DESIGN OF A GIGABIT DSL MODEM USING SUPER ORTHOGONAL COMPLETE COMPLEMENTARY CODES FOR MUI-FREE COMMUNICATION

by

Jacques Herman van Wyk

Submitted in partial fulfillment of the requirements for the degree
Philosophiae Doctor (Electronic Engineering)

in the

Department of Electrical, Electronic and Computer Engineering
Faculty of Engineering, Built Environment and Information Technology

UNIVERSITY OF PRETORIA

May 2017

SUMMARY

DESIGN OF A GIGABIT DSL MODEM USING SUPER ORTHOGONAL COMPLETE COMPLEMENTARY CODES FOR MUI-FREE COMMUNICATION

by

Jacques Herman van Wyk

Promoter(s):	Prof. L.P. Linde
Department:	Electrical, Electronic and Computer Engineering
University:	University of Pretoria
Degree:	Philosophiae Doctor (Electronic Engineering)
Keywords:	Gigabit Digital Subscriber Line (GDSL), MC-CDMA, Super Orthogonal Complete Complementary (SOCC), Code Allocation Algorithm (CAA), MUI-free, NEXT / FEXT crosstalk mitigation

Every year the demand for faster connections are increasing. This is mainly driven by an increasing amount of information that needs to be transported between two or more points. Networks that still consist of copper wires are slowly being replaced with fibre links, but the so called 'last mile' parts of the network, closer to the customer, still contain copper wires. Due to complete fibre solutions still being too expensive, Telcos are looking to reuse the existing copper as much as possible.

The primary problem addressed in this thesis is to develop a Multi-carrier Code Division Multiple Access (MC-CDMA) Digital Subscriber Line (DSL) modem, capable of delivering 1 Gbps aggregated throughput over a 200 m single twisted-pair of 0.5 mm copper wire. A secondary problem is too much self-interference within Digital Subscriber Line (DSL) systems. Self-interference is defined as the disturbance or interference that is created by similar DSL technology (i.e. one VDSL service on another VDSL service) operating within the same frequency band. The interference, referred to as *Crosstalk* is due to magnetic cross-coupling of signals between adjacent twisted pairs. Far end crosstalk (FEXT) for short loops is still a huge problem. Current techniques like Vectoring makes use of pre-coding in downstream transmission and makes use of Multi-user Detection and Interference

Cancellation (MUD-IC) in upstream transmission. Overall these techniques (pre-coding and MUD-IC) have a high computational overhead. Using Super Orthogonal Complete Complementary (SOCC) spreading codes the effect of crosstalk is mitigated, since the SOCC spreading/despreading process inherently provide IC and does not require overhead for pre-coding and MUD-IC.

The designed GDSL modem provides Multi-user interference (MUI)-free communication in a highly crosstalk dominated environment (Near end crosstalk and Far-end crosstalk) by incorporating Super Orthogonal Complete Complementary (SOCC) spreading into the existing xDSL modem architecture.

A novel code allocation algorithm was also developed to provide all users with equal transfer ratios (i.e. transferred bits to offered bits), even with bad line profiles and a high amount of offered bits. Implementation and simulation of existing network characteristics, including attenuation, Near-end Crosstalk (NEXT) and Far-end Crosstalk (FEXT) used ITU and NIPPC standards as guidelines.

1 Gbps aggregate throughput was obtained for the GDSL system over a single pair of 0.5 mm diameter copper wire over a distance of 190 m with only GDSL modems present, or 185 m to 148 m, depending on whether ADSL2+ or VDSL2 Profile 30a bypass profiles are implemented. Performance analysis in a practical MIMO crosstalk environment showed that the GDSL system have acceptable BER performance for a fully loaded system of 64 users, even for very short loops (severe FEXT).

ACKNOWLEDGEMENT

To my loving wife, Karin,

my family who supported me through my years of study

and God Almighty for giving me talents, and the opportunities to use them.

"'I Am the Way, and the Truth, and the Life"' (John 14:1)

"The best way to predict the future is to invent it" - Alan Kay - 1971

I would like to express my gratitude to:

- **Prof. Louis P. Linde** - Shoe, we made it! Thanks for your guidance - as a good friend, a colleague and as promoter.
- **Maryna Bekker**, **Mari Ferreira** and **Heleen Gous** for being my virtual moms, listening when things got too much, providing moral support, friendly smiles and friendship.
- **Prof. John M. Cioffi**, for his help with NIPP standards and for the little time I could spend at Stanford.
- Industry partners (Telkom and Bytes Universal Systems (previously UNISYS South Africa)) and the National Research Foundation for their financial support towards CeTEIS.
- Friends and students for moral support, discussions and advice.
- Examiners for their valuable input to improve this thesis and make it even better.

LIST OF ABBREVIATIONS

0-9

2B1Q	Two binary one quaternary
4B3T	Four binary three ternary
4G	4th Generation

A

ACF	Auto-correlation function
ADSL	Asymmetric Digital Subscriber Line
AMI	Alternate Mark Inversion
ANSI	American National Standards Institute
AOFDM	Adaptive Orthogonal Frequency Division Multiplexing
AWGN	Additive White Gaussian Noise

B

BCH	Bose, Chaudhuri, and Hocquenghem
BER	Bit Error Rate
BPSK	Binary Phase Shift Keying
BpRB	Bits per Resource Block
BpT	Bits per Tone

C

CAA	Code Allocation Algorithm
CAZAC	Constant Amplitude Zero Autocorrelation
CC-MC-CDMA	Complete Complementary Multicarrier Code Division Multiple Access
CCC	Complete Complementary Code
CCDF	Complementary Cumulative Distribution Function
CCF	Cross-correlation Function
CCR	Code change rate
CDMA	Code Division Multiple Access
CI	Carrier Interferometry
CIMA	Carrier Interference Multiple Access
CO	Central Office
COFDM	Coded Orthogonal Frequency Division Multiplexing
CP	Cyclic Prefix
CpRB	Code per Resource Block

D

DAC	Digital-to-Analog-Converter
DMT	Discrete Multi-tone
DS	Downstream
DS-CDMA	Direct Sequence Code Division Multiple Access
DSL	Digital Subscriber Line
DSM	Dynamic Spectral Management
DSLAM	Digital Subscriber Line Access Multiplexer

E

EC	Echo cancellation
EO	Extended Orthogonal
EOCC	Extended Orthogonal Complete Complementary

F

FDD	Frequency Division Duplex
FDM	Frequency Division Multiplexing
FEXT	Far-end Crosstalk
FFT	Fast Fourier Transform
FIR	Finite Impulse Response
FS	Frequency Spreader/Spreading
FTP	Foiled Twisted Pair
FTTB	Fiber to the Business/Building
FTTdp	Fibre to the distribution point
FTTE	Fiber to the Enclosure
FTTH	Fiber to the Home
FTTN	Fiber to the Node
FZC	Frank-Zadoff-Chu

G

Gbps	Gigabit per second
GCL	General Chirp-like
GDSL	Gigabit Digital Subscriber Line
GLS	Generalized Loosely Synchronous
GTU-C	Gigabit Terminal Unit-Central Office
GTU-R	Gigabit Terminal Unit-Remote

H

HSDPA	High Speed Data Packet Access
HSPA+	High Speed Packet Access Enhanced

I

IC	Interference Cancellation
IEC	International Electrotechnical Commission
IFFT	Inverse Fast Fourier Transform
ISDN	Integrated Digital Service Network
ISI	Inter symbol Interference
ITU	International Telecommunications Union
IFW	Interference-free Window

L

LA	Large area
LAS	Large Area Synchonized
LS	Loosely Synchronous
LTE	Long Term Evolution

M

M-QAM	M-level Quadrature Amplitude Modulation
MAI	Multiple Access Interference
MC-CDMA	Multi-carrier Code Division Multiple Access
MC-DS-CDMA	Multi-carrier Direct Sequence Code Division Multiple Access
MIMO	Multiple Input Multiple Output
MMSE	Minimum Mean Square Error
MSAN	Multi-Service Access Node
MSB	Most significant bit
MT-CDMA	Multitone Code Division Multiple Access
MUD	Multiuser Detection
MUI	Multiuser Interference

N

NEXT	Near-end Crosstalk
NIPPC	Network Interface, Power, and Protection Committee

O

OCCC	Orthogonal CCC

OFDM	Orthogonal Frequency Division Multiplexing
ORC	Orthogonal Ratio Combining
OVSF	Orthogonal Variable Spreading Factor

P

PAC	Periodic Autocorrelation
PAPR	Peak-to-Average Power Ratio
PCC	Periodic Cross-correlation
PDF	Probability Density Function
PG	Processing Gain
PO-CI	Pseudo-orthogonal Carrier Interferometry
POC	Perfectly Orthogonal Complementary
POM	Polyphase Orthogonal Matrix
POTS	Plain Old Telephone Service
PN	Pseudo-noise
PR	Pseudo-random
PSD	Power Spectral Density

Q

QLN	Quiet Line Noise
QS-CDMA	Quasi-Synchronous CDMA

R

RB	Resource Block
RE-ADSL	Reach Extended ADSL
RMS	Root-mean-square
RS	Reed-Solomon

S

SC	Single Carrier
SCC	Super Complete Complementary
SINR	Signal-to-Interference Noise Ratio
SNR	Signal-to-Noise Ratio
STP	Shielded Twisted Pair
SOC	State Owned Company
SOCC	Super Orthogonal Complete Complementary

T

TDD	Time Division Duplex
TS	Time Spreader/Spreading

U

US	Upstream
UTP	Unshielded Twisted Pair
UTRA	Universal Terrestrial Radio Access

V

VDSL	Very-high-speed Digital Subscriber Line

LIST OF SYMBOLS

b	coded bitstream
$\bar{b}_n$	vector of bits representing symbol d_n for subchannel n
c_i	spreading code i
d	Line length experiencing crosstalk
d_n	M-QAM symbol for subchannel n
f	Frequency
i	Spreading sequence index
k	Active user index
l	Line length
m	Resource block index
n	Subchannel index
n_{pilot}	Subchannel index for pilot tone(s)
r	Counter from first active RB to the last active RB
$\mathbf{s_i}$	Spreaded symbol i
$Bits\_left$	Offered bits left
$Bits\_used$	Bits sent
$BpRB$	Bit allocation profile per RB
C	Capacity
C_l	Capacitance
$CpRB_{start}$	Start index of spreading codes to be used in a specific RB
$CpRB_{end}$	End index of spreading codes to be used in a specific RB
$Codes\_RB$	Number of spreading codes allocated to a RB
G	Conductance
H_{lin}	Linear channel attenuation
H_{log}	Logarithmic channel attenuation
K	Number of active users
L_{fsp}	Frequency spreading sequence length
L_{tsp}	Time spreading sequence length
L	Inductance
M	Number of Resource Blocks (RBs)
N	Number of subchannels / FFT size
N_0	One-sided AWGN noise power spectral density

$\mathbb{N}_0$	natural numbers (including zero)
$\mathbb{N}_1$	natural numbers (without zero)
P	Number of allocated codes from $CpRB_{start}$ to $CpRB_{end}$
R	Code rate
R_b	Bit rate
R_l	Resistance
R_s	Symbol rate
RB_bits	Number of bits allocated to be sent in a RB
RB_bits_adj	Adjusted number of bits allocated to be sent in a RB, based on integer $Codes\_RB$
RB_start	First subchannel index of a resource block (RB)
RB_stop	Last subchannel index of a resource block (RB)
SNR_{index}	10-bit unsigned value of SNR_{used}
$SNR_{indexed}$	Quantized representation of SNR_{used}
$SNR_{measured}$	Measured SNR
SNR_{used}	$SNR_{measured}$ - Γ
$\mathbf{S}$	Spreading vector
Z_o	Characteristic Impedance
α	dynamic range, defined as the ratio between the signal level at the transmitter and the noise level at the receiver
Δf	Subchannel spacing
ε_b	bit energy
ε_s	symbol energy
γ	Propagation constant
Γ	SNR margin
σ^2	variance
ρ_{xy}	Cross-correlation between sequences x and y
ω	Radian frequency

TABLE OF CONTENTS

LIST OF TABLES

LIST OF FIGURES

CHAPTER 1 INTRODUCTION

"Still it is far too complex to implement a full-scale crosstalk canceler." - M.K. Rudberg [1] - Sep 1999

"As DSPs gets cheaper, smaller, and less power-consuming, crosstalk cancellation will become more attractive; ..." - J.A.C. Bingham [2] - 2000

"Graphics Processing Units (GPUs) have become a common place in the consumer market and are finding their way beyond graphics processing..."' - Linjia Hu et al. [3] - 2013

"G.Fast chipsets give copper a new lease on life - G.Fast offers a partial solution for ISPs that need to remain competitive but want to circumvent the heavy investment of fiber-to-the-home deployment." - Versa Technology Blog - 28 October 2016

1.1 MOTIVATION AND OBJECTIVES

Every year the demand for faster connections is increasing. This is mainly driven by an increasing amount of information that needs to be transported between two or more points. Networks that still consist of copper wires are slowly being replaced with fibre links, but the so called 'last mile' parts of the network, closer to the customer, still contain copper wires. Due to complete fibre solutions still being too expensive, Telcos are looking to reuse the existing copper as much as possible. The primary problem addressed in this thesis is to develop a Multi-carrier Code Division Multiple Access (MC-CDMA) Digital Subscriber Line (DSL) modem, capable of delivering 1 Gbps aggregated throughput over a 200 m long single twisted-pair of 0.5 mm diameter copper wire. A secondary problem is too much self-interference within Digital Subscriber Line (DSL) systems. Self-interference is defined as

the disturbance or interference that is created by similar DSL technology (i.e. one VDSL service on another VDSL service) operating within the same frequency band. The interference, referred to as *Crosstalk* is due to magnetic cross-coupling of signals between adjacent twisted pairs. This makes current DSL systems interference limited. Many solutions were developed to mitigate or combat the crosstalk effect, some very successfully (like Vectoring) [4] to improve the system performance in the presence of crosstalk. FEXT for short loops is still a huge problem. As a secondary objective the latest in orthogonal spreading codes, particularly Super Orthogonal Complete Complementary (SOCC) codes will be incorporated and a novel code allocation scheme will be developed to allocate codes uniquely to each user, thus ensuring multi-user interference (MUI) free communication. In the case of DSL, MUI is the crosstalk interference experienced between users. Implementation and simulation of existing network characteristics, including attenuation, Near-end Crosstalk (NEXT) and Far-end Crosstalk (FEXT) will use ITU and NIPPC standards [5–7] as guidelines.

1.2 OVERVIEW OF CURRENT LITERATURE

The appeal of wide-bandwidth digital access has grown enormously with the Internet. Higher-speed access means faster file transfer, and reduced waiting times, thus enhancing the use of more bandwidth-intensive Internet applications. Additional high-speed access services, including multiplexed digital voice, digital video, and business teleconferencing, can be implemented through or in addition to Internet data. xDSL is an increasingly popular access technology for providing high-speed access through copper lines, and was the focus of research at Stanford University [8].

Telephone companies are still considering existing twisted-pair loops in their next generation broadband access networks. Fibre to the home (FTTH) is still prohibitively expensive in a marketplace that is now driven by competition rather than cost. Fibre to the node (FTTN), which encompasses Fibre to the curb (FTTC) and Fibre to the basement/building (FTTB), is an attractive alternative to FTTH. Fibre to the distribution point (FTTdp) is something between FTTN and FTTH - With fibre running to within a few metres of the property, FTTdp brings fibre much closer than FTTN, and almost as close as FTTH. This means near-gigabit network speeds can be achieved over the very short run of copper between the premises and the distribution box (which can later be replaced with fibre for FTTH). A large part of the competition includes wireless services like 3G, 3.5G (HSDPA and HSPA+), LTE and LTE-Advanced. The LTE specification provides downlink peak rates of 300 Mbps, uplink peak rates

of 75 Mbps and transfer latency of less than 5 ms. Practically, much lower rates and higher latency are obtained between shared users.

Two of the enabling technologies for FTTN are *Asymmetric Digital Subscriber Line* (ADSL) and *Very-high-bit-rate Digital Subscriber Line* (VDSL), which can support various topologies. DSL installations and use are multiplying rapidly worldwide, especially in urban/sub-urban areas. Nearly all developed countries have matured deployments of the dominant technology of today, ADSL [9]. In South Africa, Telkom SA (SOC) started the deployment of Multi-service Access Nodes (MSANs) [10] in parts of their network in order to support next generation FTTC/FTTN technologies like VDSL/VDSL2. VDSL services at 20, 40 and 100 Mbps downstream were supported at time of writing. There is also a rapid deployment of FTTH solutions, mainly up to 100 Mbps, some even to 1 Gbps. An overview of some of the dominant xDSL technologies are provided in Chapter 2 (Background).

As the demand for more bandwidth increases, new technology must make provision to support higher bit rates. One of the latest in the series of xDSL standards is VDSL2, standardized as ITU G993.2 [11]. It is intended to offer between 6 and 60 Mbps downstream for wires shorter than 1.5 km [12]. Alternatively, VDSL2 can support symmetric services up to 23 Mbps, which makes VDSL2 attractive for many applications and even opens the market for new services not possible on asymmetric-based services. G.fast [7, 13] is the latest of the xDSL standards and supports a more hybrid solution of fibre and copper (FTTdp), mainly to provide 1 Gbps and higher throughput.

The first mention of **GDSL** was in a ITU Working group contribution [14] and more publicly in a paper by Lee *et al.* [15], where MIMO transmission methods were applied to multi-wire communication systems. Using a MIMO channel model, it was found that symmetric data rates of more than 1 Gbps were achievable over four twisted pairs (Category 3) for a 300 m range. Similar results were also obtained for a quad-core cable. Huawei published a paper on their Giga DSL solution [16]. It provided an aggregated (combined upstream and downstream) 1 Gbps over a single 100 m long 0.5 mm diameter copper wire using a 100 MHz frequency band with Time division duplex (TDD) and 2048 subcarrier OFDM.

1.2.1 Transmission performance

Transmission performance is detrimentally affected by the crosstalking environment, which includes other DSLs. Two areas of potential DSL transceiver improvements have been identified, namely: *Multiuser detection* and *Multiuser coding*.

1.2.1.1 Multiuser detection

Multiuser detection for DSL was first proposed by the DSL Friendly group in [17]. The basic concept is that a single DSL receiver attempts to decode not only its signal, but also those of its crosstalking neighbours. Although the performance of the main DSL transceiver should be improved, due to the mitigation of crosstalking users through a demodulation-remodulation process (multi-user interference cancellation), the complexity of the receiver is increased.

1.2.1.2 Multiuser coding

When considering multiuser detection, one may consider the use of codes which allow crosstalkers to be more easily separated from the desired DSL signal in the detector. Of particular interest is a method of choosing energy and loading tables of advanced Discrete Multi-tone (DMT) modems when taking into account the type of crosstalkers present as well as the associated crosstalk coupling functions. DMT is closely related to the Orthogonal Frequency Division Multiplexing (OFDM) technique used in wireless systems, since both use IFFT/FFT structures (subchannels are created), but with DMT the modulation scheme used within each of the subchannels (tones) can be varied according to channel conditions.

Most research focus has been placed on different modulation techniques and coding schemes to improve capacity.

1.2.2 Noise mitigation techniques

Honig *et al.* [18] considered the suppression of Near-end Crosstalk (NEXT) and Far-end Crosstalk (FEXT) by using linear pre- and post-filtering. A Minimum mean square error (MMSE) linear equalizer was completely specified in terms of the near and far-end channel transfer functions, bandlimited to the Nyquist frequency. The behavior of the MMSE was studied, assuming Finite Impulse Response (FIR) transmitter and receiver filters, as a function of how the matrix taps are allocated between these filters, as well as the timing phase. It was found that the mean square error is a very sensitive function of timing phase, but nearly independent of how taps are allocated between transmitter and receiver filters. NEXT and FEXT could be eliminated completely under certain conditions.

Ginis *et al.* [19] showed that the precoding scheme can also prove valuable for Multiple-Input-Multiple-Output (MIMO) zero-forcing equalization. However, in a point-to-multipoint scenario (broadcasting), joint processing at the receiver side is not feasible (due to different line lengths (timing)). Equalization has to be performed at the transmitter side [20].

1.3 CONTRIBUTIONS AND RESEARCH OUTPUTS

In this thesis, the following contributions were made:

- A MC-CDMA DSL modem was designed that obtains 1 Gbps over a single 0.5 mm diameter twisted-pair copper wire of 190 m length, in contrast to either 1 Gbps over 4 pairs of 200 m length 0.5 mm diameter wire, or 1 Gbps over a single pair of 100 m length 0.5 mm diameter wire;
- A novel code allocation algorithm (CAA) was developed and implemented. This algorithm uniquely allocates SOCC spreading codes to each active user in each resource block and ensures that each user overall obtain the same transfer ratio (transmitted bits to offered bits);
- Frequency spreading / despreading using Super Orthogonal Complete Complementary codes was implemented. This SOCC frequency spreading block, together with the CAA, can modularly be added to existing xDSL architectures to provide MUI-free communication;

- Orthogonal code division (using spreading) vs. existing pre-coding was implemented to mitigate MUI, even in severe crosstalk conditions. Vectored DSL makes use of pre-coding in downstream transmission and makes use of Multi-User Detection (MUD) interference cancellation (IC) in upstream transmission [4]. Overall these techniques (pre-coding and MUD-IC) have a high computational overhead. Using SOCC spreading codes the effect of crosstalk is mitigated, since the SOCC spreading/despreading process inherently provide IC and does not require overhead for pre-coding and MUD-IC.

The following patent was filed:

1. J.H. van Wyk "'Unique Spreading Code Allocation Algorithm based on Data Rate and Channel Conditions"', Preliminary South Africa Patent 2016/04353.

The following peer-reviewed journal articles were accepted:

1. J.H. van Wyk, L.P. Linde, "'Design of a Gigabit DSL modem using super orthogonal complete complementary codes"', *Trans. Emerging Tel. Tech. (2016)*, vol. 27, no. 11, pp. 1454-1460. Published online in Wiley Online Library (Available: http://wileyonlinelibrary.com). DOI: 10.1002/ett.3071
2. J.H. van Wyk, L.P. Linde, "'Performance evaluation of a Gigabit DSL modem using SOCC codes under practical crosstalk conditions"', *SAIEE Africa Research Journal.* (to be published December 2017).

The following international conference publications were presented:

1. J.H. van Wyk, L.P. Linde, "'Combatting multi-user interference in ADSL systems using time spreading"', *Proc. CCECE 2003*, Montreal, Canada, 3-7 May 2003.
2. J.H. van Wyk, L.P. Linde, "'Design of a CC-MC-CDMA system for Gigabit DSL (GDSL)"', *Proc. ITNG 2009*, Las Vegas, Nevada, USA, 27-29 April 2009.

The following national conference publications were presented:

1. J.H. van Wyk, L.P. Linde, "'Towards Gigabit DSL (GDSL): Design of a CC/MC-CDMA modem"', *Proc. SATNAC 2007*, Sugar Beach Resort, Mauritius, 9-13 September 2007.
2. J.H. van Wyk, L.P. Linde, "'Towards Gigabit DSL (GDSL): System Feasibility Study"', *Proc. SATNAC 2008*, Wild Coast Sun, Eastern Cape, 7-10 September 2008.

1.4 THESIS OVERVIEW

In Chapter 2 relevant background literature is provided. In Chapter 3 the GDSL channel- and system capacity, channel impulse response, signal to noise margin, background noise and measurement, crosstalk coupling models (NEXT, FEXT as well as MIMO crosstalk model), transmit/receive filters and power spectral densities are described. In Chapter 4 the GDSL system architecture is described, i.t.o. the GDSL transmitter / receiver , as well as sub-systems related to these. It also discusses the idea of Resource Blocks (RB) that are used, the correlation properties of the SOCC spreading codes, modem operation, notching of specific frequency bands and co-location with other xDSL services. In Chapter 5 the simulation models, basic transceiver simulation results and bit error rate analysis of the proposed SOCC codes are discussed in a NEXT/FEXT environment. In Chapter 6 the novel RB code allocation algorithm (CAA) is provided. This algorithm operates on the RB profile and offered bits to be transferred, to allocate unique spreading codes in each RB, to ensure each user achieve the same transfer ratio. In Chapter 7 some concluding remarks are made.

CHAPTER 2 BACKGROUND

2.1 DIGITAL SUBSCRIBER LINE TECHNOLOGY

x-type Digital Subscriber Line (xDSL) is an access technology, where the x can be replaced by several letters of the alphabet. This family of technologies can be used to convert the current Public Switched Telephone Network (PSTN) into a high-speed digital network for residential and business users. xDSL technologies have been developed and implemented to circumvent the circuit-switched voice network's limited 4 kHz spectrum, and allow the use of a much broader frequency spectrum. It allows the reuse of the existing copper network, while allowing the gradual transition from copper to fibre. Some xDSL members have the distinct advantage of operating simultaneously and without interfering with conventional voice services. Various speeds and services, over different distances, can be obtained for each member of the xDSL family.

DSL started with the introduction of Basic rate access DSL (also known only as DSL). Some of the current standardized systems found around the world are:

1. *Basic rate access DSL (ISDN)* - It was a 160 kbps one-pair full-duplex system, used in the USA only to provide access to ISDN and in Europe for 2 x 64 kbps digitized voice services. ITU recommendation G.961 defined three variations / systems: [2]

   (a) Two binary one quaternary (2B1Q) coding with echo-cancellation (EC); used in North America and much of Europe.

   (b) Four binary three ternary (4B3T) coding with EC; used in some European countries.

   (c) Alternate mark inversion (AMI) coding with synchronized TDD; used in Japan.

2. *T1* - A 1.544 Mbps dual simplex on two pairs using AMI coding and repeaters spaced every 1.83 km; used in North America.

3. *E1* - It is similar to T1, but operates at 2.048 Mbps with repeaters spaced every 2 km; used in South Africa and the rest of the world. It is by far the most severe source of crosstalk into ADSL and VDSL [2, 21, 22].

4. *High-Speed DSL (HDSL)* - 1.536 Mbps two-pair and 2.048 Mbps two- and three-pair, full-duplex systems using 2B1Q coding and EC. It is now standardized as ITU Recommendation G.991.1.

5. *HDSL2* - A 1.536 Mbps one-pair full-duplex system using a mixture of FDM and EC, and very sophisticated trellis coding. It was developed to replace existing T1/E1 installations and is standardized as G.991.2.

6. *Asymmetric DSL (ADSL)* - ANSI T1.413 [23] and G.992.1 (G.DMT) [5] define an ADSL system that supports downstream and upstream rates up to 8 Mbps and 1 Mbps, respectively [24], within a radius of approximately 3.66 km from the Central Office (CO). Reduced downstream rates of around 1 Mbps can be obtained for a radius of approximately 6 km [25]. There is also an Annex A (ADSL over POTS) and an Annex B (ADSL over ISDN) frequency plan. G.992.2 [26], better known as G.Lite, defining a simpler system allowing variable rates up to 2 Mbps downstream, which is line compatible with G.992.1.

7. *ADSL2* - ADSL2 (G.992.3 or G.DMT.bis) [27] increased the data rates to 12 Mbps downstream and, depending on Annex version, up to 3.5 Mbps (Annex J) upstream, using the same bandwidth as ADSL. This is achieved using improved modulation techniques. A reach extended version RE-ADSL (Annex L) and a splitter-less version (G.992.4) is also available, but it is not used much due to its low rates (1.5 Mbps downstream and 0.5 Mbps upstream) and high noise characteristics.

8. *ADSL2+* - ADSL2+ (G.992.5 or G.DMT.bis+) [28] doubles the bandwidth used to 2.2 MHz, supporting 20 Mbps downstream (24 Mbps for Annex M) and up to 1.1 Mbps upstream (3.3 Mbps for Annex M) depending on the distance from the DSLAM to the customer's premises.

9. *Very high-speed DSL (VDSL)* - VDSL (G.993.1) [6] is mainly used in a hybrid twisted-pair/fibre optic systems where a large part of the copper network from the Central Office (CO) is replaced with fibre. Various topologies exist, such as Fibre to the Exchange (FTTE), FTTN, FTTB and FTTC [29]. VDSL distance vary from 0.3 km to 1.83 km for the twisted-pair and up to 52 Mbps downstream and 16 Mbps upstream [2,30,31] using a frequency band up to 12 MHz. VDSL uses up to 7 different frequency bands, which enables customization of data rate between upstream and downstream.

10. *VDSL2 - VDSL2 (G.993.2)* [11] use frequencies of up to 30 MHz to support symmetric data rates exceeding 100 Mbps (in both the upstream and downstream directions), which is achieved at a range of about 300 m.

11. *G.fast (G.9700 and G.9701)* [7, 13] - G.fast modulates data using DMT modulation, as in ADSL, VDSL and VDSL2. It uses up to 12 bits per tone and specify 106 MHz profiles, with 212 MHz profiles planned for future amendments. G.9701 (G.fast-phy) is the G.fast physical layer specification. To enable co-existence with ADSL2 and various VDSL2 profiles, the start frequency can be adjusted to 2.2, 8.5, 17.664, or 30 MHz, respectively.

12. *XG-Fast* [32] - XG-Fast has a hardware proof-of-concept platform (no standardization yet), with rates of 8.8 Gbps over a single 30 m length of 0.6 mm twisted pair, using full duplex transmission and a signal bandwidth of 500 MHz. With two pairs and using TDD instead of FDD, 10 Gbps is achieved. It is envisioned to be deployed for dense deployment of 5G small cells.

Strictly speaking, T1 and E1 is not a DSL technology, since it was originally used to provide trunks between COs, but they were later used as high speed links from COs to customer sites (digital subscriber lines) [24].

2.2 MULTI CARRIER CODE DIVISION MULTIPLE ACCESS

Many researchers were motivated to investigate the suitability of combining Multi-carrier modulation (MCM) with CDMA techniques for wideband multiple access communications [33]. The combination, known as Multi-carrier CDMA (MC-CDMA), allows one to benefit from the advantages of both

schemes. The three most popular proposals are multi-tone CDMA (MT-CDMA) [34], multi-carrier direct-sequence CDMA (MC-DS-CDMA) [35–37] and MC-CDMA [38–40]. An overview of MC-CDMA is also provided by Hara *et al.* [40]. In all three schemes, many subchannels are available for transmission of user data. OFDM is robust to frequency-selective fading, but can suffer from complex subcarrier synchronization and high sensitivity to frequency offset and non-linear amplification [40]. For Multi-carrier transmission it is best to have frequency non-selective fading over each subchannel. Using OFDM also provides the advantage that it lowers the symbol rate in each subchannel, leading to a longer symbol duration, which makes it easier to quasi-synchronize the transmission [41]. Using IFFT/FFT, signals can easily be transmitted and received without increasing the complexity, and have the feature of high spectral efficiency due to minimally-dense carrier spacing [40]. Using CDMA, each user is usually assigned a CDMA code, which is used to differentiate between signals belonging to different users, by performing a correlation process at the receiver. MC-CDMA provides high-bandwidth efficiency, high capacity and a low complexity implementation [42].

In MC-CDMA the original data is spread over different subcarriers, using a given spreading code in the frequency domain. A fraction of the symbol, represented by a chip of the spreading code, is transmitted through a different subcarrier. The capacity of MC-CDMA is limited by multiple access interference (MAI), as in DS-CDMA, and inter-channel interference (ICI) due to carrier-frequency offset. Performance and robustness to frequency offset can then be gained at the price of an increase in computational complexity and bandwidth efficiency. To achieve high performance, channel-dependent multiuser detection is needed [33]. However, relative to DS-CDMA, MC-CDMA have the following distinctive advantages:

- Synchronization: Block synchronization can be achieved and maintained in MC-CDMA due to long chip/symbol duration. This is instrumental to multiuser detection.
- Loading: With information being transmitted in parallel narrowband streams, it is convenient to employ adaptive loading techniques to distribute transmission power efficiently based on subchannel signal-to-interference noise ratio (SINR) to achieve optimum efficiency.

MC-DS-CDMA is an enhanced version of MC-CDMA, where additional time-domain spreading is performed after the IFFT process on the transmitter side. This extra spreading facilitates joint exploitation of the frequency and time diversities in a multiple-access environment [43]. Different spreading codes can be used on each subchannel, providing an additional time spreading factor L_{tsp}.

All signals are spread across all $N = L_{fsp}$ subchannels, providing better narrowband fading/interference resistance. The effective spreading factor is $L_{fsp}.L_{tsp}$ (due to both frequency and time spreading), allowing it to handle a heavily loaded system $K > L_{fsp}$ and L_{tsp} [33], where K is the number of users in the system.

2.3 RELATED RESEARCH

2.3.1 Spreading codes

When considering traditional CDMA systems using Walsh-Hadamard spreading sequences, the system is interference limited. Inter symbol interference (ISI) is due to non-zero autocorrelation sidelobes of the spreading sequences, while MAI or MUI is due to non-zero cross-correlation [40]. Walsh-Hadamard and Orthogonal Variable Rate Spreading Factor (OVSF) codes will also not be orthogonal at all in asynchronous transmission channels. To combat ISI, each of the sequences in the set must be easy to distinguish from a time-shifted version of itself, while MAI is combatted if each sequence is easily distinguished from every other sequence in the set. To guarantee small MUI in such systems, the designer is forced to construct a set of sequences having both good even and odd periodic cross-correlation function (CCF)s, whereas the corresponding auto-correlation function (ACF)s are important in the presence of multipath interference. Pursley [44] showed that MUI strongly impacts the received signal to noise ratio, given as:

$$SNR = \left(\frac{N_0}{2E_b} + \frac{1}{6L^3} \sum_{x=1, x \neq y}^{K} \sum_{l=1-L}^{L-1} |\rho_{xy}(l)|^2 \right)^{-1} \tag{2.1}$$

where E_b is the bit energy, N_0 is the one sided noise power spectral density, L is the sequence length, K is the number of active users and ρ_{xy} is the cross-correlation between sequences x and y. It is thus ideal to eliminate cross-correlation between used sequences [45]. *Overall, a set of sequences with good autocorrelation (strong autocorrelation peak), no cross-correlation between sequences, and a large number of sequences within a family of a certain length L are required.* Auto-correlation is the correlation between any sequence and itself, and cross-correlation is the correlation between one sequence and another one. Correlation can also be performed aperiodically (linear shifting of sequences) or periodically (cyclically shifting sequences).

2.3.1.1 Pseudorandom sequences

In most of the literature on periodic sequences, the terms pseudo-random (PR) sequence, pseudo-noise (PN) sequence and maximal length sequence (or m-sequence) are used synonymously. Sarwate *et al.* [46] presented a survey on PN-sequences i.t.o. their periodic and aperiodic cross-correlation properties. Due to these PN sequences having non-ideal correlation properties (autocorrelation not zero for all time shifts except $t = 0$ and cross-correlation not zero for all time shifts) they were not considered in this thesis.

2.3.1.2 Large Area Synchronized Codes

Stańczak *et al.* [47] looked at systematic methods and theory for the construction of LAS codes. LAS codes are constituted by the combination of Large Area (LA) codes and Loosely Synchronous (LS) codes. Large area synchronized (LAS) codes exhibit a so-called Interference Free Window (IFW) within which the aperiodic off-peak autocorrelation is zero, and the cross-correlation is zero. LAS codes were not considered in this thesis due to their non-ideal cross-correlation properties outside the IFW. To reduce multiple access interference and inter-symbol interference in a time dispersive channel, LS codes have perfect auto-correlation and cross-correlation functions in the vicinity of zero shift. By reducing both ISI and MAI, the "near-far effect" could be reduced significantly, and the spectral efficiency can be enhanced. Due to the IFW, i.e. within the interval $\{-d, ..., d\}$ it is necessary to insert guard intervals (or zero gaps) between sequences of length equal to the maximum dispersion delay d of the channel, leading to an undesired reduction of spectral and energy efficiency. IFW was introduced because perfect synchronization is difficult to achieve in practical systems, especially wireless systems. The IFW needs to be increased as synchronization becomes less ideal. It is well known that the ISI and MAI in non-synchronous CDMA systems strongly depend on the aperiodic correlations of the spreading sequences [46], which for LAS codes are not good outside the IFW.

Zhou *et al.* [48] performed a theoretical analysis of LA code properties for LAS-CDMA, using (17,136,2559) LA codes.

Ni *et al.* [49, 50] studied the achievable network performance of a UTRA-like FDD/CDMA system by simulation, and compared OVSF codes with LS codes. It was found that network performance of

LS-codes-based systems was substantially better than OVSF-based systems.

Lai *et al.* [51,52] looked at LA code construction, a method of triangular array formations of correlation value distribution positions, as a potential high spectral efficiency system for 4G. The proposed LAS-CDMA system must be synchronized within the IFW and zero strings with different sizes must be inserted between elements of the orthogonal code. LAS-CDMA is a multiple access scheme, based on 2 families of CDMA codes, LA codes and LS codes. Different users within a cell use different LS codes. The LS codes are pulse position modulated by an LA code, with different cells using different LA codes.

Xu *et al.* [53] presented an OFDMA scheme based on LAS-codes for use in Powerline Communications to increase data throughput, system capacity and spectral efficiency in Home Networks.

Wang *et al.* [54] proposed a novel access method with LS codes in MC-CDMA. Theoretical analysis and simulation results showed that, by using the LS-code access scheme, the sensitivity to frequency offset in a MC-CDMA system can effectively be eliminated. It was shown for the case of no carrier frequency offset that both Walsh-Hadamard and LS codes are orthogonal, which leads to both of them having no MAI or ICI. However, in the case of some frequency offset, although both of them have no MAI due to orthogonality, LS-code-based systems performed better than Walsh-Hadamard based systems.

Tang *et al.* [55] developed a systematic construction of new families of Generalized LS (GLS) codes with favourable ICI correlation properties, while maintaining the desirable IFW property. These GLS codes can be obtained by choosing different Hadamard matrices and different uncorrelated complementary pairs. BER results showed that GLS families constructed from Hadamard matrices and the Kerdock code achieved a performance gain over scrambled LS codes.

2.3.1.3 Carrier Interferometry (CI) codes

Nassar *et al.* [56] introduced the idea of Carrier Interference Multiple Access (CIMA). Like MC-CDMA, CIMA accomplishes spectral spreading by transmission of identical data over several carriers simultaneously. However, unlike any existing CDMA technique to date, this method does not provide

user orthogonality through the use of spreading codes (based on PN sequences), but rather through multiple carrier interference. Orthogonality amongst users is always attained whether the number of users is less than or equal to the dimensions / carriers, and pseudo-orthogonality when the number of users exceeds the number of carriers. In AWGN channels, CIMA supports a greatly simplified receiver structure.

Natarajan *et al.* [57, 58] introduced a large set of CI spreading codes that doubles the user capacity in MC-CDMA systems without any cost in bandwidth and negligible cost in performance. It uses complex spreading sequences, consisting of two sets with minimum cross correlation between sets. It was demonstrated that Carrier Interferometry (CI) codes significantly outperforms other large code sets such as extended Gold and quadriphase sequences introduced by Popovic [59]. It also overcomes the strict length restrictions and/or user capacity limitations of the complex spreading sequences proposed in [60]. In [61] CI/MC-CDMA performance was shown to match that of orthogonal MC-CDMA using Hadamard-Walsh codes up to the MC-CDMA K user limit; and also provided the added flexibility of an additional $K-1$ users with pseudo orthogonal positioning. When compared to MC-CDMA schemes capable of supporting greater than K users, CI/MC-CDMA performance exceeded that of MC-CDMA. It was also shown to be robust against phase jitters and frequency offsets.

Natarajan *et al.* [62] analyzed crest factor considerations in MC-CDMA systems employing carrier interferometry codes. It was shown that the crest factor in downlink transmission demonstrated the desirable properties of low mean and low variance. The poor crest factor observed in the uplink was characterized and it was shown how this can be effectively combated by use of Schroeder's analytical crest factor reduction techniques [63].

Wu *et al.* [64] demonstrated that CI codes achieved lower cross correlation than Hadamard-Walsh codes after transmission over a frequency selective channel. Lower cross correlation means better orthogonality between codes and lower MAI at the receiver.

Wiegandt *et al.* [65] introduced a novel carrier interferometry phase coding scheme to enhance the performance in OFDM systems without bandwidth expansion or decreased user throughput. It was shown to gain 14 dB over conventional OFDM, equalling the performance of Coded OFDM (the addition of channel coding, redundancy and frequency diversity which is added to OFDM), but the overall user throughput was reduced and receiver complexity increased. CI/OFDM entails the

simultaneous modulation of each bit onto all carriers and then assigning a unique phase code set to the carriers of each bit to assure orthogonality.

Chung *et al.* [66] proposed an Adaptive OFDM system based on CI codes. In AOFDM, an adaptive modulation scheme is allocated to an OFDM symbol, rather than each subcarrier. When compared to a fixed OFDM system, it offers both performance improvement and high throughput per user, even in hostile fading conditions.

Taylor *et al.* [67] investigated the performance of CI and Pseudo-Orthogonal CI (PO-CI) implementations of MC-CDMA, compared with traditional MC-CDMA (with Hadamard-Walsh spreading codes). It was found that BPSK CI outperformed both MC-CDMA and COFDM, while BPSK PO-CI offered twice the capacity of MC-CDMA, with the same performance. For higher modulations however, CI system's performance was the same as MC-CDMA, whilst the performance of PO-CI was found to be very poor. CI systems also performed better in the presence of phase noise. MMSE was implemented as a receiver structure, but Orthogonal Ratio Combining (ORC) can also be used.

Wu *et al.* [68] introduced CI codes to spread OFDM symbols over all N subcarriers, allowing OFDM to exploit frequency diversity, improving performance (without loss of throughput) and suppressing narrowband interference. OFDM is sensitive to narrowband interference, which is well-known for ADSL. As a consequence, BER performance degrades rapidly. Adaptive loading (Waterfilling) is used to combat narrowband interference, through reliable real-time channel feedback from receiver to transmitter. In the CI/OFDMA system, compared to other orthogonal spreading codes, CI codes provide excellent peak-to-average power ratios, overcoming one of OFDM's disadvantages. CI codes may also be designed for any length N, ensuring flexible system design.

2.3.1.4 Orthogonal codes

Park *et al.* [69] proposed an orthogonal code which, for a period N, has zero autocorrelation except for every Nth term. From Suehiro *et al.* [70], an orthogonal sequence is defined as a periodic sequence whose autocorrelation function is zero except for the period-multiple-shift terms. The system thus does not suffer from inter-user interference over a period of N chips. Disadvantages include high time-consumption to generate codes and to reconstruct information symbols. Receivers also have to wait N^2

time units to decode N information symbols and lastly, a dummy symbol must be included. A modified sequence which overcomes these disadvantages was also suggested and investigated [70].

2.3.1.5 Polyphase sequences

Polyphase sequences originated in 1953 when Frank [71] designed N-phase codes of length N^2, identical to Heimiller [72], but without the relatively prime limitation of Heimiller. Frank's [71] sequences had one main peak and very small side peaks for the autocorrelation function.

Golomb *et al.* [73] examined the effect of various transformations on the original (± 1) Barker sequences and on four-valued ($\pm 1, \pm j$) Barker sequences, and then exhibited constructions for generalized Barker sequences of a variety of lengths and all possible alphabet sizes. A Barker sequence is a sequence a_r of $\pm$ls of some finite length L_c such that the correlation function C(τ) defined by $\mathrm{C}(\tau) = \sum_{r=1}^{k-\tau} a_r a_{r+\tau}^*$ satisfies $|C(\tau)| \leq 1$ for $\tau \neq 0$. Chang *et al.* [74] studied n-phase Barker sequences.

Chu [75] described the construction of complex codes of the form $e^{j\alpha_k}$ whose discrete circular autocorrelations are zero for all shifts. From this work one can obtain L sequences of length L. Chu sequences are defined as

$$a_k = \begin{cases} e^{i\frac{M\pi k^2}{L}} & L \text{ even} \\ e^{i\frac{M\pi k(k+1)}{L}} & L \text{ odd} \end{cases} \tag{2.2}$$

where M is relatively prime to L. Variations such as cyclic shifts, addition of a constant to the exponential part or conjugating the entire code will not affect the autocorrelation function. Certain linear phase shifts of the form $e^{i2\pi qk/L}$, where q is an integer, when introduced into the code, will also not affect the correlation.

Frank sequences are described by a matrix of the form [72]:

$$\begin{bmatrix} 1 & 2 & 3 & 4 & \cdots & L \\ 2 & 4 & 6 & 8 & & 2L \\ 3 & 6 & 9 & 12 & & 3L \\ 4 & 8 & 12 & 16 & & 4L \\ \vdots & & & & & \vdots \\ L & . & . & . & . & L^2 \end{bmatrix} \tag{2.3}$$

The matrix elements represent multiplying coefficients of a basic phase angle $2\pi p/L$, where $p, L > 0$ and p is relatively prime to L. Frank sequences are generated taking a row at a time.

Frank [76] reviewed previous work on polyphase complementary codes (Golay [77] and Sivaswamy [78]) and described various transformations on polyphase codes to preserve their complementary properties. For binary sequences - a) interchange sequences in pairs, b) negate one sequence of each pair and c) reverse the order of all sequences. For the polyphase case c) must be combined with complex conjugation. The number of mutually orthogonal sets cannot exceed the number of sequences in the set. Frank sequences exist in perfect square length only.

Popovic [79, 80] describes the large subclass of General Chirp-like (GCL) sequences which incorporate all the known different classes of polyphase sequences with ideal periodic autocorrelation and with minimum alphabets, such as generalised Frank sequences, Chu, Ipatov and Milewski sequences. GCL sequences belong to a class of modulatable orthogonal sequences [81]. For Frank sequences, the sequence length $L = m^2$, where m is the alphabet size (number of sequences). For Chu sequences of length L, the alphabet size is $L = s.m^2$ for s and m any positive integer. For Zadoff-Chu sequences of arbitrary length L the alphabet size is generally equal to $2L$. If it can be reduced for odd L to alphabet size L, it is called Ipatov sequences [79]. Milewski sequences [82] are of length $L = g^{2h+1}$ with alphabet size g^{h+1}, where g and h are any positive integers. A special case of Frank sequences is the Constant Amplitude Zero Auto-correlation (CAZAC) sequence of 1 1 1 -1. Zadoff-Chu sequences are defined as [83]

$$a_k = \begin{cases} e^{-i\frac{\pi Mk^2+2\pi qk}{L}} & k = 0,1,2,\ldots,L-1 \; for \; L \; even \\ e^{-i\frac{\pi Mk(k+1)+2\pi qk}{L}} & k = 0,1,2,\ldots,L-1 \; for \; L \; odd \end{cases} \tag{2.4}$$

Stańczak *et al.* [45] addressed the design of good spreading sequences with small-valued auto- and cross-correlation functions. The design was applied to two known unit-magnitude sequences: Binary Rudin-Shapiro sequences and sequences with quadratic phase function, which are similar to the well-known Frank-Zadoff-Chu (FZC) sequences [75]. These sequences have been extensively investigated in literature due to their excellent periodic correlation properties. An upper bound of $\sqrt{L+1}$ on the inverse merit factor was provided. Chu sequences however only provide the largest family of codes for a given length L, if L is a prime number.

Park *et al.* [84] suggested a new class of polyphase sequences, named Park-Park-Song-Suehiro (PS) sequences. The autocorrelation sequence is zero except at periodic intervals, and the cross-correlation between properly selected sequences is zero. It was shown that the performance of the system is independent of the number of users and offers better performance than PN sequences. The sequence is also ideal for Quasi-Synchronous CDMA (QS-CDMA) systems. PS sequences also do not suffer from the prime number limitation, as for Chu sequences.

Lu *et al.* [85] used Zadoff-Chu sequences to be able to support a large number of users and have perfect auto- and cross-correlation properties, similar to complete complementary codes. During the generation of the Zadoff-Chu sequences, only prime numbers are used for the separate sequences. It was found that polyphase sequences can be cyclically rotated, but that relatively prime sequences as 'seed' sequences are not mutually orthogonal, according to Popovic [79].

The cross-correlation of polyphase sequences are defined as [86]:

$$R_{l_p,l_q}[0] = \frac{1}{L}\sum_{k=0}^{L-1} g_L^{l_p}[k]\left(g_L^{l_q}[k]\right)^* = \begin{cases} 1 & l_p = l_q \\ 0 & l_p \neq l_q \end{cases} \tag{2.5}$$

Hu *et al.* [87] presented a genetic algorithm to numerically optimize the design of orthogonal code sets.

Tsai *et al.* [86] developed a systematic approach to construct variable spreading factor polyphase codes that exhibited better auto-and cross-correlation properties than Hadamard codes. OFDM-CDMA systems employing polyphase codes have better PAPR performance than those using Hadamard codes.

Pereira *et al.* [88] presented a method to generate a prime number L of perfect sequences with length L, which have one more perfect sequence than Chu polyphase sets, with the same maximum periodic cross-correlation value of $\sqrt{L}$.

2.3.1.6 Complementary codes (CC)

Complementary codes originated in the early 60s, when Welti [89] described quaternary codes whose autocorrelation consist of a single pulse. Each code can be paired to another code (its mate) in such a way that the cross-correlation of mates are identically zero. Lüke [90] presented construction methods of sets of two and higher dimensional Welti codes, which allows the construction of mutually orthogonal complementary codes in one or more dimensions.

Golay [77] and Turyn [91] first studied binary complementary codes whose autocorrelation function is zero for all even shifts except the zero shift [92]. When the cross-correlation is considered, it is not zero. Golay complementary pairs are only available in lengths of $K.2^k$, where $k \in \mathbb{N}_0$ and K is the kernel length given by 2,10 and 26 [77, 93].

Sivaswamy [78] introduced multiphase complementary codes, based on work by Golay.

Suehiro *et al.* [81] investigated N-shift cross-orthogonal sequences, a class of binary codes whose elements are either 1 of -1, with autocorrelation of zero for all even and odd shifts, except the zero shift. These sequences have the properties of complementary codes, meaning that the sum of the autocorrelation of a pair of binary codes is also zero. Furthermore, the cross-correlation for any pair of sequences is zero for all possible shifts [92]. These codes were proposed for a synchronous multi-user system, resulting in no crosstalk, and no distortion from autocorrelation sidelobes or signal non-periodicity. The concept of complementary codes was extended by Tseng *et al.* [94], Sivaswamy [78] and Frank [76].

Bömer *et al.* [95] presented properties, existence conditions and recursive construction procedures for sets of periodic complementary binary sequences. Two or more sequences are called a set of periodic complementary binary sequences if the sum of their respective autocorrelation functions is a delta function. A periodic complementary sequence may alternatively be defined by a two-dimensional periodic autocorrelation function of a binary array, which can be used in time-frequency-coding applications (Golomb *et al.* [96]).

Huang *et al.* [97,98] presented polyphase scalable complete complementary sequences by transforming Golay-paired Hadamard matrices to polyphase ones. Starting from a 2x2 polyphase Golay-paired

matrix, as shown in Equation (2.6) and a recursive construction formula, shown in Equation (2.7), the Golay-paired matrix $\mathbf{H}_N$ of order $N = 2^n$ can be derived. w_n ($n \geq 0$) are arbitrary polyphase elements satisfying $|w_n|$=0 and $\tilde{\mathbf{H}}_{2^n}$ is the equivalent matrix obtained by exchanging the upper and lower half of $\mathbf{H}_{2^n}$.

$$\mathbf{H}_2 = \begin{bmatrix} 1 & w_0 \\ 1 & -w_0 \end{bmatrix} \tag{2.6}$$

$$\mathbf{H}_{2^{n+1}} = \begin{bmatrix} \mathbf{H}_{2^n} & w_n\tilde{\mathbf{H}}_{2^n} \\ \mathbf{H}_{2^n} & -w_n\tilde{\mathbf{H}}_{2^n} \end{bmatrix} \tag{2.7}$$

Chen *et al.* [99] showed that the processing gain of CC codes is equal to the congregated length of the flock of element codes. Every CC code is divided into several segments (called element codes) which should be transmitted in different frequency channels. Zero cross-correlation and zero out-of-phase autocorrelation are ensured for any relative shift between two codes. The system showed excellent orthogonality among codes even in asynchronous conditions. Using orthogonal subcarriers, spaced $1/T_c$ (where T_c denotes the chip duration), different element codes can be send separately to further enhance bandwidth efficiency. A dedicated pilot signal should be added to the system. They used an 'offset stacked' spreading method, which inherently supports multiple data rates with the same processing gain. Due to the summation of spreaded signals, a multilevel $(L+1)$-QAM modem is required for element code length L.

Matsufuji *et al.* [100] discussed complementary arrays and their construction. Complementary arrays can be constructed by interchanging, inversion and interleaving of complementary arrays, similar to guidelines for complementary sequences as presented by Golay [77].

Tu *et al.* [101] proposed a generating function based on XOR and AND operations for generating a Hadamard matrix of order 2^n as well as complementary sequence sets, based on Suehiro's method [81]. The following conditions were lacking from Tu:

1. The condition for orthogonality, i.e. $A_n.A_n^T = I_n$;
2. ensuring *mutually* orthogonal complementary sets based on the periodic autocorrelation function between complementary sets.

In their paper, Tu *et al.* describe the generation of a Hadamard matrix of order 2^n by using a generating function $f(\overrightarrow{x}, \overrightarrow{y})$ to produce

$$\mathbf{H}_{2n} = \left[(-1)^{f(\overrightarrow{x},\overrightarrow{y})}\right] \tag{2.8}$$

where x and y denote the column and row index of $\mathbf{H}$ respectively. $f(\overrightarrow{x}, \overrightarrow{y})$ is a generating function expressed as:

$$f(\overrightarrow{x}, \overrightarrow{y}) = \sum_{k=0}^{n-1} (x_{i_k} \cdot y_k \oplus u_k \cdot x_k \oplus v_k \cdot y_k) \oplus w \tag{2.9}$$

where $\cdot$ denotes binary AND and $\oplus$ denotes binary XOR. The row vector $\mathbf{i} = (i_o, i_1, \ldots, i_{n-1})$ is any permutation of sequence $(0, 1, \ldots, n-1)$, $\{u_k, v_k; 0 \leq k \leq n-1\} \in \{0,1\}$ and $w \in \{0,1\}$.

For any generated Hadamard matrix to be orthogonal,

$$\mathbf{H}_{2n}.\mathbf{H}_{2n}^T = N.\mathbf{I}_N \tag{2.10}$$

where $\mathbf{I}_N$ is the identity matrix of order $N = 2^n$.

Example:

For $i_0, i_1, u_0, u_1, v_0, v_i, w$=0, the following matrix is generated:

$$H_4 = \begin{bmatrix} 1 & 1 & 1 & 1 \\ 1 & 1 & -1 & -1 \\ 1 & 1 & -1 & -1 \\ 1 & 1 & 1 & 1 \end{bmatrix}$$

Applying Eq. (2.10):

$$H_4.H_4^T = \begin{bmatrix} 4 & 0 & 0 & 4 \\ 0 & 4 & 4 & 0 \\ 0 & 4 & 4 & 0 \\ 4 & 0 & 0 & 4 \end{bmatrix}$$

which is not orthogonal.

In order for two or more Hadamard matrices of order 2^n to be mutually orthogonal,

$$PAC = \sum_{m=1}^{N} \mathcal{F}^{-1}\left\{\mathcal{F}\{\mathbf{H}_a(m,:)\}.(\mathcal{F}\{\mathbf{H}_a(m,:)\})^*\right\} = [N^2, 0_{N-1}] \tag{2.11}$$

and

$$PCC = \sum_{m=1}^{N} \mathcal{F}^{-1}\left\{\mathcal{F}\{\mathbf{H}_a(m,:)\}.(\mathcal{F}\{\mathbf{H}_b(m,:)\})^*\right\} = [0_N] \tag{2.12}$$

where *PAC* is the periodic autocorrelation function, *PCC* is the periodic cross-correlation function, $\mathcal{F}^{-1}$ is the inverse fast Fourier transform, $\mathcal{F}$ is the fast Fourier transform, m is the m-th row of $\mathbf{H}_a$ and $\mathbf{H}_b$, $()^*$ is the complex conjugate and 0_{N-1} is a row vector of $N-1$ zeros. $N = 2^n$ is the order of the matrices $\mathbf{H}_a$ and $\mathbf{H}_b$. In general $b \leq a$, and $\mathbf{H}_a$ and $\mathbf{H}_b$ will be a set of matrices generated using Eqns. (2.8) and (2.9).

Doing an exhaustive search, the following mutually orthogonal matrices sets are found for n=2 (N=4):

$$\mathbf{H}_{4A} = \begin{bmatrix} 1 & 1 & 1 & 1 \\ 1 & 1 & -1 & -1 \\ 1 & -1 & 1 & -1 \\ 1 & -1 & -1 & 1 \end{bmatrix} \quad \mathbf{H}_{4B} = \begin{bmatrix} 1 & 1 & -1 & -1 \\ 1 & 1 & 1 & 1 \\ 1 & -1 & -1 & 1 \\ 1 & -1 & 1 & -1 \end{bmatrix}$$

$$\mathbf{H}_{4C} = \begin{bmatrix} 1 & -1 & 1 & -1 \\ 1 & -1 & -1 & 1 \\ 1 & 1 & 1 & 1 \\ 1 & 1 & -1 & -1 \end{bmatrix} \quad \mathbf{H_{4D}} = \begin{bmatrix} 1 & -1 & -1 & 1 \\ 1 & -1 & 1 & -1 \\ 1 & 1 & -1 & -1 \\ 1 & 1 & 1 & 1 \end{bmatrix}$$

The four matrices can be generated using Eqns. (2.8) and (2.9) with the following values for **i**, **u**, **v** and w:

Matrix	**i**	**u**	**v**	w
H_{4A}	[0 1]	[0 0]	[0 0]	0
H_{4B}	[0 1]	[0 1]	[0 0]	0
H_{4C}	[0 1]	[1 0]	[0 0]	0
H_{4D}	[0 1]	[1 1]	[0 0]	0

Other four matrix sets can be obtained by following Golay's rules for complementary series [77], or as described by Matsufuji *et al.* [100] for complementary arrays. These include:

1. Interchanging corresponding rows of mutually orthogonal arrays;
2. Reversing corresponding rows of mutually orthogonal arrays;
3. Altering corresponding rows of mutually orthogonal arrays.

It should be noted that different four matrix sets are not necessarily mutually orthogonal between matrices of the different sets. For example, interchanging rows 2 and 3 for $\mathbf{H}_{4A,4B,4C,4D}$ leads to:

$$\mathbf{H_{4E}} = \begin{bmatrix} 1 & 1 & 1 & 1 \\ 1 & -1 & 1 & -1 \\ 1 & 1 & -1 & -1 \\ 1 & -1 & -1 & 1 \end{bmatrix} \quad \mathbf{H_{4F}} = \begin{bmatrix} 1 & 1 & -1 & -1 \\ 1 & -1 & -1 & 1 \\ 1 & 1 & 1 & 1 \\ 1 & -1 & 1 & -1 \end{bmatrix}$$

$$\mathbf{H_{4G}} = \begin{bmatrix} 1 & -1 & 1 & -1 \\ 1 & 1 & 1 & 1 \\ 1 & -1 & -1 & 1 \\ 1 & 1 & -1 & -1 \end{bmatrix} \quad \mathbf{H_{4H}} = \begin{bmatrix} 1 & -1 & -1 & 1 \\ 1 & 1 & -1 & -1 \\ 1 & -1 & 1 & -1 \\ 1 & 1 & 1 & 1 \end{bmatrix}$$

where

$$PCC_{4A,4E} = [0\ 8\ 0\ 8]$$

which is not perfect.

Long *et al.* [102] mentioned that CCC can also be used for channel estimation, synchronization, reduction of PAPR, preamble design, sequence design and target detection (RADAR).

Zeng *et al.* [103] discussed two dimensional complementary array sets, where the number and sizes of sub-arrays can be changed.

Zhou *et al.* [93] showed that no component-sequence-balanced Golay complementary pairs exist, but that whole-sequence-balanced Golay complementary pairs exist. Primitive Golay complementary pairs are known for lengths 2, 10 and 26, which are used to construct pairs of other lengths. A Golay complementary pair exist *iff* $L_c = 2^a 10^b 26^c, a, b, c \in \mathbb{Z}$. For $L_c \leq 1000$, the admissible lengths for whole-sequence-balanced Golay complementary pairs are 4, 16, 64, 100, 256, 400 and 676.

2.3.1.7 Complete Complementary codes (CCC)

Complete complementary codes were suggested by Suehiro *et al.* [81], in which the concept of complementary codes was extended to the generation of the complete complementary code families

whose auto-correlation function is zero for all even and odd shifts except the zero shift and whose cross-correlation function for any combination of two sequences is zero for all possible shifts. It should be noted that, unlike complementary codes, complete complementary codes are ideal orthogonal codes, whose auto-correlation function for any one code and cross-correlation function between any two codes are perfect even in asynchronous transmissions. CCC is very much different from Walsh-Hadamard codes or OVSF codes, whose orthogonality does not exist if they are used in asynchronous transmission channels [104].

Torii *et al.* [105] showed the construction of periodic complete complementary codes composed of expanded modulatable orthogonal sequences of period N^2.

Farkaš *et al.* [106, 107] constructed a new family of two- and three-dimensional orthogonal CCCs (2D-OCCC and 3D-OCCC) based on the original one dimensional CCCs. Both retain auto-correlation and cross-correlation properties for every 2D and 3D shifts respectively in every direction. Set size and element's size are both directly dependent on the maximum number of users K. 3D-OCCC may be useful for Space-Time-Frequency-coding.

Švač *et al.* [42] presented a new class of complete complementary codes named variable two-shift auto complementary sets. The proposed class of CC codes can support a larger number of users than CC codes and show greater flexibility for resource allocation, while keeping ideal aperiodic auto- and cross-correlation functions.

From Chen [104] the cross-correlation $\rho(\mathbf{S}_1, \mathbf{S}_2; i)$ between sequences $\mathbf{S}_1$ and $\mathbf{S}_2$ with the i-th chip shift is defined as:

$$\rho(\mathbf{S}, i) \equiv \begin{cases} \frac{1}{L} \sum_{j=1}^{L-i} s_{1,j} s_{2,j+i}^* & i = 0, 1, \ldots, L-1 \\ \frac{1}{L} \sum_{j=1-i}^{L} s_{1,j} s_{2,j+i}^* & i = -1, \ldots, -L+1 \end{cases} \tag{2.13}$$

where $()^*$ is the complex conjugate operation, $\mathbf{S}_n = (s_{n,1}, \ldots, s_{n,L_e})$ and L_e is the element code length. M sets of M sequences $\{S_{1,1}, \ldots, S_{1,M}\}, \ldots, \{S_{M,1}, \ldots, S_{M,M}\}$ are called a complete complementary code of order M if every set is an auto-complementary code and every pair of distinct sets chosen from

the M sets are a cross-complementary code, or

$$\begin{cases} \sum_{j=1}^{M} \rho(\mathbf{S}_{k,j};\, i) = 0 & i \neq 0;\; k \;=\; 1,\ldots,\, M \\ \sum_{j=1}^{M} \rho(\mathbf{S}_{k,j}, \mathbf{S}_{i,j};\, i) = 0 & for\ any\ i;\; k,l \;=\; 1,\ldots,M;\; k \neq l \end{cases} \tag{2.14}$$

The auto-correlation function and cross-correlation function of complete complementary codes are defined based on the element codes (or flocks), which will be assigned to a user for CDMA. Each flock here consists of M element codes, which should be used jointly, instead of individually as is the case for all traditional CDMA systems.

The major problem with complete complementary codes is their small set-size, or parameter K. The set size (number of flocks) of a complementary code set is always equal to the flock size (number of element codes in one flock) and is $K = M = \sqrt{L_e}$. The processing gain (PG) of CCC is equal to $L_e\sqrt{L_e}$, where L_e is the length of the element code. In order to increase the set size to support more users in a CDMA system based on complementary codes, extended complementary codes were introduced by Suehiro *et al.* [81].

2.3.1.8 Extension of sequences

Lu *et al.* [85] have shown that the number of users supported by CC codes is limited, due to the relatively small family size. Zadoff-Chu sequences were proposed to extend CC codes, referred to as Extended Orthogonal (EO) Polyphase codes. More importantly, the extension was based on orthogonal design and that the number of EO users that can be supported is equivalent to the order (or the number of rows) of the orthogonal matrix.

Gerakoulis *et al.* [108] presented a method to generate orthogonal codes by using Kronecker matrix products, called EO codes. These are used to construct concatenated orthogonal sequences. Examples of PN-sequences, Walsh-Hadamard and Quaternion codes, Complex orthogonal and the Polyphase Orthogonal Matrix (POM), as well as their extension, were shown.

It should be noted that extended complementary codes will not support more users in the same CDMA system.

2.3.1.9 Super Orthogonal Complete Complementary (SOCC) codes

Super orthogonal complete complementary codes were proposed by Chen [104] to overcome several problems of CCC and extended CC, as listed below:

- To maintain a sufficiently large set size, both CCC and extended CC have to use very long element codes.
- The use of very long element codes will also make it very difficult to increase the data transmission rate with a fixed signal processing power. With the increase of data rate, the bit duration will be substantially reduced, thus making the chip width even shorter.
- For CCC the ratio between the flock size (or the set size) and element code length L_e is a fixed number, equal to $\frac{\sqrt{L_e}}{L_e}$. There is no way to change this ratio. All ideally orthogonal complementary codes have the property that their set size (K) is always equal to their flock size (M). Therefore, if we can make the flock size larger, we can increase the set size as well, to support more users. Unfortunately, the rigid ratio between the flock size and element code length makes it impossible to increase the set size under a fixed processing gain, which is equal to the product of flock size and element code length ($M.L_e$).

Super complementary codes have the superior property that their set size can reach its maximal value, being equal to the processing gain of the super complementary codes.

2.3.2 MC-CDMA

Tulino *et al.* [109] analyzed the spectral efficiency of random spread synchronous multi-carrier CDMA for uplink and downlink, either conditioned on the subcarrier fading coefficient or unconditioned thereon. Jointly optimized, MMSE, decorrelator and single-user matched filter receivers were considered. The conditioned spectral efficiency has been shown to converge asymptotically in the number of users and subcarriers to an expression that depends on the empirical instantaneous fading profile across subcarriers.

2.3.3 Time and frequency spreading

Yang *et al.* [110] provided a comparative discussion in terms of the characteristics of the three typical CDMA schemes: SC DS-CDMA, MC-CDMA and MC DS-CDMA (also known as T-F-Spreading). The MC-DS-CDMA system uses DS-based time-domain spreading to increase the processing gain associated with each subcarrier signal, together with the frequency domain spreading across several subcarriers to further increase the total attainable processing gain.

Zhao *et al.* [111] derived a general formula (lower bound) for the complementary cumulative distribution function (CCDF) of the PAPR of an MC-DS-CDMA signal.

2.4 CHAPTER SUMMARY

In this chapter an overview of applicable background literature were provided. In Section 2.1 a high level overview of DSL as an access technology was provided. In Section 2.2 an overview of MC-CDMA was provided, as well as the reasons for using MC-CDMA for the GDSL design. In Section 2.3 an overview of different spreading codes were provided.

It is very important to note that a set of sequences with good autocorrelation (strong autocorrelation peak), no cross-correlation between sequences, and a large number of sequences within a family of a certain length L are required for MUI-free communication. Codes should also have good *periodic* properties, since they will be implemented in a block format (Resource Blocks). Orthogonal complementary codes also have very good partial correlation properties, which make them very suitable to reduce MAI and MI when they are used in a CDMA system that supports high-speed bursty type [112]. Complete complementary codes have ideal auto-correlation functions and cross-correlation functions regardless of the transmission mode. That is to say, their ideal auto-correlation functions and cross-correlation functions should be ensured in both synchronous and asynchronous transmission channels [112]. Thus, although some orthogonal sequences have good correlation properties, SOCC spreading sequences meet all requirements stated above, for both synchronous and asynchronous transmission between users.

CHAPTER 3 CHANNEL MODELLING

3.1 CHAPTER OVERVIEW

Gigabit DSL is envisioned to operate over up to a 200 m length of 0.5 mm diameter copper wire. The modelling of copper wire have been studied in great detail [113]. In this chapter the system - and channel capacity is described in Section 3.2. The channel impulse response and cyclic extension is described in Section 3.3. In DSL systems a SNR margin is added, as described in Section 3.4. To obtain an insertion loss model for any line topology encountered in practice, a simulation channel model can be determined. Primary and secondary parameters are the main variables which can be measured and calculated, as described in Section 3.5. These parameters are used to obtain a two-port network model (ABCD matrix) for the line, as described in Section 3.6. Sections 3.7 and 3.8 describe the noise and crosstalk impairments encountered in the GDSL environment, which will be extensively used in the simulation. The transmit and receive filters are explained in Section 3.9 and the PSDs under channel conditions are discussed in Section 3.10.

3.2 CHANNEL AND SYSTEM CAPACITY

The channel characteristics of DSL systems depend on the frequency, f, while the channel is sampled using a tone spacing Δf which is usually a multiple of 4.3125 kHz. In order to determine a protocol-independent channel capacity C as a function of the copper loop length l (which affects the channel attenuation profile H_{ins}), the bandwidth B (in Hz) and the dynamic range α (defined as the ratio between the signal level at the transmitter and the noise level at the receiver), is given by [32]:

$$C = \Delta f \sum_{n=1}^{N} \log_2 \left(1 + \alpha \left| H_{ins}(n.\Delta f + \tfrac{\Delta f}{2}) \right|^2 \right) \tag{3.1}$$

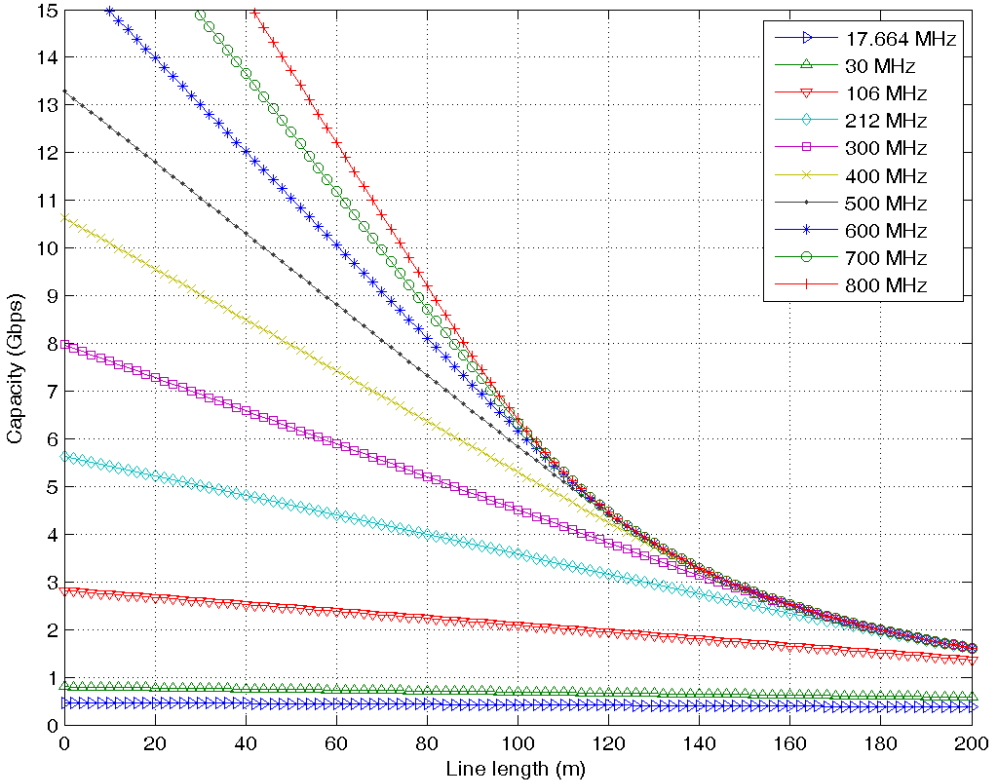

Figure 3.1. Protocol-independent capacity vs line length for a 0.5 mm twisted-pair for different system bandwidths.

where Δf is the subchannel spacing (Hz), $\left|H_{ins}(n.\Delta f + \frac{\Delta f}{2})\right|^2$ is the channel attenuation at frequency $n.\Delta f + \frac{\Delta f}{2}$, $n \in \{0,1,2,...,N-1\}$ is the subchannel index and $N = B/\Delta f$ is the total number of subchannels. The protocol-independent capacity of a 0.5 mm twisted-pair cable vs. line length, with a 80 dB dynamic range, is shown in Figure 3.1 [32]. With an additional SNR margin of 10 dB, and a bandwidth B = 17.664 MHz, the capacity for a 200 m length 0.5 mm diameter line is slightly above 300 Mbps, while for B = 100 MHz or greater the capacity is just above 1 Gbps. The benefit of increasing the signal bandwidth rapidly declines with the line length. Large bandwidth requirements are expected to reduce the achievable dynamic range due to hardware limitations.

The objective is to design a GDSL modem operating at 1 Gigabit per second (1 Gbps). SNR_{index} is defined as:

$$SNR_{index} = \|2.(SNR_{measured} - \Gamma + 32)\| \tag{3.2}$$

where $SNR_{measured}$ is the measured SNR of the channel (in dB), Γ is the SNR margin (in dB) and $\|\cdot\|$

is the nearest integer function. SNR_{index} is then limited to between 0 and 254 (10-bit unsigned integer). $SNR_{indexed}$ is then calculated as:

$$SNR_{indexed} = -32 + SNR_{index}/2; \tag{3.3}$$

Based on $SNR_{indexed}$, the bits allocated per subchannel n, $n \in \{0...4095\}$, as used by existing DSL systems, is calculated as:

$$b_n = \log_2(1 + SNR_{indexed}) \tag{3.4}$$

$$= \log_2(1 + \frac{SNR_{measured}}{\Gamma}) \tag{3.5}$$

The system capacity (throughput in Mbps) was calculated as:

$$C = \sum_{n=0}^{N-1} 0.9 \cdot b_n \cdot \Delta f \tag{3.6}$$

$$= \sum_{n=0}^{N-1} 0.9 \cdot b_n \cdot 0.051750 \tag{3.7}$$

where N is the total number of subchannels, the factor of 0.9 assumes that only 90% of the subchannel bandwidth is used (other 10% for overheads) and 0.051750 is the subcarrier spacing in MHz.

3.3 CHANNEL IMPULSE RESPONSE AND CYCLIC PREFIX

The channel impulse response as a function of line length is shown in Figure 3.2. For the maximum line length of 200 m, the time dispersion t_{CP} will be around 0.94 μs. In typical systems, in order to combat inter-symbol-interference (ISI), a guard band or cyclic-prefix (CP) should be included. The number of samples L_{CP} to be added is related to t_{CP} by:

$$t_{CP} = \frac{1}{T'}.L_{CP} \tag{3.8}$$

where $1/T'$ is the sampling frequency (211.968 MHz) and L_{CP} is the number of samples used for the cyclic prefix. L_{CP} is 200 samples (4.9% of the total 4096 symbols). The transmit symbols is constructed from the IFFT samples $x(n)$ by prepending the last L_{CP} samples of the IFFT output $x(n)$ to the $2N$ output IFFT samples $x(n)$ as the cyclic prefix (CP). At the receiver, the cyclic prefix is removed before decoding.

Chen [104] proved that SOCC codes do not need cyclic prefixing in order to ensure MUI-free communication for either periodic (synchronous) of aperiodic (asynchronous) transmission. Thus no cyclic

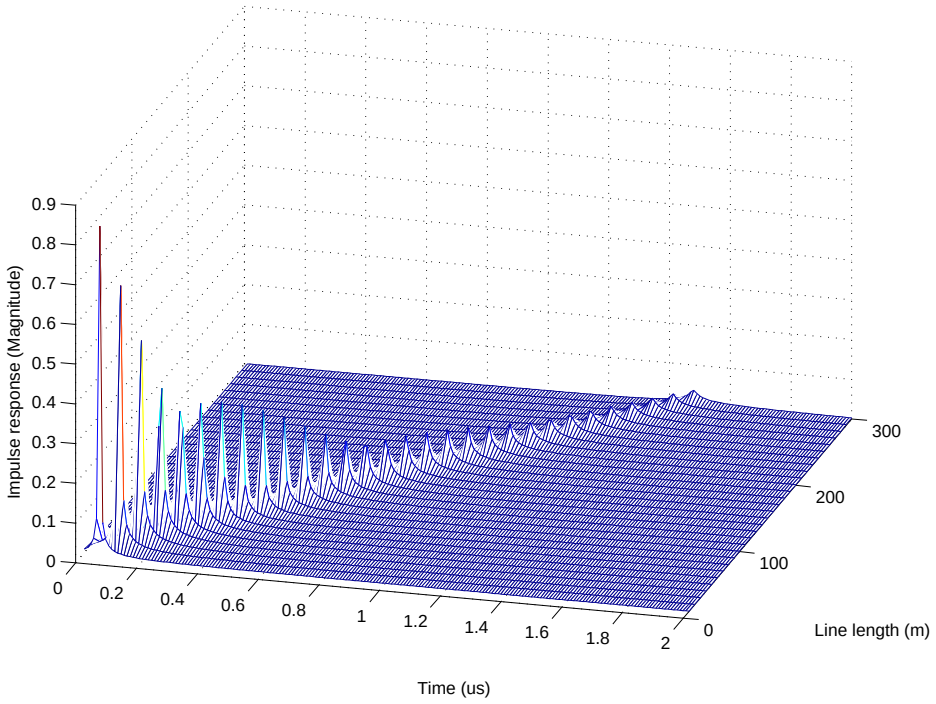

Figure 3.2. Channel impulse response vs. line length.

prefix is added for similar OFDM blocks (an upstream / downstream FFT block). However, to combat interference between downstream and upstream transmission using TDD, a guard band or cyclic-prefix can be added to the last OFDM block sent in each direction for added protection.

3.4 SIGNAL TO NOISE (SNR) MARGIN

DSLs are designed with a 9.8 dB SNR margin, which will provide a 10^{-7} target bit error rate (BER) when the crosstalk signal power is 9.8 dB higher than the defined worst-case crosstalk model. For uncoded QAM systems the SNR gap at 10^{-7} BER is 10 dB [114]. The SNR margin provides for cable variations (aging, splices and wet cables), additional noise in CO and customer premises wiring, other noise sources, imperfect transceiver designs and manufacturing variations. The SNR margin is defined as the difference between the measured SNR of the channel (including background noise and other interference) and the SNR profile that is used by the system [24, 115].

3.5 RLCG MODELS

Twisted-pair local loops are characterized by their primary parameters, R_l (resistance), C_l (capacitance), L (inductance) and G (conductance). These parameters vary with frequency for different cable types and wire gauges. According to Annexure C of the ANSI T1.413-2003 standard [23], G is assumed zero, C_l is a constant for all frequencies, and the variation of R_l and L with frequency can be accurately modelled as:

$$R_l = \sqrt[4]{roc^4 + ac.f^2} \tag{3.9}$$

$$L = \frac{l_o + l_\infty.\left(\frac{f}{f_m}\right)^{b_L}}{1 + \left(\frac{f}{f_m}\right)^{b_L}} \tag{3.10}$$

where R_l is the resistance of the line [Ω/km] at a specific frequency f [Hz], roc is the copper DC resistance [Ω/km] and ac a constant characterizing the rise of resistance with frequency due to the "skin effect". L is the inductance of the line [H/km] at a specific frequency f [Hz], l_o and l_∞ are the low-frequency and high-frequency inductances [H/km] respectively, b_L is chosen to characterize the transition between low and high frequencies in the measured inductance values and f_m is in Hz [23, 24].

Several types of copper wire used in the main network have been characterized in terms of these parameters, as shown in Table 3.1 [23, 24] for frequencies up to 30 MHz. In this study the parameters were also used for frequencies above 30 MHz. A submission to the ITU Study Group 15 [116] showed that the extended models (above 30 MHz) show similarities to the existing models (up to 30 MHz). The resistance R_l vs. frequency f, using Equation (3.9), is shown in Figure 3.3 and the inductance L vs. frequency f, using Equation (3.10), in Figure 3.4. The twisted-pair secondary parameters can be expressed as:

$$Z_o = \sqrt{\frac{R_l + j\omega.L}{G + j\omega.C_l}} \tag{3.11}$$

$$\gamma = \sqrt{(R_l + j\omega.L)(G + j\omega.C_l)} \tag{3.12}$$

where $\omega = 2\pi f$, Z_o is the characteristic impedance and γ is the propagation constant of the twisted-pair at a specific frequency f [24, 117]. The characteristic impedance Z_o vs. frequency f is shown in Figure

Table 3.1. Cable parameters for different wire types (up to 30MHz).

Wire Type	roc (Ω/km)	ac	l_o (H/km)	l_∞ (H/km)	f_m (Hz)	b_L	C_l(F/km)
0.32mm	$0.4090 \cdot 10^3$	0.3822	$0.6075 \cdot 10^{-3}$	$0.5000 \cdot 10^{-3}$	$0.6090 \cdot 10^6$	5.2690	$40 \cdot 10^{-9}$
0.4mm	$0.2800 \cdot 10^3$	0.0969	$0.5873 \cdot 10^{-3}$	$0.4260 \cdot 10^{-3}$	$0.7459 \cdot 10^6$	1.3850	$49 \cdot 10^{-9}$
0.5mm	$0.1792 \cdot 10^3$	0.0561	$0.6746 \cdot 10^{-3}$	$0.5327 \cdot 10^{-3}$	$0.6647 \cdot 10^6$	1.1950	$50 \cdot 10^{-9}$
0.63mm	$0.1130 \cdot 10^3$	0.0257	$0.6994 \cdot 10^{-3}$	$0.4772 \cdot 10^{-3}$	$0.2658 \cdot 10^6$	1.0956	$45 \cdot 10^{-9}$
0.9mm	$0.0551 \cdot 10^3$	0.0090	$0.7509 \cdot 10^{-3}$	$0.5205 \cdot 10^{-3}$	$0.1238 \cdot 10^6$	0.9604	$40 \cdot 10^{-9}$
Dropwire 10"	$0.1809 \cdot 10^3$	0.0497	$0.7289 \cdot 10^{-3}$	$0.5434 \cdot 10^{-3}$	$0.7189 \cdot 10^6$	0.7558	$51 \cdot 10^{-9}$
Flat pair	$0.0412 \cdot 10^3$	0.0001	$1.0000 \cdot 10^{-3}$	$0.9110 \cdot 10^{-3}$	$0.1742 \cdot 10^6$	1.1950	$22.68 \cdot 10^{-9}$
UTP Cat.5	$0.1766 \cdot 10^3$	0.0500	$1.0908 \cdot 10^{-3}$	$0.5045 \cdot 10^{-3}$	$0.0326 \cdot 10^6$	0.7050	$48.55 \cdot 10^{-9}$

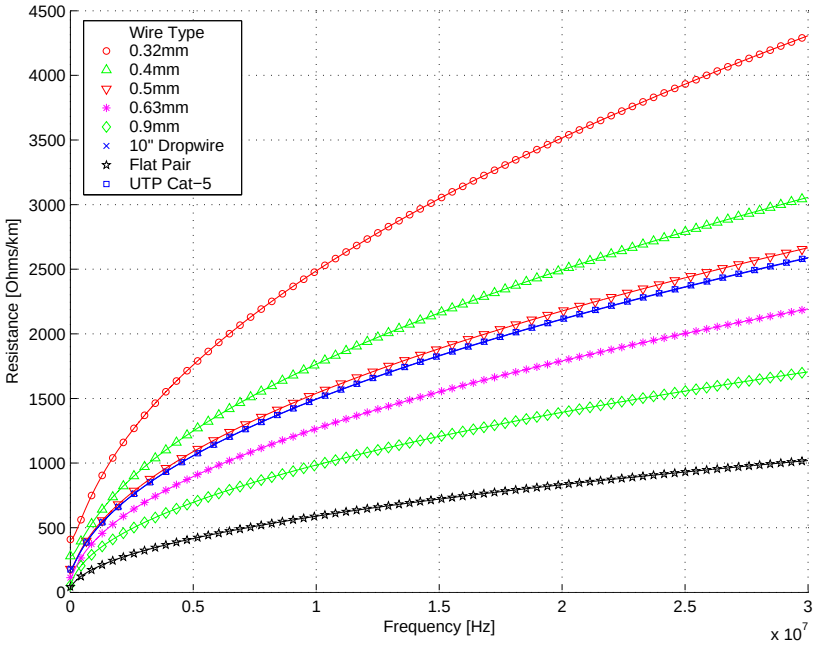

Figure 3.3. Resistance vs. frequency.

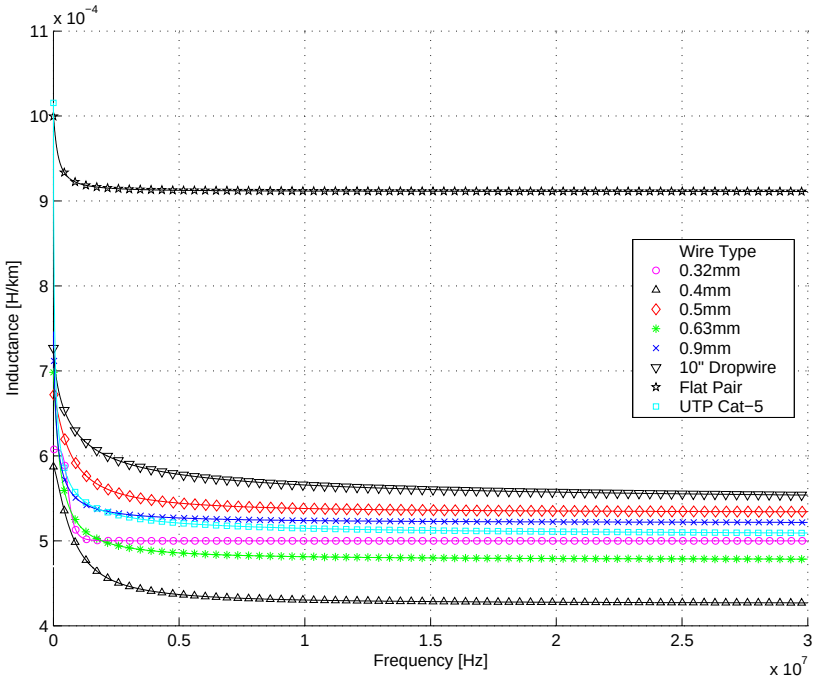

Figure 3.4. Inductance vs. frequency.

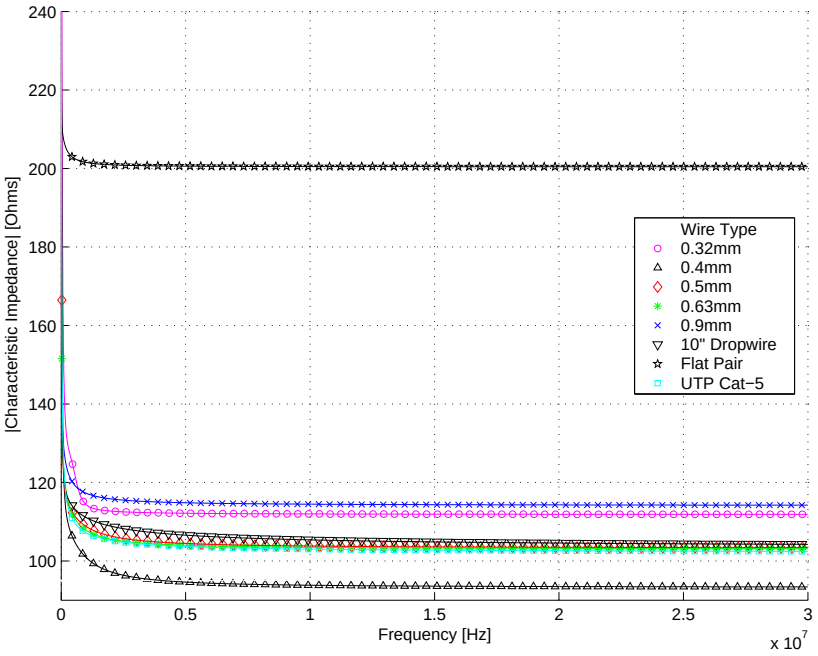

Figure 3.5. Characteristic Impedance vs. frequency.

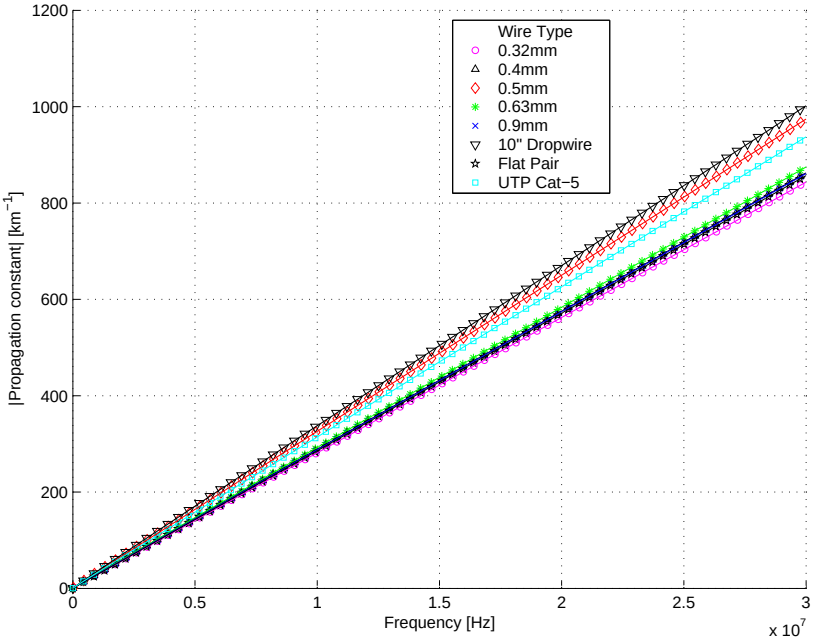

Figure 3.6. Propagation constant vs. frequency.

3.5 using Equation (3.11) and the propagation constant γ vs. frequency f in Figure 3.6 using Equation (3.12). Figures 3.3-3.6 should look similar to [24, 117].

3.6 TWO-PORT NETWORKS AND ABCD PARAMETERS

Local loops usually consist of several sections of cable with different lengths and wire gauges, with or without bridged taps, and terminated with resistive impedance. Two-port networks, and specifically ABCD matrixes can be used to represent each segment or section of a line. By multiplying the ABCD matrixes of each segment, an ABCD matrix is obtained which represents the complete line.

For a series impedance Z_{ser}, the ABCD matrix is:

$$\begin{bmatrix} A & B \\ C & D \end{bmatrix} = \begin{bmatrix} 1 & Z_{ser} \\ 0 & 1 \end{bmatrix} \tag{3.13}$$

For a shunt impedance Z_{par}, the ABCD matrix is:

$$\begin{bmatrix} A & B \\ C & D \end{bmatrix} = \begin{bmatrix} 1 & 0 \\ Z_{par}^{-1} & 1 \end{bmatrix} \tag{3.14}$$

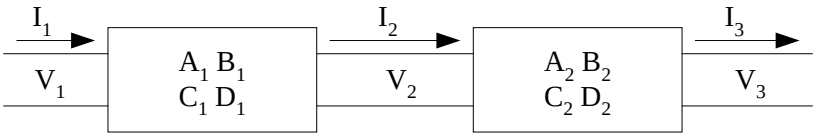

Figure 3.7. Two-port networks in series.

For two-port networks in series, shown in Figure 3.7, the ABCD matrix is:

$$\begin{bmatrix} A & B \\ C & D \end{bmatrix} = \begin{bmatrix} A_1A_2 + B_1C_2 & A_1B_2 + B_1D_2 \\ C_1A_2 + D_1C_2 & C_1B_2 + D_1D_2 \end{bmatrix} \tag{3.15}$$

Bridged taps are open-circuited twisted pairs, which are connected in shunt with working twisted pairs. Bridged taps create reflections of the main signal which affect both the transmitter and the receiver [117, 118]. For GDSL, bridged taps should be totally avoided, as it creates notches in the spectrum - any unnecessary impairment(s) should be removed as far as possible. The ABCD parameters are related to the characteristic impedance Z_o and propagation constant γ as follows:

$$A = D = \cosh(\gamma.l) \tag{3.16}$$

$$B = Z_o.\sinh(\gamma.l) \tag{3.17}$$

$$C = \frac{1}{Z_o}.\sinh(\gamma.l) \tag{3.18}$$

where l is the length [km] of the line segment under consideration [119].

The insertion loss function (also referred to as "Linear Channel Attenuation") of the twisted-pair loop with source impedance Z_s and terminal impedance Z_t is [24, 119]:

$$H_{ins}(f) = Hlin(f) = \frac{Z_s + Z_t}{A.Z_t + B + C.Z_s.Z_t + D.Z_s} \tag{3.19}$$

The attenuation through the cable, in [dB], is expressed as [119]:

$$\begin{aligned} L_{att}(f) = Hlog(f) &= 10.log_{10}|\,H_{ins}(f)\,|^2(dB) \\ &= 20.log_{10}\,|\,H_{ins}(f)\,|\,(dB) \end{aligned} \tag{3.20}$$

where $|\cdot|$ is the absolute value of $H_{ins}(f)$. The channel attenuation, as a function of frequency and line length, is shown in Figure 3.8. A comparison between the Channel attenuation (dB) vs. frequency

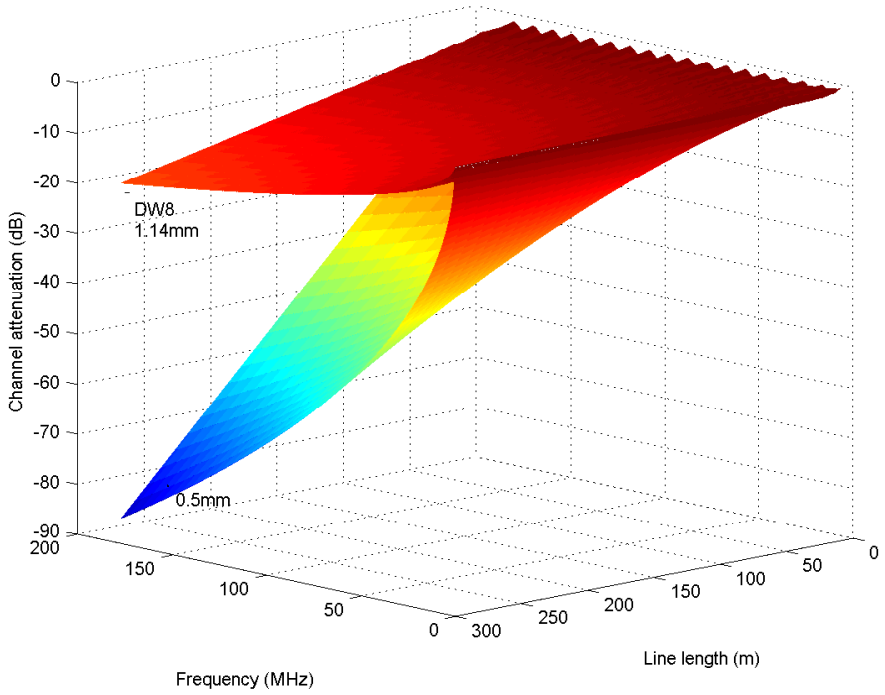

Figure 3.8. Channel attenuation vs. frequency and line length.

(kHz) for 100 m, 200 m and 300 m lengths respectively of 0.5 mm diameter twisted-pair wire is shown in Figure 3.9.

Following the guidelines as specified in G.993.1 [6], the Gigabit Terminal Units (GTUs), $Hlog(f)$ is measured by the GTU-R during the loop diagnostic mode and initialization. The measurement is updated during `Showtime`. `Showtime` is the normal operational state for DSL modems, during which data is transferred, in contrast to the `Idle` or `Init` states [120]. $Hlog(f)$ is sent to the GTU-C during the loop diagnostic mode and is sent on request to the GTU-C any time. In loop diagnostic mode, both $Hlin(f)$ and $Hlog(f)$ is measured, because the corrections that can be done, relative to the receiver and/or transmitter filter characteristics with $Hlin(f)$ and $Hlog(f)$, may differ. $Hlin(f)$ and $Hlog(f)$ is measured over either 1 ms, 10 ms, 100 ms or 1 s time period in loop diagnostic mode. The value of $Hlog(f)$ is represented using a granularity of 0.1 dB and an $Hlog(f)$ dynamic range of approximately 102 dB (+6 dB to -96 dB). $m(n)$ is defined as:

$$m(n) = \left\| ((6 - Hins_{(dB)}(n)).10) \right\| \tag{3.21}$$

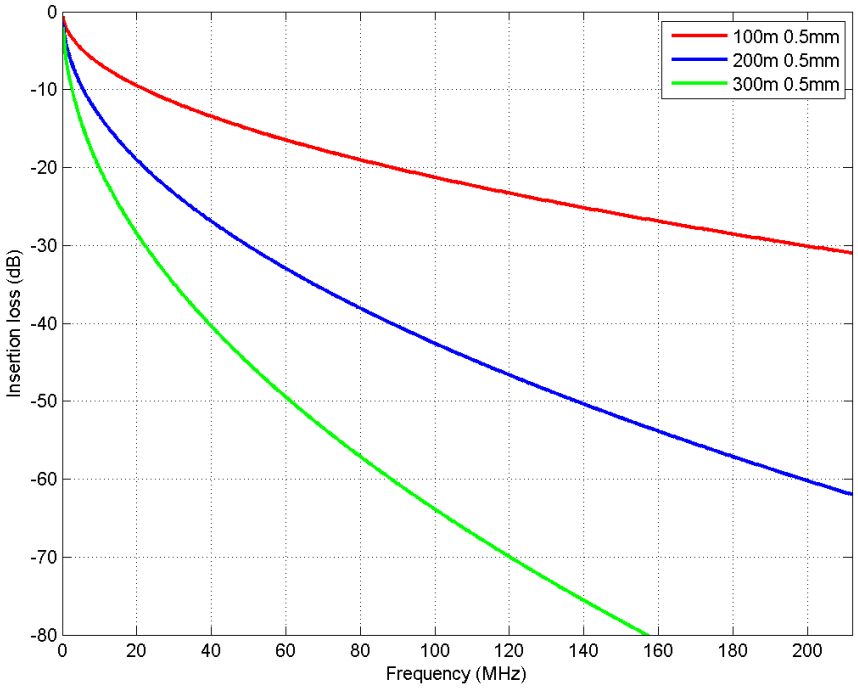

Figure 3.9. Channel attenuation comparison for 100 m, 200 m and 300 m 0.5 mm twisted-pair wire.

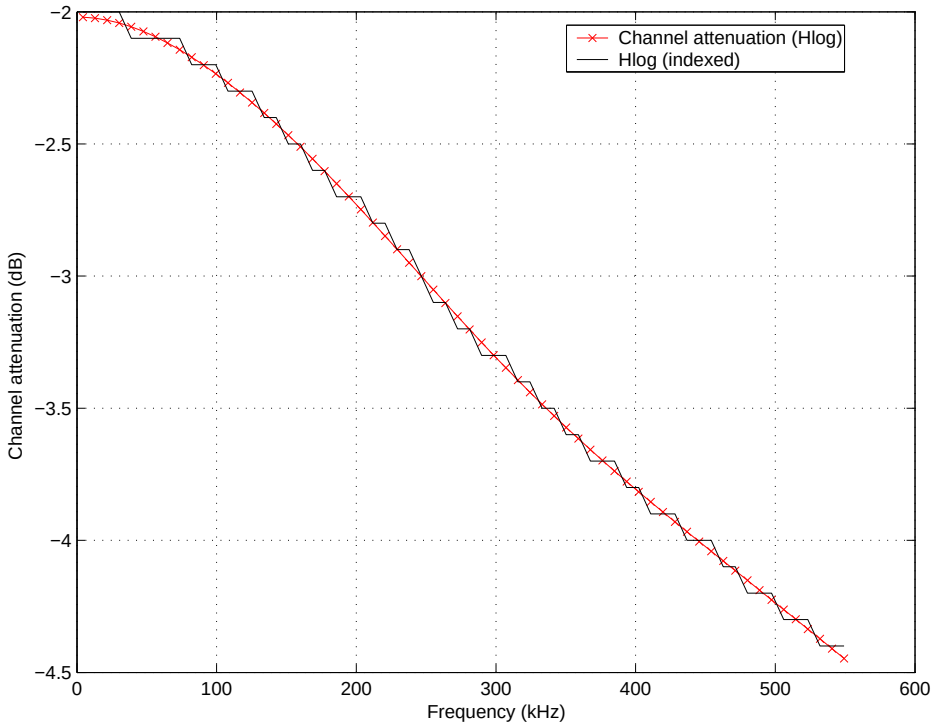

Figure 3.10. Channel attenuation *Hlog* (measured) and *Hlog* (indexed) vs. frequency.

and

$$Hlog(n) = 6 - m(n)/10 \tag{3.22}$$

where $m(n)$ is the 10-bit unsigned value of $Hins(n)$, $n \in \{0...4095\}$ is the subchannel index and $\|\cdot\|$ is the nearest integer function. A simulation of the approximation is shown in Figure 3.10.

3.7 BACKGROUND NOISE

In the GTUs, the quiet line noise PSD (QLN) for a particular sub-carrier is the RMS level of the noise present on the loop when no GDSL signals are present on the loop. QLN is measured by the GTU-R during the loop diagnostic mode and initialization. The measurement is not updated during `Showtime`. QLN is sent to the GTU-C during the loop diagnostic mode and is sent on request to the GTU-C any time. The GTU-C sends QLN to the GTU-R on request during `Showtime`. The quiet line noise $QLN(n)$ is the average of all power values of quiet line noise measured for a specific sub-carrier. The value of $QLN(n)$ (dB) is defined as:

$$w(n) = \|(-23 - QLN(n)).2\| \tag{3.23}$$

and

$$QLN(n) = -23 - (w(n)/2) \tag{3.24}$$

where $w(n)$ is the 10-bit unsigned value of $Hins(n)$, $n \in \{0...4095\}$ is the subchannel index [6] and $\|\cdot\|$ is the nearest integer function. This data format supports a $QLN(n)$ granularity of 0.5 dB with a range of values for $QLN(n)$ from -160 to -23 dBm/Hz. In Figure 3.11 a simulation is shown of the QLN that will be measured by the modem ($QLN_{measured}$) and the indexed (or quantized) version of it ($QLN_{indexed}$).

3.8 CROSSTALK COUPLING

Consider Figure 3.12. Near-end crosstalk is described as the interference (coupling) of a disturbing transmitter's signal, on the same side as the desired receiver. Far-end crosstalk is described as the interference (coupling) of a disturbing transmitter's signal, on the other side of the line, on the received signal. In terms of upstream and downstream transmission:

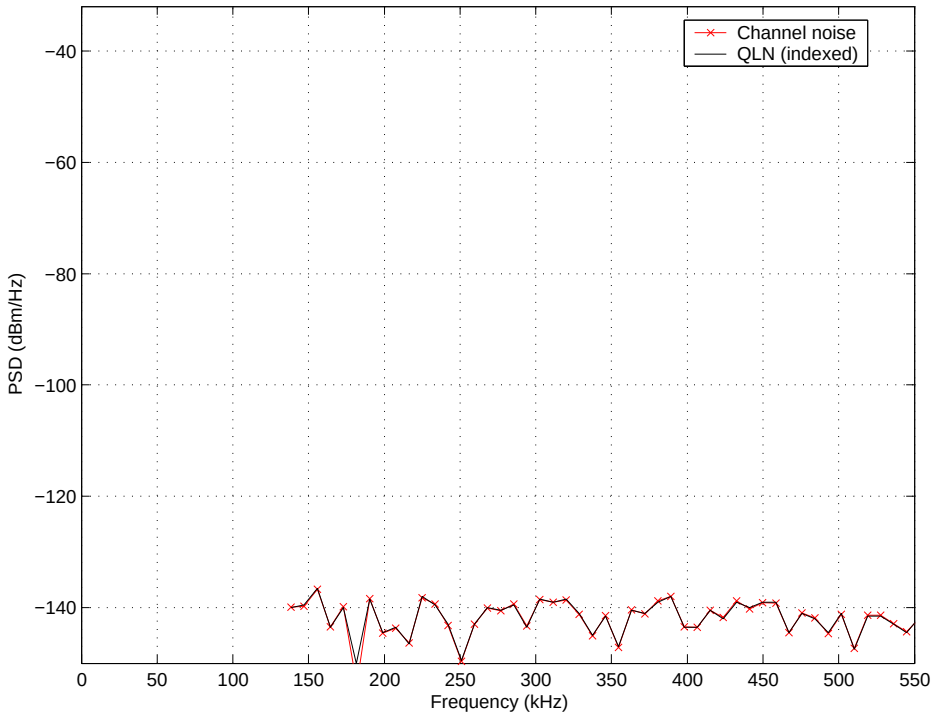

Figure 3.11. Channel Noise - $QLN_{measured}$ vs. $QLN_{indexed}$.

- the desired upstream(downstream) receiver will experience NEXT interference from a disturbing downstream(upstream) transmitter at the same side;
- the desired upstream(downstream) receiver will experience FEXT interference from a disturbing upstream(downstream) transmitter from opposite sides.

It is for the reason stated above that NEXT can be eliminated by using either FDD or TDD. FEXT is still an issue, since the transmitter-receiver combinations are in the same direction (upstream or downstream).

3.8.1 NEXT and FEXT model

The transfer function for a 99% worst-case Near-end crosstalk (NEXT) channel can be expressed as [21, 24, 119]:

$$|H_{NEXT,99}(f)|^2 = x_n \cdot f^{1.5} \tag{3.25}$$

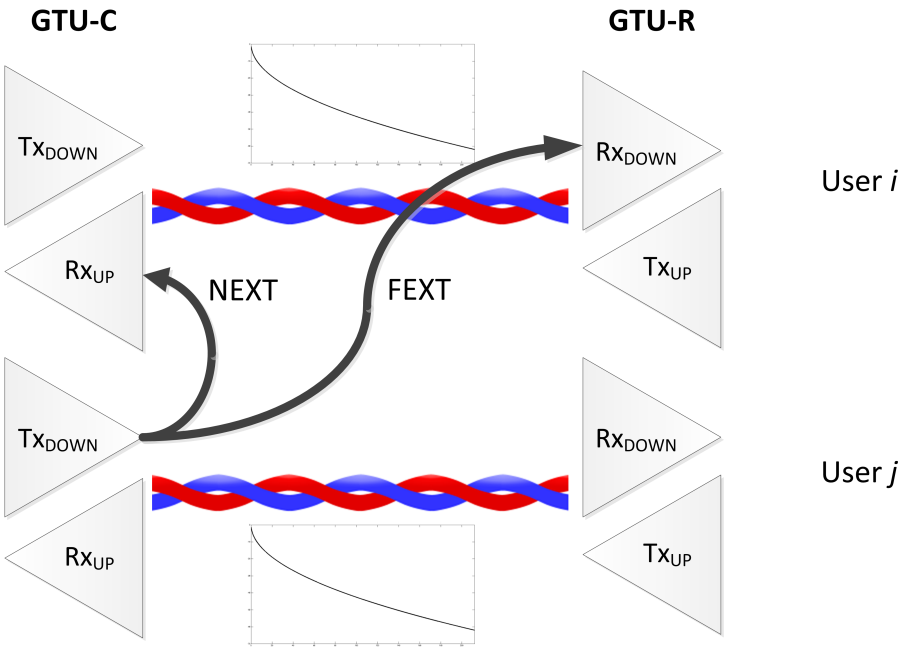

Figure 3.12. Illustration of NEXT and FEXT interference.

and the PSD as:

$$PSD_{NEXT} = PSD_{Disturber} \cdot |H_{NEXT,99}(f)|^2 \tag{3.26}$$

where $x_n = 8.814 \cdot 10^{-14}$ and f is the frequency [Hz].

Far-end crosstalk (FEXT) is dependent on the characteristics of the line. The original signal at the transmitter (of a disturber) will be attenuated due to the inherent propagation loss of the line. In a real network, FEXT is not just a function of the crosstalk in the cable, but also of the cable topology [21], i.e.

$$|H_{FEXT,99}(f)|^2 = x_n \cdot d \cdot |H_{ins}(f)|^2 \cdot f^2 \tag{3.27}$$

and the PSD as:

$$PSD_{FEXT} = PSD_{Disturber} \cdot |H_{FEXT,99}(f)|^2 \tag{3.28}$$

where $x_n = 2.625 \cdot 10^{-16}$, d is the crosstalk coupling length [m], $H_{ins}(f)$ is the insertion loss for the line under consideration, $|\cdot|^2$ is the modulus-squared function, and f is the frequency [Hz]. In Figure 3.13 a comparison is shown between NEXT and FEXT for different line lengths (l = 10 m , l = 100 m and l = 200 m respectively) for a 0.5 mm diameter copper wire. In Figure 3.14 a comparison is shown between NEXT, FEXT (d = 10 m), FEXT (d = 100 m) and FEXT (d = 200 m) for a 200 m length of

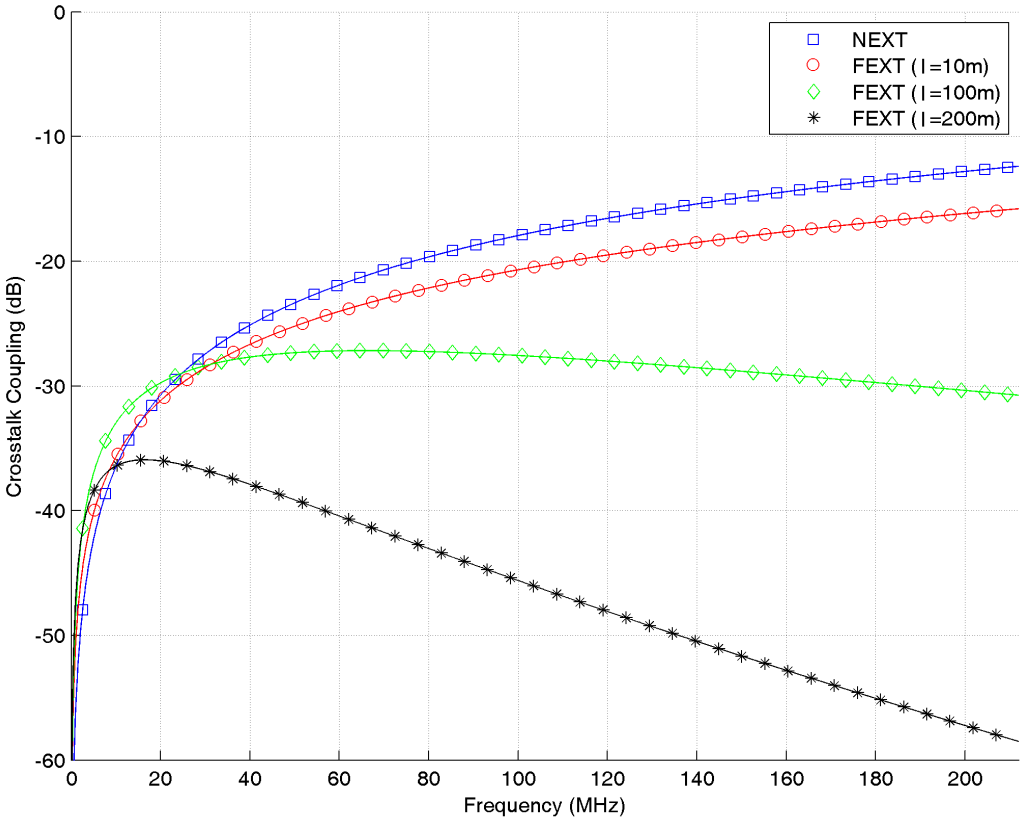

Figure 3.13. NEXT and FEXT Crosstalk coupling for different line lengths (l = 10 m, 100 m and 200 m respectively) vs. frequency.

0.5 mm diameter wire line. It should be observed that the FEXT coupling increases (lower negative value) as the coupling length d increases. The FEXT coupling will also approach NEXT coupling in the high frequency region as the line length l is decreased. In ADSL and VDSL systems, where the line length was still relatively long (the so called 'last-mile'), NEXT was eliminated by using a FDD approach, using different sub-channels for upstream and downstream transmission. One approach to control crosstalk was to control certain transmission parameters such as tone power levels. These "spectrum management" restrictions are conservatively designed so that 99% of all operational cases operate properly. FEXT had PSD levels close to or below the noise level due to large line attenuation, specifically at higher frequencies. With VDSL / VDSL2 the FEXT from VDSL systems (often called 'self-FEXT') is the major performance constraining factor, especially as the loop length becomes shorter.

One of the problems with reducing the line length is that FEXT becomes a real issue in terms of crosstalk interference, especially self-FEXT. As the line attenuation decreases for shorter loops, FEXT

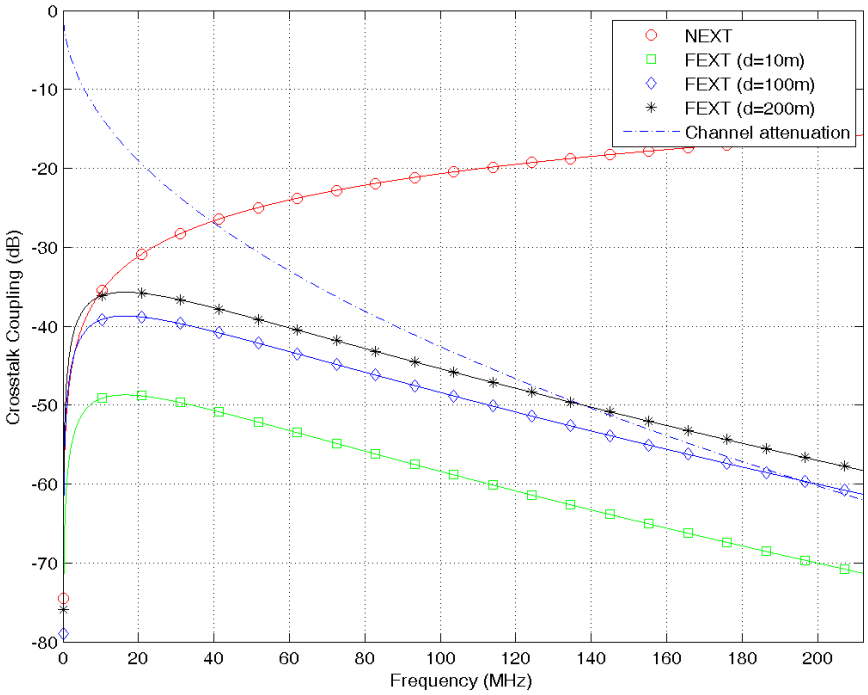

Figure 3.14. NEXT and FEXT Crosstalk coupling comparison for a 200 m length 0.5 mm diameter twisted pair for different coupling lengths (d=10 m, 100 m and 200 m respectively) vs. frequency.

noise starts to approach the same levels as NEXT noise. FEXT remains a problem for the FDD approach - a solution was to apply dynamic spectral management (DSM) Level 1. DSM Level 2 performs spectrum balancing jointly across multiple lines to mitigate crosstalk, while DSM Level 3 applies Vectored DSL to effectively remove crosstalk. Vectored DSL makes use of pre-coding in downstream transmission and makes use of Multi-User Detection (MUD) and Interference Cancellation (IC) in upstream transmission [4]. Overall these techniques (pre-coding and MUD-IC) have a high computational overhead. In this thesis we are using spreading with SOCC codes to mitigate the effect of crosstalk, which inherently provide IC and does not require overhead for pre-coding and MUD-IC.

3.8.2 MIMO Crosstalk Channel Model

In 2009 the Network Interface, Power, and Protection (NIPP) Committee: Network Access Interfaces (NAI) Subcommittee conducted a study [121] that provided a stochastic model for a multiple input,

multiple output, far-end crosstalk coupling channel for DSL transmission systems, and is duplicated below (since reference is not available online).

"The model was derived using a statistical analysis of measurements of ingress energy into pairs of a cable, from other pairs in the same cable, using an actual loop plant. The probability density function (PDF) of the model is asymmetric, meaning that the crosstalk coupling from line (or pair) 1 to 2 is different from the crosstalk coupling from line 2 to 1. The difference seems to vary between 0 dB to 3 dB. The MIMO crosstalk model is also based on a 99% worst case model for single or multiple binders of up to 25 pairs each (up to 100 pairs total), 0.4 mm or 0.5 mm cable type. The transfer function for the MIMO FEXT model is given as:

$$H_{FEXT}(f,d) = |H_{FEXT,99}(f,d)| .e^{j\varphi(f)} . 10^{\frac{X_{dB}}{20}} \tag{3.29}$$

where f is the frequency [Hz], d is the coupling length [m], $H_{FEXT,99}$ is the 99% worst-case crosstalk coupling model in linear scale, $\varphi(f)$ is the phase of the crosstalk channel transfer function and X_{dB} is the amplitude offset of the crosstalk transfer function [dB], relative to the amplitude of the 99% worst case model. The phase $\varphi(f)$ is equal to the phase of the direct channel transfer function plus an offset:

$$\varphi(f) = \tan^{-1}\left(\frac{imag\,(H_{ins}(f))}{real\,(H_{ins}(f))}\right) + \varphi_0 \tag{3.30}$$

where the phase offset φ_0 is a uniformly distributed random variable over the range [0, 2π]."

An interesting observation from the practical measurements was "...it is also clear that the phase of the crosstalk channel has the same slope as the phase of the direct channel". Thus, the crosstalk channels are only affected by the amplitude $X_{dB}(f)$. Also note that "...the amplitude offset $X_{dB}(f)$ can be considered to be independent of the frequency". Thus, the frequency variation of the amplitude offset is ignored and approximated by X_{dB}.

For this study a standard 100x100 matrix of X_{dB} (representing a 100-pair cable with four 25-pair binders) will be used [121]. Row 70 (Pair i = 70 as desired channel) had the lowest minimum crosstalk coupling (thus the worst profile) and will be used for the MIMO channel profiling. $X_{i,j}$ vs. Pair j as shown in Table 3.2.

Table 3.2. Crosstalk coupling $X_{i,j}$(dB) for $i = 70$ (worst-case).

Pair j =>	54	70	68	55	69	72	73	63	74	61
	0.26	0	-1.07	-2.26	-5.56	-7.36	-7.79	-7.87	-8.4	-8.98
Pair j =>	77	39	65	96	27	99	34	81	66	87
	-10.41	-11.01	-12.06	-12.79	-12.96	-13.43	-13.51	-13.51	-13.54	-14.36
Pair j =>	84	75	71	59	35	85	45	36	79	26
	-14.88	-14.98	-15.09	-15.34	-15.99	-16.63	-17.09	-17.3	-17.42	-17.71
Pair j =>	20	8	19	91	32	82	6	44	76	98
	-17.92	-18.22	-18.22	-18.27	-18.83	-19.1	-19.56	-19.98	-19.99	-20.3
Pair j =>	9	80	48	1	62	23	43	46	24	95
	-20.49	-20.61	-20.75	-21.12	-21.19	-21.34	-21.59	-22.21	-22.7	-22.73
Pair j =>	52	58	5	78	3	33	64	28	13	97
	-23.03	-23.19	-23.37	-23.44	-24.27	-24.92	-24.96	-24.98	-25.03	-25.4
Pair j =>	10	90	31	57	89	21	30	83	51	22
	-25.43	-26.25	-26.4	-26.56	-26.87	-27.03	-27.41	-27.57	-27.86	-28.38
Pair j =>	2	88	12	92	29	41	11	49	18	53
	-28.43	-28.52	-28.63	-28.82	-29.13	-29.4	-29.72	-30.12	-30.12	-30.13
Pair j =>	86	42	67	93	50	60	37	17	47	25
	-30.24	-30.4	-30.49	-30.79	-31.16	-31.28	-31.47	-31.52	-31.6	-31.92
Pair j =>	40	38	100	56	14	16	94	15	4	7
	-32.06	-32.27	-32.69	-33.46	-34.11	-36.32	-40.31	-40.59	-41.26	-41.28

Although the MIMO model was derived for FEXT, it is also applicable to NEXT, as $X_{i,j}$ is the crosstalk coupling between pairs i and j. $H_{NEXT}(f)$ and $H_{FEXT}(f,d)$ is thus defined as:

$$H_{NEXT}(f) = H_{NEXT,99}(f) \cdot 10^{\frac{X_{dB}}{20}} \tag{3.31}$$

$$H_{FEXT}(f,d) = H_{FEXT,99}(f,d) \cdot 10^{\frac{X_{dB}}{20}} \tag{3.32}$$

These equations have been used for the performance analysis of the GDSL system.

3.9 TRANSMIT AND RECEIVE FILTERS

The GDSL modems implement square root raised cosine filters at the output of the transmitter and input to the receiver. The transfer function $G(f)$ in the frequency domain is given in Equation (3.33)

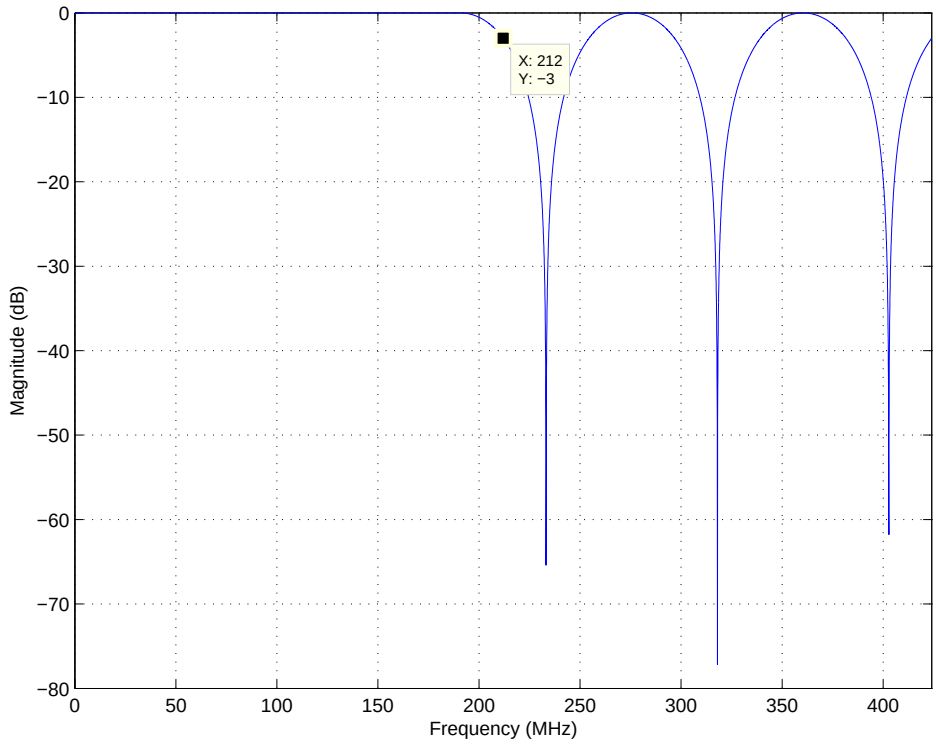

Figure 3.15. Square root raised cosine filter frequency response.

and shown in Figure 3.15.

$$G(f) = \begin{cases} T_{system}\,, & 0 \leq |f| \leq \frac{1}{2T_{system}}(1-\alpha) \\ \frac{T_{system}}{\sqrt{2}}\sqrt{1-\sin\frac{\pi T_{system}}{\alpha}(f-\frac{1}{2T_{system}})}\,, & \frac{1}{2T_{system}}(1-\alpha) < |f| \leq \frac{1}{2T_{system}}(1+\alpha) \end{cases} \tag{3.33}$$

3.10 POWER SPECTRAL DENSITIES AND CHANNEL CONDITIONS

Figure 3.16 shows the power spectral densities (PSD) of the transmitted pilot tones (in this example -60 dBm/Hz), the received pilot tones, the background noise, 99% worst case NEXT noise level and 99% worst case FEXT noise levels for different coupling lengths, for a 200 m length of 0.5 mm diameter twisted pair. The channel attenuation was also added in order to compare the profile of the received pilot tones with the profile of the transmitted pilot tones. Figure 3.17 shows the measured SNR ($SNR_{measured}$), the SNR used for bit loading (SNR_{used}) and the indexed SNR ($SNR_{indexed}$). A zoomed-in version (0 - 553.6 kHz) is shown in Figure 3.18. The effect of NEXT and FEXT interferers was not taken into consideration and a SNR larger than 96 dB was used to illustrate the clipping effect

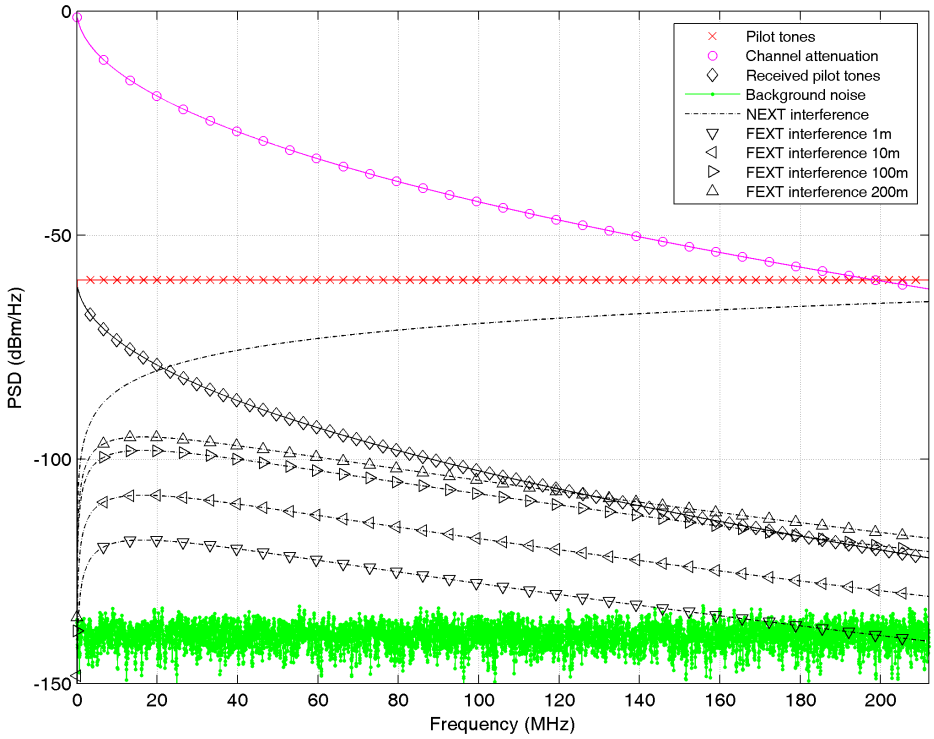

Figure 3.16. Power spectral density of pilot tones, channel attenuation, received tones, background noise, 99% worst case NEXT noise level and 99% worst case FEXT noise levels for different coupling lengths.

of SNR_{index} (Equations 3.2 and 3.3). A zoomed-in version (0 - 553.6 kHz) of the channel attenuation and quiet line noise (QLN) are shown in Figure 3.19 and Figure 3.20.

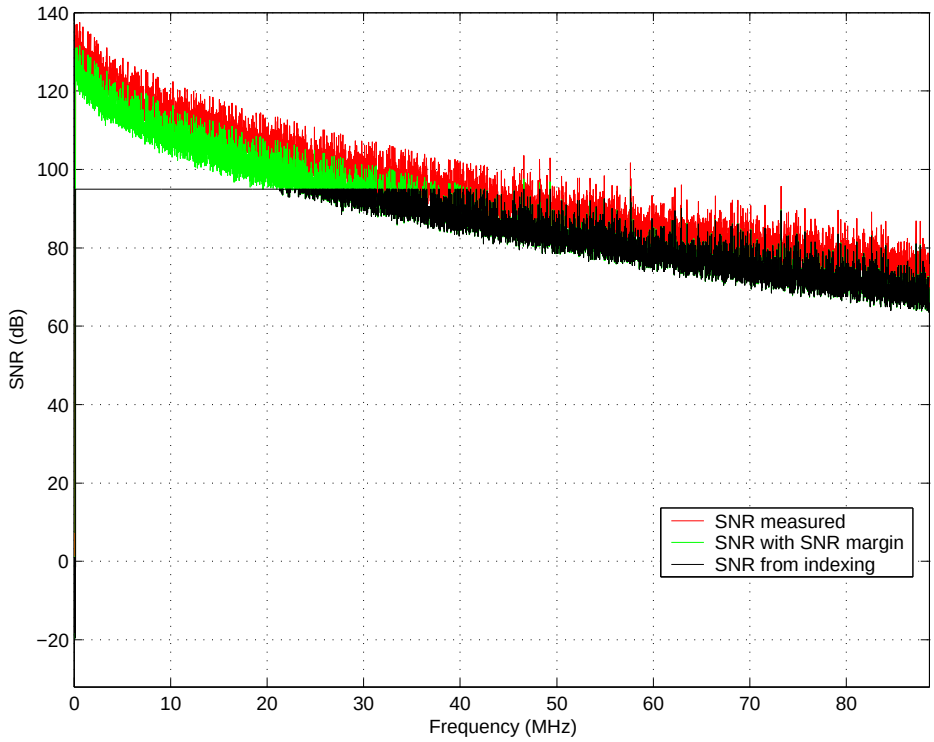

Figure 3.17. Power spectral density of $SNR_{measured}$, SNR_{used} and $SNR_{indexed}$.

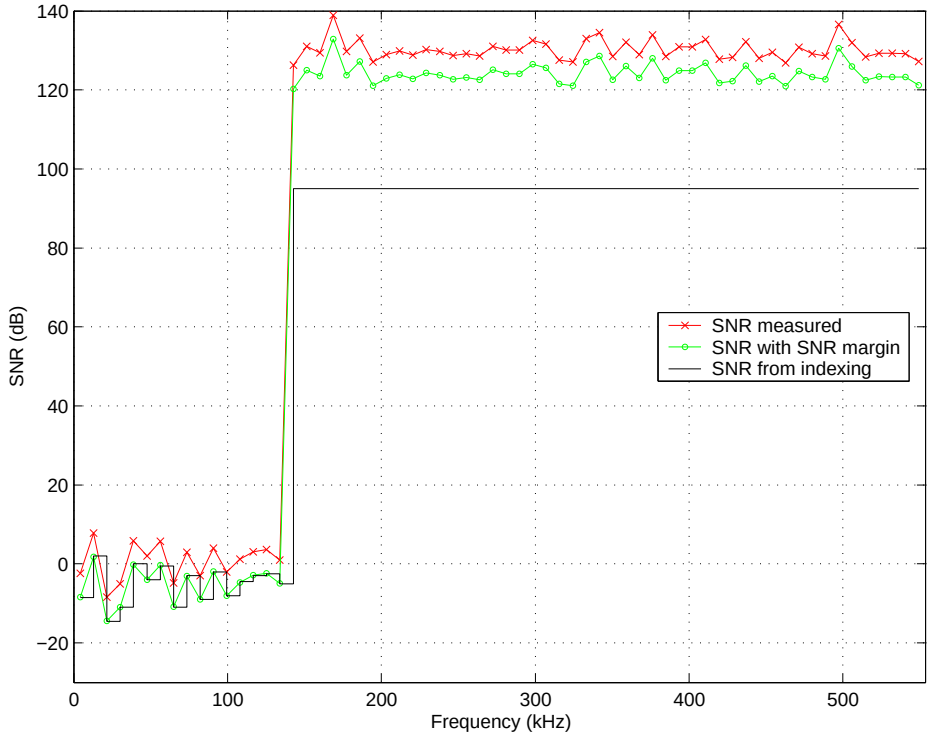

Figure 3.18. Zoomed Power spectral density of $SNR_{measured}$, SNR_{used} and $SNR_{indexed}$ (0 - 553.6 kHz).

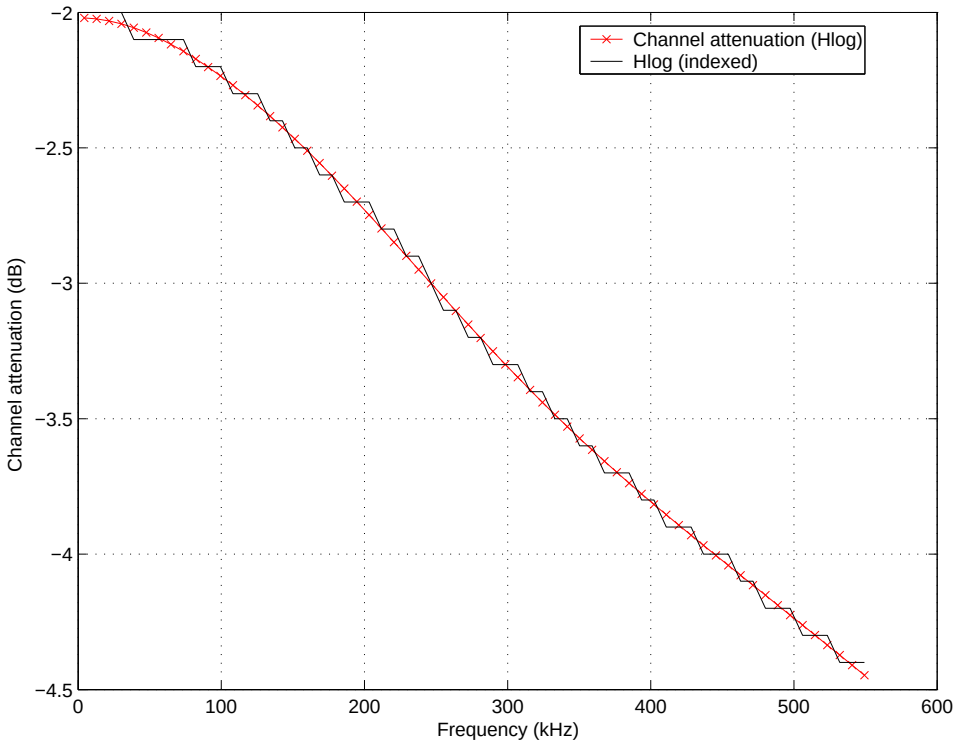

Figure 3.19. Zoomed portion of channel attenuation ($Hlog$) and $Hlog_{indexed}$.

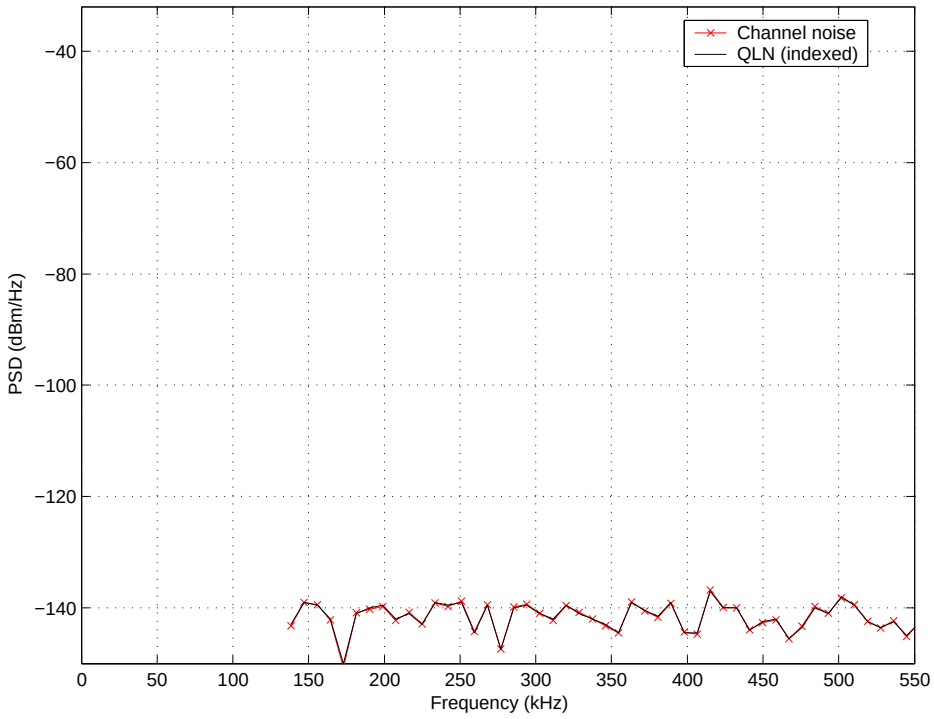

Figure 3.20. Zoomed portion of Quiet Line Noise (QLN) and $QLN_{indexed}$.

CHAPTER 4 SYSTEM ARCHITECTURE

4.1 INTRODUCTION

This chapter describes the system architecture of the GDSL modem. System specifications are described in Section 4.2. These specifications were determined based on existing standards and guidelines for future systems. In Section 4.3 the GDSL modem frequency band is compared with existing xDSL systems to show which frequency bands it will use to make it compatible with existing xDSL systems and to allow bypass policies where needed. The transmitter and receiver structure is shown in Section 4.4, as well as its sub-components. The concept of Resource Blocks is discussed in Section 4.5. The correlation properties of the SOCC spreading codes is discussed in Section 4.6. Modem operation (initialization, messaging modulation, link states and initialization procedures) are discussed in Section 4.7. To protect certain radio services, such as amateur radio bands, certain bands need to be masked out - this is described in Section 4.8. Co-location with other DSL services, bypass profiles and the effect on system throughput are discussed in Section 4.9.

4.2 SYSTEM SPECIFICATION

Based on information from the G.fast specification [7, 13], it was decided that the system should have the following specifications:

- Bandwidth (BW): 211.968 MHz
- Subcarrier spacing (Δf): 51.750 kHz
- Number of subchannels (N): 4096
- Power level: -60 dBm/Hz (or 23.263 dBm or 211.968 mW (for 200 m))

- Noise level: -140 dBm/Hz

4.3 FREQUENCY BAND PLAN COMPARISON

Figure 4.1 shows a comparison between ADSL, ADSL2+, VDSL2, G.fast and the proposed GDSL. GDSL defines 63 bands (or resource blocks) of 65 subchannels each. These bands can either be allocated for upstream / downstream operation if Frequency Division Duplex (FDD) is used, or all bands are utilized and upstream/ downstream operation is defined by Time division duplex (TDD).

4.4 TRANSCEIVER STRUCTURE

ADSL and VDSL standards [5, 6] use DMT modulation. It is a special implementation of multicarrier modulation, based on the IFFT/FFT transform pair that can conveniently be implemented in a fully digital way with relatively low complexity.

A block diagram of the GDSL transmitter is shown in Figure 4.2. A block diagram of the GDSL receiver is shown in Figure 4.3. The GDSL modulator is responsible for the allocation of the required number of bits per subchannel (tone ordering), the conversion of these bits to an appropriate symbol (M-QAM modulation), frequency spreading and multiplexing of symbols; conversion to the time domain using the IFFT process and lastly transmission over the subscriber line.

Standard bit loading, as used in existing DSL systems, is performed, as well as the optimal power is assigned for each subchannel, according to the measured signal-to-noise ratio (SNR_{used}) for that specific subchannel [22, 122]. The developed Code Allocation Algorithm (discussed in Chapter 6) ensures a constant bits per Resource Block ($BpRB$) profile for each RB. The CAA also determines the number of allocated spreading codes allocated per RB. The number of bits transmitted per OFDM block is a function of the number of active RBs, the number of allocated spreading codes per active RB, as well as the number of bits to allocate per spreaded symbol (BpRB).

The serial-to-parallel converter converts the incoming serial bit stream b into parallel data streams $\bar{b}_n$ based on the bits per tone profile (specifically $BpRB$). The QAM modulator maps the designated

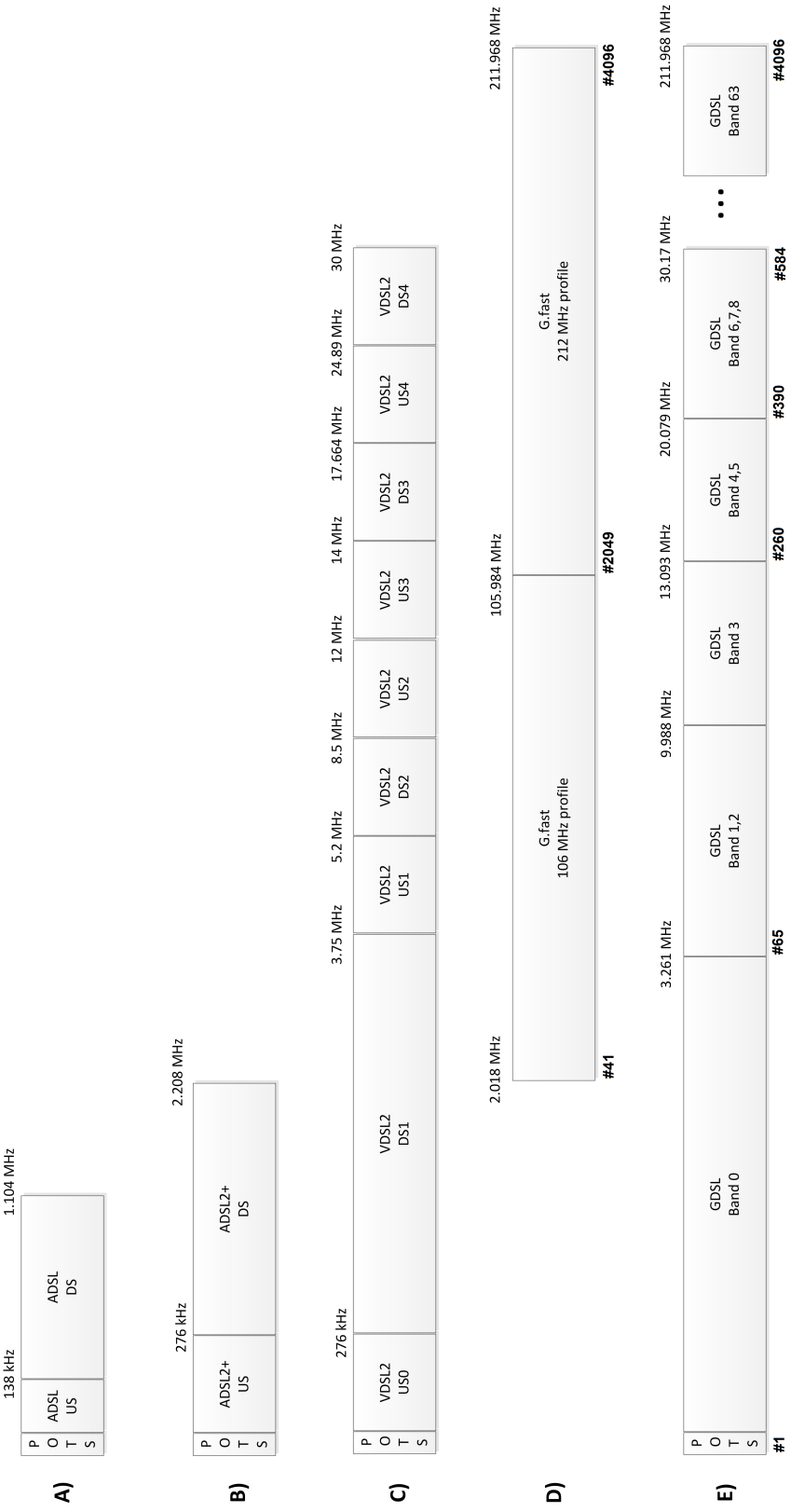

Figure 4.1. Frequency band plan comparison for (A) ADSL, (B) ADSL2+, (C) VDSL2, (D) G.fast and (E) GDSL.

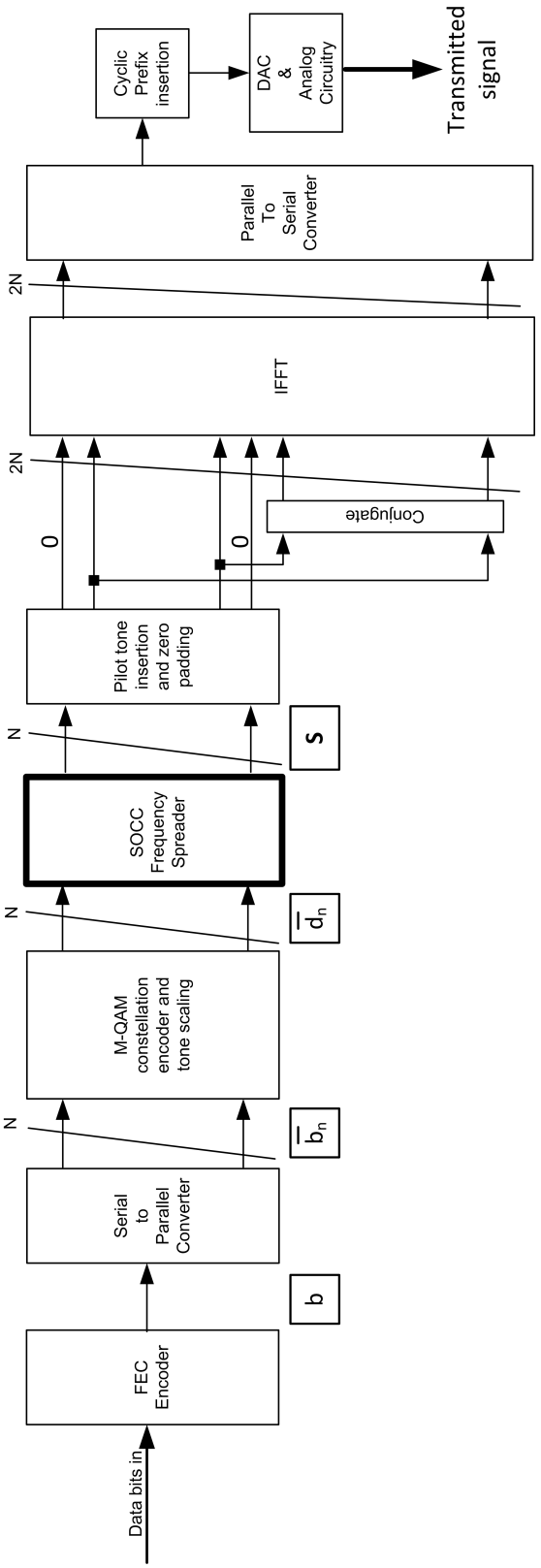

Figure 4.2. GDSL Transmitter Block diagram. Republished with permission of IEEE, from [114]; permission conveyed through Copyright Clearance Center, Inc.

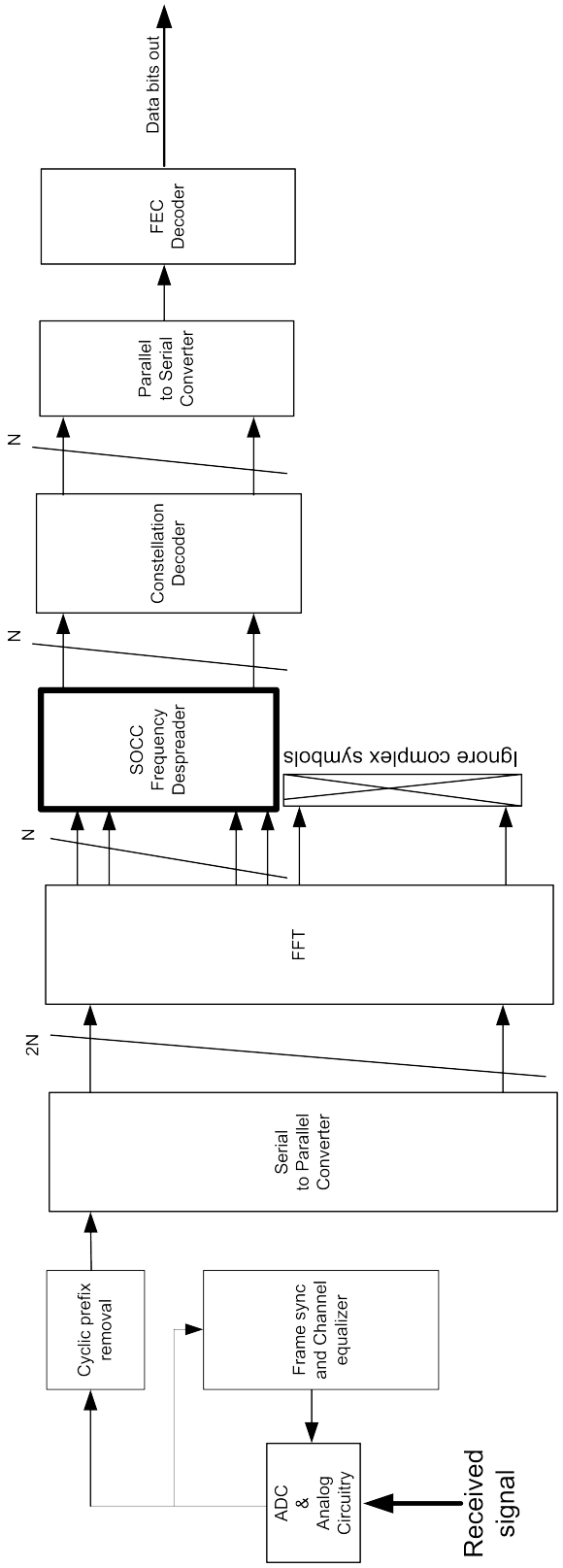

Figure 4.3. GDSL Receiver Block diagram. Republished with permission of IEEE, from [114]; permission conveyed through Copyright Clearance Center, Inc.

number of bits $\bar{b}_n$ into unique Gray-encoded M-QAM symbols ($\bar{d}_n$). These symbols are then scaled to obtain the correct power (energy) level (called tone scaling). Tone scaling also tries to obtain an average energy profile across all symbols. The modulator is discussed in more detail in Section 4.4.2 and the tone scaling process in Section 4.4.3.

The M-QAM symbols ($\bar{d}_n$) are then spread in frequency by the SOCC Frequency Spreader (L_{fsp} = 64 or 256) to obtain the spreading vector **S**. Pilot tones are added where needed. A 2N-point conjugate symmetric IFFT is performed to produce only real-valued time samples t_N. A cyclic prefix can be added to protect against time dispersion (as discussed in Section 3.3), lastly followed by the DAC and Analog circuitry to produce the transmitted signal.

Following a similar reasoning for a MC-CDMA system as provided by Hanzo *et al.* [123], the transmitted signal of the kth user per OFDM block, $s^k(t)$ is written as:

$$s^k(t) = \sum_{m=1}^{M} \sum_{n=RB_{start}(m)}^{RB_{stop}(m)} \sum_{i=CpRB_{start}(m)}^{CpRB_{stop}(m)} d_h^k . c_n^i . e^{2\pi . (RB_{start}+n).\Delta f . t} p(t - h.T) \tag{4.1}$$

where m is a counter over all active Resource Blocks (M active blocks), $RB_{start}(m)$ and $RB_{stop}(m)$ are the start and stop subchannel index of active RB m, $CpRB_{start}(m)$ and $CpRB_{stop}(m)$ are the start and stop index of spreading codes s_i to be used in active RB m, d_h^k is the hth M-QAM symbol of the kth user, c_n^i represent the nth chip of the allocated spreading sequences from $CpRB_{start}$ to $CpRB_{stop}$, $RB_{start}.\Delta f$ is the lowest subchannel frequency, Δf is the subchannel spacing and $p(t - h.T)$ is a rectangular signalling pulse shifted in time, given by:

$$p(t) \triangleq \begin{cases} 1 & for \;\; 0 \leq t \leq T \\ 0 & otherwise \end{cases} \tag{4.2}$$

4.4.1 Error correction coding / decoding

Current versions of xDSL modems employ Reed Solomon (RS) block codes, which is a subset of non-binary Bose, Chaudhuri, and Hocquenghem (BCH) codes. BCH codes form a large class of powerful random error-correcting cyclic codes. This class of codes is a remarkable generalization of the Hamming code for multiple-error correction. RS codes, specified as RS(p,q) and operating over a Galois field $GF(256)$, operate on 8-bit symbols and have p symbols per block. q determines the

number of data symbols in the block and $p-q$ is the number of parity check symbols that are added during the encoding process. For DSL, parity check symbol sizes of 0, 2, 4, 6,...,16 and 32-255 data symbols are typically specified.

Low-density parity-check (LDPC) codes are a class of highly efficient linear block codes. LDPC can provide performance very close to the Shannon bound (the theoretical channel capacity). LDPC codes were invented by Gallager in his PhD thesis in 1960 [124], but due to the computational effort in implementing the encoder/decoder and the introduction of Reed-Solomon codes, they were mostly ignored until the mid 1990s, when work of MacKay, Luby and others noticed the advantages of LDPC.

LDPC codes are now used in many recent high-speed communication standards, such as Digital video broadcasting (DVB-S2) [125], WiFi (IEEE 802.11n) [126], 10GBase-T Ethernet (IEEE 802.3an) [127] and ITU-T G.hn (G.9960) [128].

In order to limit the overhead introduced by implementing LDPC encoding/decoding, high coding rate ($R \geq 0.9$) LDPC codes were needed. The DVB-S2 standard only provides a coding rate of up to $R = 9/10$ of data block size 64,800. As the design of LDPC codes was not the major objective of this thesis, existing LDPC generator source code was used, as provided by Prof. R.M. Neal on his website [129]. This software generates a parity check matrix *pchk*. To make the generated LDPC parity check matrix systematic for use within Matlab (LDPCEncoder), the following procedure was used:

- Convert the *pchk* matrix into the *alist* format;
- The *alist* file is converted to a binary H_b matrix using A2H.p perl script from [130];
- The binary H_b matrix is imported into Matlab;
- Determine a sparse version H_s of the transpose of H_b (`Hs=sparse(Hb')`);
- Determine an identity matrix H_I (`HI=speye(size(Hs,1))`);
- Determine the systematic H parity matrix (`H = [Hs HI]`).

Code rates $R = 0.9$, 0.9375 and 0.95 were considered. A BER simulation, using the simulation model shown in Figure 4.4, was performed using a QPSK-based system to determine the performance of

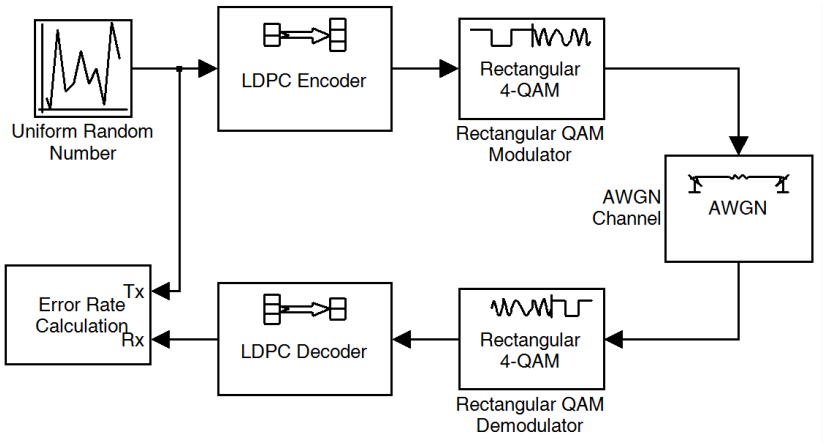

Figure 4.4. Simulation model to test the performance of different LPDC models.

different coding rates LDPC codes for data sizes of 8,192 and 16,384 bits, and to compare these against an equivalent uncoded QPSK system, as well as the DVB-S2 (R = 9/10) LDPC code, as shown in Figure 4.5. SOCC spreading was not added, but similar results are expected, since SOCC spreading does not change the BER performance of M-QAM based systems, as illustrated in Figure 4.14. Similar coding rate R systems have similar performance. The size of the blocks do not seem to influence performance too much. As expected, the coding gain reduces when the coding rate R approaches 1. In order to allow for other overheads i.t.o. protocols, messages etc. a coding rate of $R = 0.95$ was used to provide some coding gain. There is a trade-off between high throughput rates (R approaching 1) and better error protection (higher coding gain or lower code rate R). Since this GDSL system is a high throughput system and the coding gain that is obtained going from $R = 0.95$ to $R = 0.9$ is only about 1 dB, it was decided to rather go for high throughput than coding gain. Error protection i.t.o. coding gain can be increased (lower R) but throughput will decrease.

4.4.2 M-QAM mapping

The GDSL modem will utilize Differential PSK (DPSK) for all messages and pilot tone channels, as discussed in Section 4.7.3 and Gray-encoded M-QAM mapping for user data.

The transmitter on each side (central office GTU-C and customer GTU-R) has a specified average power spectral density (dBm/Hz) or power level (dBm) in a specified bandwidth. For ADSL and VDSL the power level is usually 14.5 dBm. According to the IEC EN55022:1998 [131] standard a quasi-peak

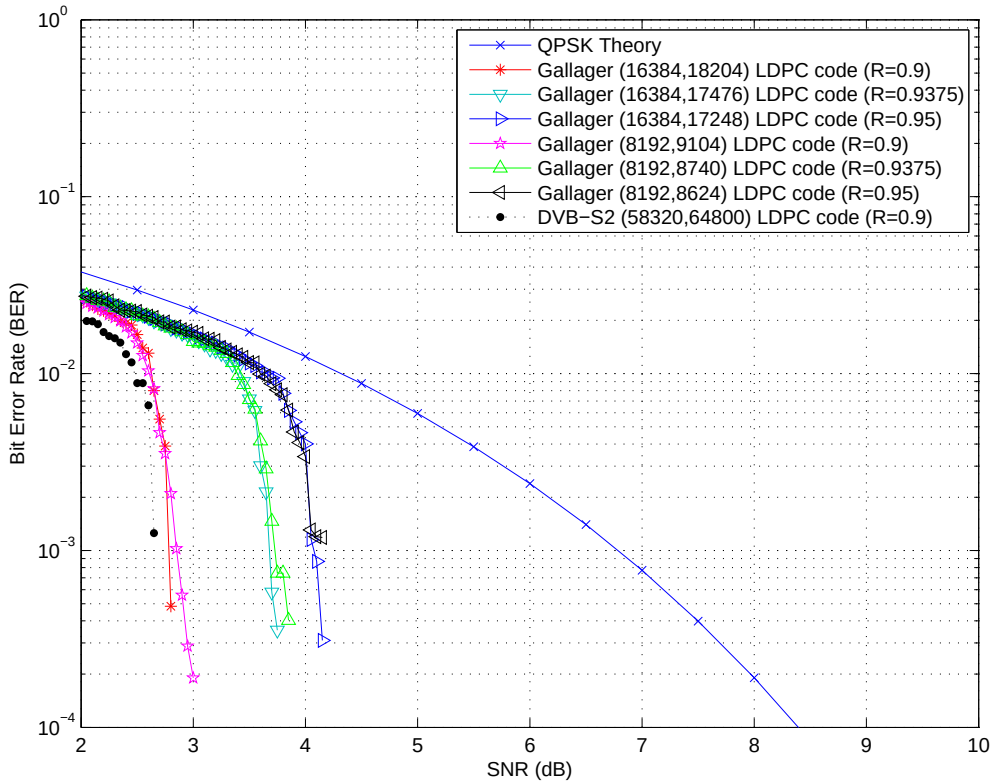

Figure 4.5. BER vs. SNR performance of $R = 0.9$, 0.9375 and 0.95 LDPC codes for data sizes 8,192 and 16,384 bits, compared to uncoded QPSK system and DVD-S2 ($R = 9/10$) LDPC.

limit for radiation caused by an electric appliance is measured at a distance of 10 m. This limit of 30 dB(μV/m) is measured in any 6 dB band of 9 kHz width in the frequency range above 30 MHz. A transmit PSD below -60 dBm/Hz ensures that this limit is on average not violated. Based on this choice, the total system power is 23.263 dBm (211.968 mW) and power per carrier = -12.861 dBm.

4.4.3 Gain scaling

The GTU may also use gain scaling in the range of 0.1888 and 1.33 (-14.5 dB to 2.5 dB) to equalize the expected error rates for all data-carrying subchannels. Each encoded complex symbol from the encoder is multiplied by a gain scaling factor g_i. Gain scaling has a flattening effect on the power spectrum of DSL systems.

4.4.4 Frequency spreading

A frequency spreader is added to the GDSL system to provide protection against variations or fading effects in the frequency domain. The spreading codes used is based on the latest orthogonal code design techniques. Specifically, SOCC binary codes will be used. Another alternative is polyphase codes based on minimum phase rotation. These codes also have perfect correlation properties, as discussed in Section 4.6, but they were not used, since SOCC codes allowed for both asynchronous and synchronous transmission between users. Spreading is also used to provide some processing gain, as will be evident from the performance analysis results in Section 4.6.

4.4.5 IFFT/FFT

In the GDSL system, modulation is performed by a $2N$-point IFFT, transferring the parallel independent subchannels in the frequency domain to the time domain. To assure that the IFFT at the transmitter side generates only real-valued outputs, the inputs of the IFFT have the following constraints [114, 132, 133], based on Hermitian symmetry:

$$x(n) = x^*(2N-n) \qquad \text{for } n = 0,1,\ldots,N-1 \tag{4.3}$$

$$x(0) = x(N) = 0 \tag{4.4}$$

where $N = 4096$, $x(n) \triangleq x_r(n) + jx_i(n)$ are the input encoded complex symbols and $x^*(\cdot)$ is the complex conjugate of the encoded complex symbol for subchannel n. This is performed in vector form using $x_{IFFT} = [\,0 \;\; x(2:N) \;\; 0 \;\; x^*(N:-1:2)\,]$

4.5 RESOURCE BLOCKS

The spreading and despreading functions of the modem should operate in blocks, called Resource Blocks (RBs) of 64 subchannels (due to the spreading code length of 64). For each RB, a dedicated pilot tone is added for block synchronization. An operational RB thus use 65 subchannels, providing 63 RBs over the bandwidth (using 4096 subchannels). The implementation of RBs is illustrated in Figure 4.6. With an ADSL bypass policy applied, it is illustrated in Figure 4.7.

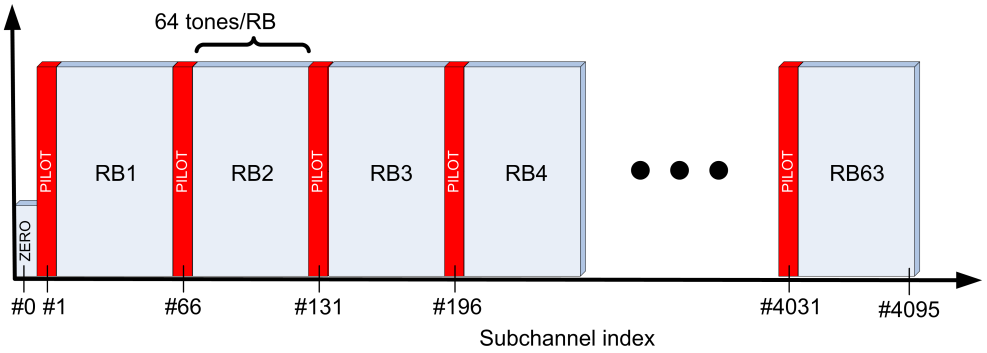

Figure 4.6. Illustration of resource block implementation vs. subchannel index.

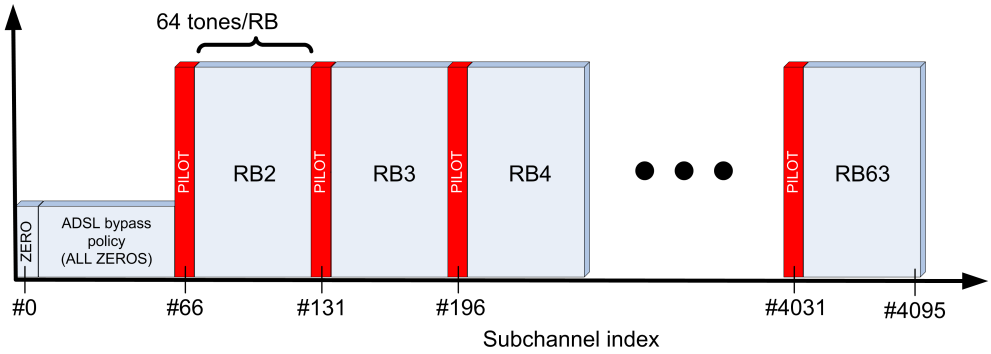

Figure 4.7. Illustration of resource block implementation with ADSL bypass policy vs. subchannel index.

4.6 SOCC CORRELATION PROPERTIES

In Figure 4.8 the normalized periodic correlation properties of the SOCC codes of length $L_{fsp} = 64$ that were used, is shown. The diagonal represents the periodic auto-correlation of each sequence (sequence i and j, $i = j$) and the rest of the graph the periodic cross-correlation between sequences (sequence i and j, $i \neq j$). A simple BER test (without any forward error correction scheme) was performed on the spreading and despreading blocks to determine if the addition of interfering signals at predefined levels (-10 dB, -20 dB, -25 dB, -30 dB and -40 dB) will affect the operation of these blocks. Results are shown in Figures 4.9 to 4.13. From these graphs it can be observed that spreading codes can be re-used in RBs where the desired user and interfering users have differences of 40 dB or more between their spectra. The simulation was only performed for a QPSK system, but similar results for other M-QAM constellations will be obtained, since the cross-correlation is a function of the spreading code length and not the modulation scheme. BER analysis were also performed for the MC-CDMA system for QPSK, 16-QAM and 64-QAM, with frequency spreading $L_{fsp} = 64$ (Figure

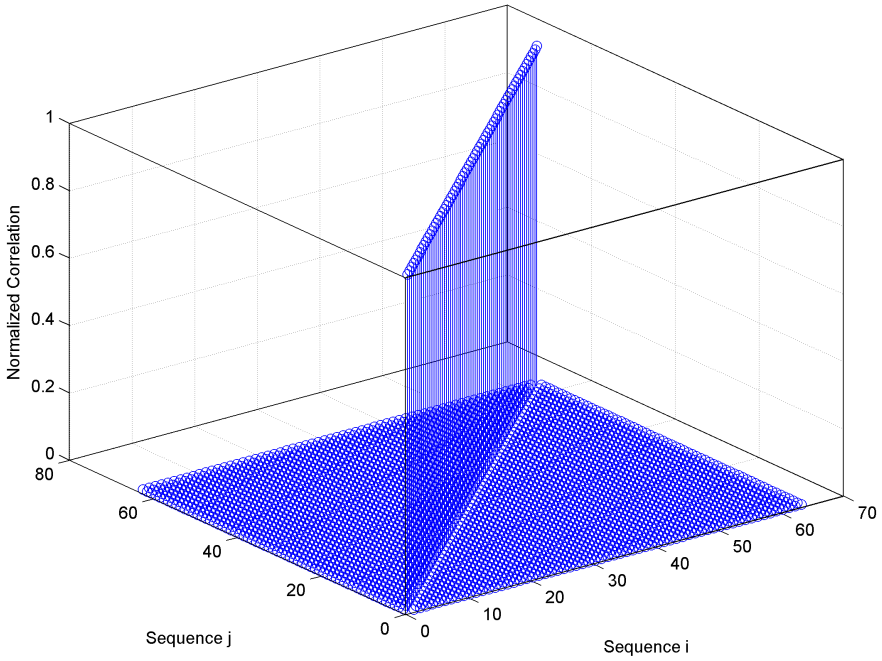

Figure 4.8. Periodic correlation properties of the SOCC codes ($L_{fsp} = 64$).

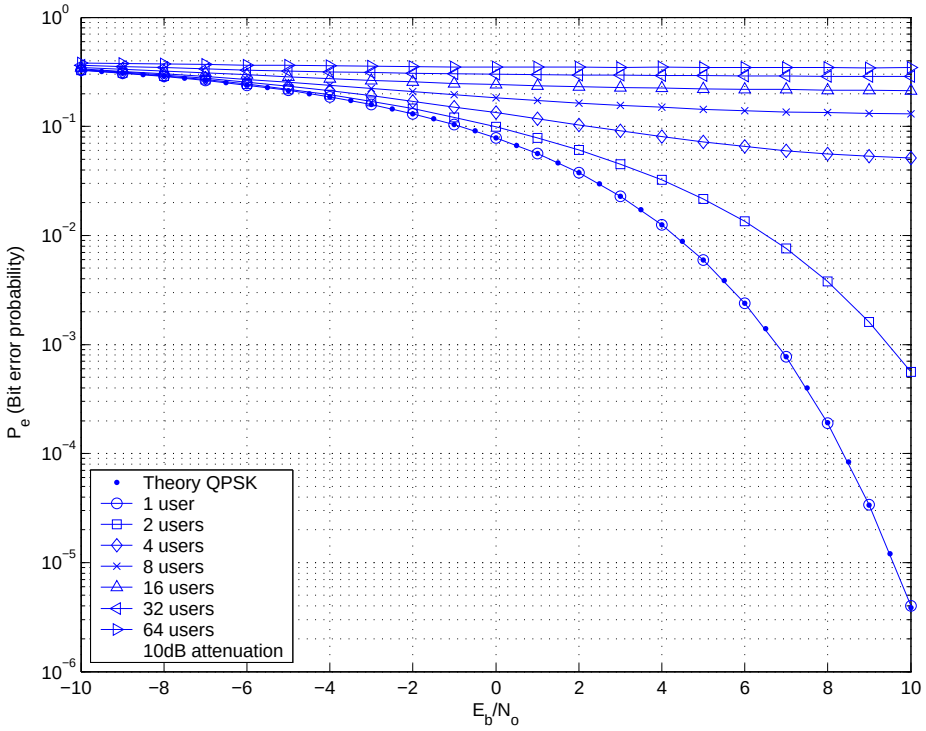

Figure 4.9. BER of the spreading/despreading block (64 subchannels) for interfering signals at 10 dB attenuation.

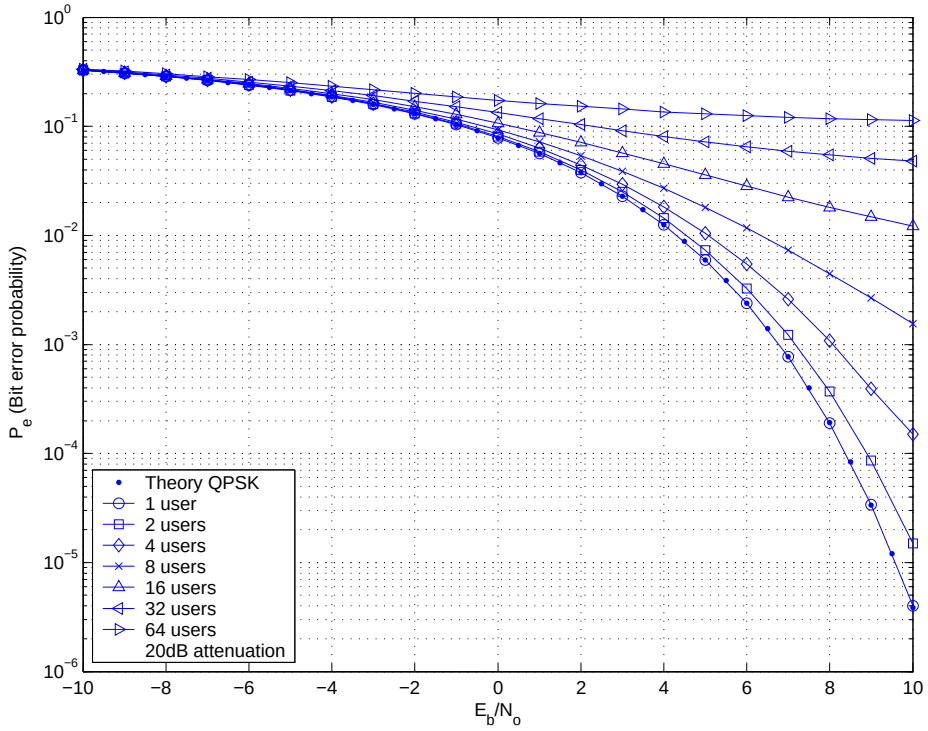

Figure 4.10. BER of the spreading/despreading block (64 subchannels) for interfering signals at 20 dB attenuation.

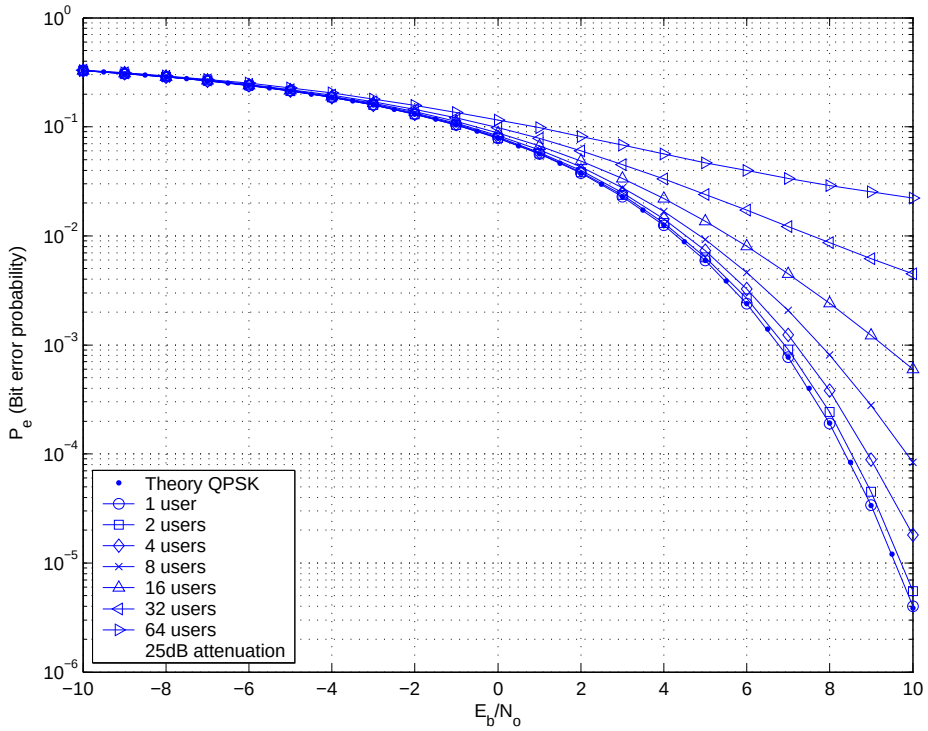

Figure 4.11. BER of the spreading/despreading block (64 subchannels) for interfering signals at 25 dB attenuation.

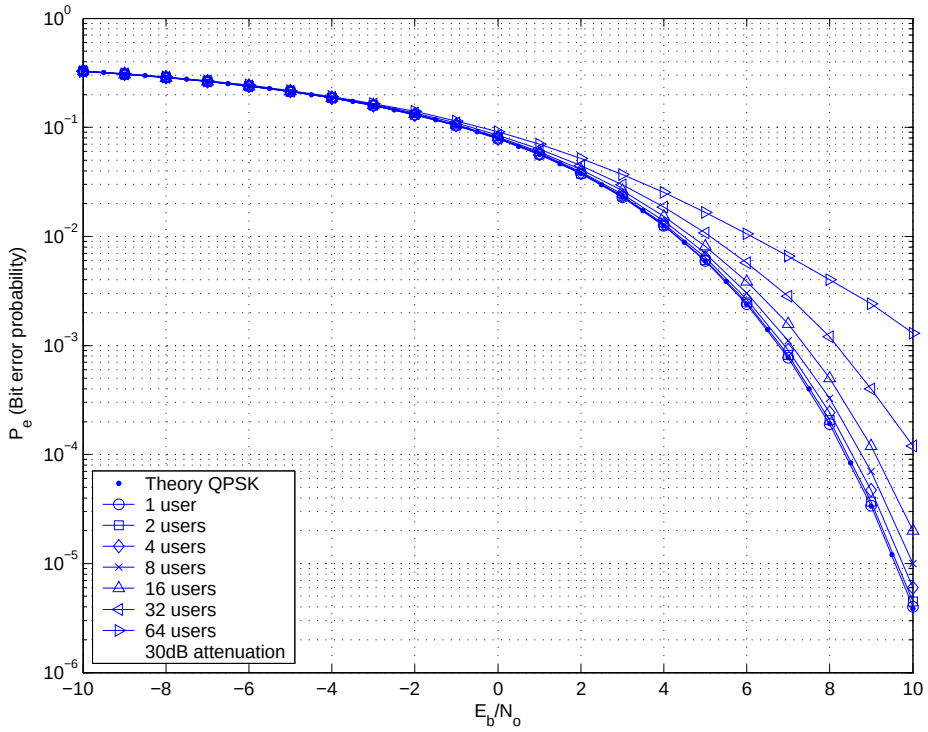

Figure 4.12. BER of the spreading/despreading block (64 subchannels) for interfering signals at 30 dB attenuation.

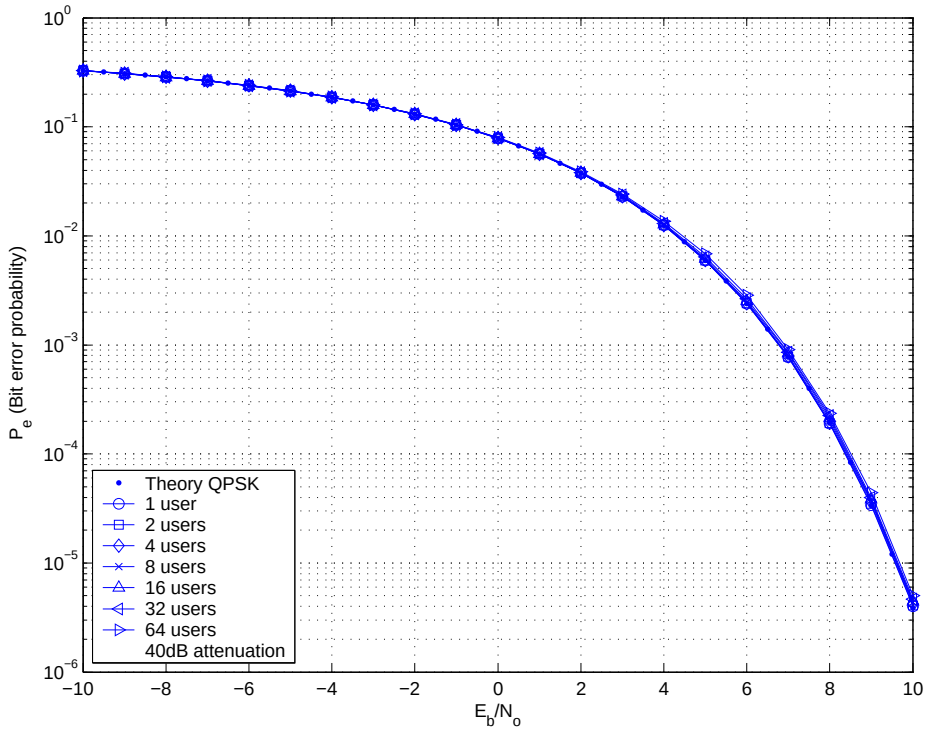

Figure 4.13. BER of the spreading/despreading block (64 subchannels) for interfering signals at 40 dB attenuation.

4.14) and L_{fsp} = 256 (Figure 4.15) to test correct operation of the modem, especially i.t.o. scaling. It can be seen that spreading does not affect the BER performance of a M-QAM-based system.

4.7 MODEM OPERATION

The modem will follow handshake procedures as described for ADSL and VDSL [5, 6] and defined by the handshake procedures for Digital Subscriber Line transceivers (ITU G.994.1) [120].

4.7.1 Modem Initialization

This section describes the Modem initialization (startup) procedure. In general, all xDSL modems have to follow handshake procedures, as described in *Handshake procedures for digital subscriber line transceivers* (ITU G.994.1) [120]. and various amendments to it - especially Amendment 4 for G.fast [134]. This thesis tried to incorporate handshake procedures that are relevant to illustrate the successful operation of the GTU-C/GTU-R modem pair. The detailed implementation of G.994.1 is outside the scope of this thesis.

4.7.2 51.750 kHz signalling family

Carrier frequencies for this GDSL family will be Q x 51.750 kHz, where $Q \in \mathbb{N}_1$. The symbol rate will be 51,750 / 8 = 6,468.75 symbols per second. In G.994.1 certain carrier sets, consisting of 3 carriers, are defined for transmission of messages. For the GDSL family, a signalling carrier, with subchannel index n_{pilot}, for pilot tones and message exchange is defined before every RB of L_{fsp} carriers. The GDSL RB carrier set thus consists of all carriers such that:

$$n_{pilot} \in \{1, 66, 131, 196, \ldots, 4031\} \tag{4.5}$$

A starting signal carrier is inserted at the starting carrier as defined by the bypass policy for other xDSL services. As an example, using the VDSL2 Profile 30a bypass policy, the starting carrier is 586. The starting carrier is inserted at 586; the GDSL RB carrier set then consist of carriers 586, 651, 716, ..., 4031 (54 RBs or RB carriers). Maximum power per carrier is limited to -12.86 dBm (-60 dBm/Hz).

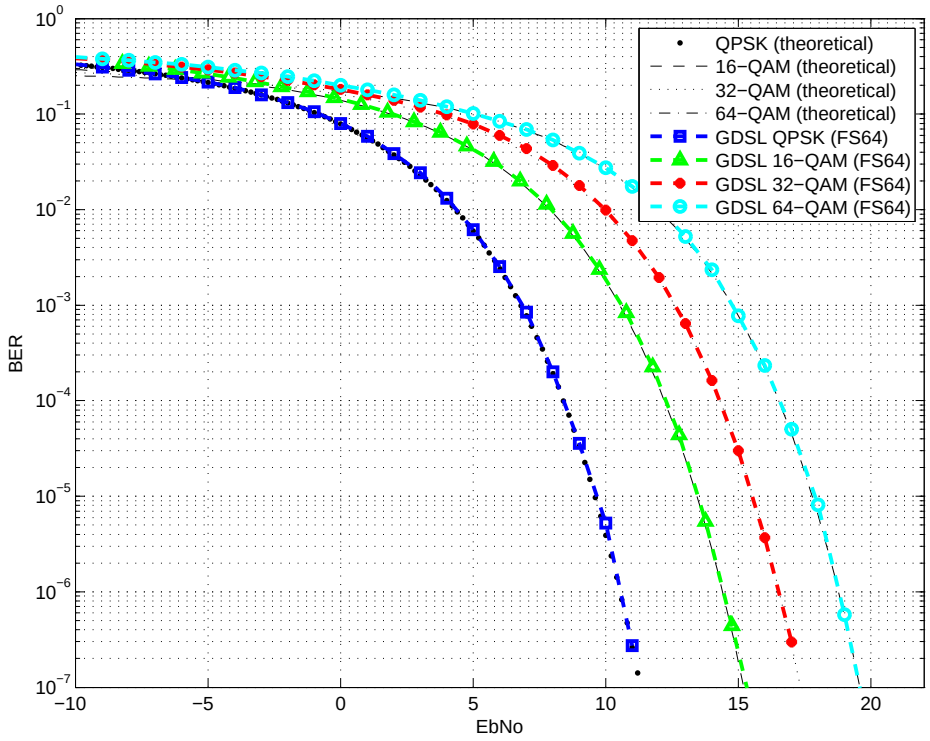

Figure 4.14. BER for GDSL system with $L_{fsp} = 64$ frequency spreading.

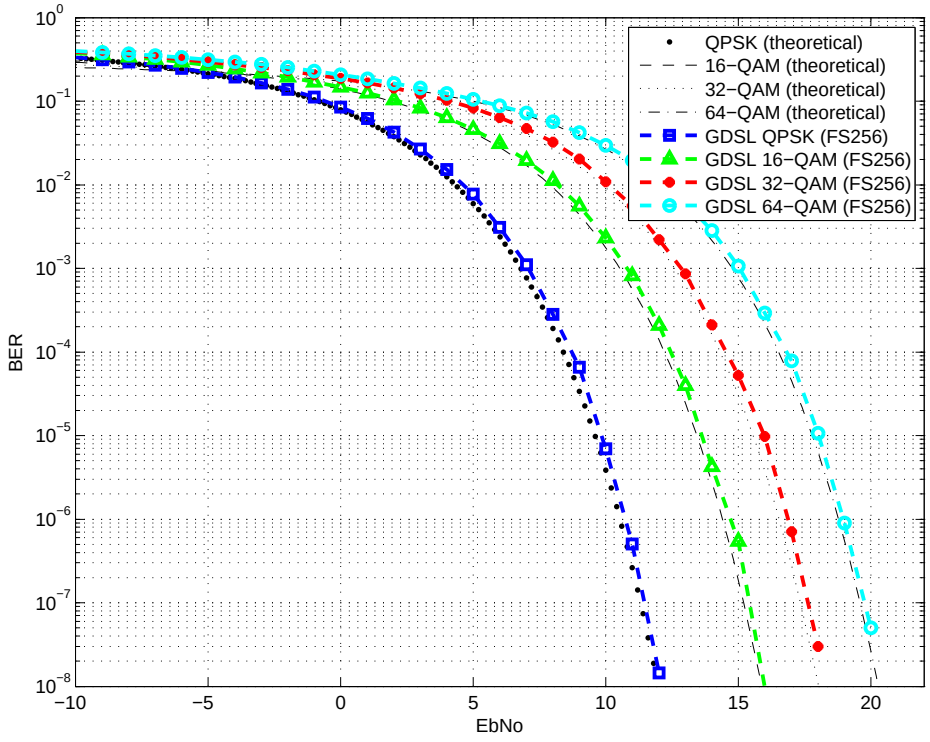

Figure 4.15. BER for GDSL system with $L_{fsp} = 256$ frequency spreading.

4.7.3 Modulation

All messages in ITU-T G.994.1 are sent with one or more carrier sets. During initialization, all carrier frequencies within a carrier set are simultaneously modulated with the same data bits using differentially encoded binary phase shift keying (DPSK). The transmit point is rotated 180° from the previous point if the transmit bit is a 1, and the transmit point is rotated 0° from the previous point if the transmit bit is a 0.

During `Showtime`, the starting carrier set can be used for general message exchange, while the individual RB carriers are used for RB related message exchange, like for example, the exchange of code masks (which spreading codes to use).

4.7.4 Link states

The link state and activation/deactivation procedures has two link states (*L0* and *L3*), and also contain the procedures that allow the modem to change from one link state to another. *L*3 is the state where the modem is provisioned through a management interface for the service desired by the operator. In this state, the modem does not transmit any signal. In the *L*3 link state, a Gigabit Terminal Unit (GTU) may determine to activate the initialization procedure defined in Section 4.7.5. *L*0 is a state achieved after the initialization procedure has completed successfully, commonly referred to as `Showtime`. In this state, the link transports user information with standard performance characteristics. The modem returns to the *L*3 state upon guided power removal (*L*3 Request), power loss or persistent link failures during `Showtime` [11].

4.7.5 Initialization procedures

During the G.994.1 handshake phase of the initialization procedure, the GTUs exchange capability lists and agree on a common mode for training and operation using the G.994.1 protocol. A successful completion of the G.994.1 handshake phase will lead to either the channel discovery phase of initialization or the loop diagnostic mode (depending on which one is selected). Failure of the G.994.1 handshake phase leads back to the *L*3 state.

During the channel discovery, training, and channel analysis and exchange phases of initialization, the GTUs train their respective transceivers after identifying the common mode of operation. During these phases, the transceivers identify channel conditions, exchange parameters for `Showtime` operation, etc. After successful completion of the initialization procedure, the transceivers switch to the *L*0 state (`Showtime`). Upon unsuccessful completion of the initialization procedure, the GTUs return to the *L*3 state.

Initialization of a GTU-C/GTU-R pair includes the following main tasks:

- Definition of a common mode of operation (profile, band plan and initial values of basic modulation parameters);
- Synchronization (sample clock alignment and symbol alignment);
- Transfer from the GTU-C to the GTU-R of transmission parameters, including information on the PSD masks to be used, RFI bands (e.g. amateur radio bands) to be protected, and target data rates in both transmission directions;
- Channel identification;
- Noise identification;
- Calculation of framer, interleaver, and coding parameters, as well as the bit loading and gain tables;
- Exchange of modem parameters (including RS / LDPC settings, interleaver parameters, framer settings, bit loading and gain tables).

The common mode of operation is negotiated during the G.994.1 handshake phase. The modem starts the initialization process by only measuring the background noise, also referred to as Quiescent Line Noise (QLN), and determining an average QLN profile (including background noise and other interferers). Random bits, represented by a Gray-encoded QPSK constellation (at maximum power per carrier of -12.86 dBm (-60 dBm/Hz)) is then sent on each carrier. Tones are attenuated through the wireline channel (as described by the Insertion loss profile of the channel - $Hlin$ is the linear profile and $Hlog$ is the logarithmic profile). Also, background noise and other interfering signals are added. The receiver receives each of the distorted tones, and needs to estimate the average received signal. The measured SNR ($SNR_{measured}$) is determined as the ratio of the received noisy signal to

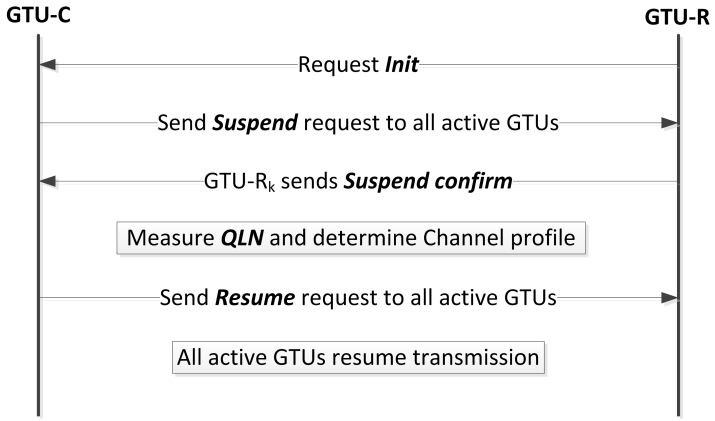

Figure 4.16. Flow diagram illustrating what happens if a GDSL modem is powered up and/or starts initialization (Init).

the QLN profile (background noise). The actual SNR profile used (SNR_{used}) for conventional DSL systems is $SNR_{margin} = \Gamma = 10$ dB (for a BER=10^{-7}) lower than the measured SNR. Since the designed system offers unique operation under crosstalk conditions, other compatible modems will be placed in a suspended transmission mode to allow a modem that is busy with initialization to only measure the background noise, and not interfering noise. Afterwards, transmission is resumed. This is illustrated in Figure 4.16. Note that the initializing modem will only start transmission on the next cycle of code allocation (referred to as the Code Change Rate (CCR)), as described in Section 6.6. The Digital Subscriber Access Multiplexer (DSLAM or GTU-C) will determine the CCR and execute the Code Allocation process (`Code_alloc_GDSL`) at the CCR intervals.

4.8 NOTCHING OF SPECIFIC FREQUENCY BANDS

GTUs can notch one or more specific frequency bands in order to protect radio services; for example, amateur radio bands or broadcast radio bands. These bands are defined as notch masks, which can be activated as needed. These bands are defined in Appendix I and II of ITU G.9700 [7].

4.9 CO-LOCATION WITH OTHER XDSL SERVICES

The proposed system is designed to provide MUI-free and FEXT-free communication for all GDSL transceivers. If other services like ADSL / ADSL2+ / VDSL / VDSL2 and its variants are also present

Table 4.1. GDSL starting carrier and corresponding starting frequency for different xDSL bypass policies

xDSL service	Bandwidth used (MHz)	GDSL starting carrier	Frequency (MHz)
ADSL	1.104	66	3.441
ADSL2+	2.208	66	3.441
VDSL2 Profile 8a/b/c	8.832	196	10.169
VDSL2 Profile 12a/b	12	261	13.533
VDSL2 Profile 17a	17.664	391	20.260
VDSL2 Profile 30a	30	586	30.351

within the same binder as the GDSL services, the GDSL modem will not be able to remove their FEXT. The best work-around is to completely avoid the effected frequency areas (not allocate any bits). This is accomplished by changing the starting subchannel (RB_{start}) of the Spreading bit allocation algorithm. Table 4.1 summarizes the applicable xDSL standards, their occupied bandwidth, the GDSL starting subchannel and the starting frequency. ADSL2+ and VDSL2 profiles are obtained from ITU G.992.5 [28] and G.993.2 [11] standards, respectively. Figure 4.17 shows the throughput rate comparison between standard bitloading (no spreading or bypass policy) and L_{fsp} = 64 spreading with ADSL2+ bypass policy applied, assuming a 10% total overhead for error correction coding and other protocol overheads. It should be observed that a GDSL system with no bypass policy can obtain 1 Gbps over a 190 m length (blue curve). When the ADSL2+ bypass policy is applied, 1 Gbps aggregate throughput can be obtained over a 185 m length of 0.5 mm diameter copper wire (red curve). Figure 4.18 shows how the spreading bit allocation is adjusted when a VDSL2 Profile 30a bypass policy is applied.

Figure 4.19 shows the throughput rate comparison between standard bitloading (with no spreading or bypass policy) and L_{fsp} = 64 spreading with VDSL2 Profile 30a bypass policy applied. It should be observed that 1 Gbps aggregate throughput can be obtained over a 148 m long 0.5 mm diameter copper pair when a VDSL2 Profile 30a bypass policy is applied.

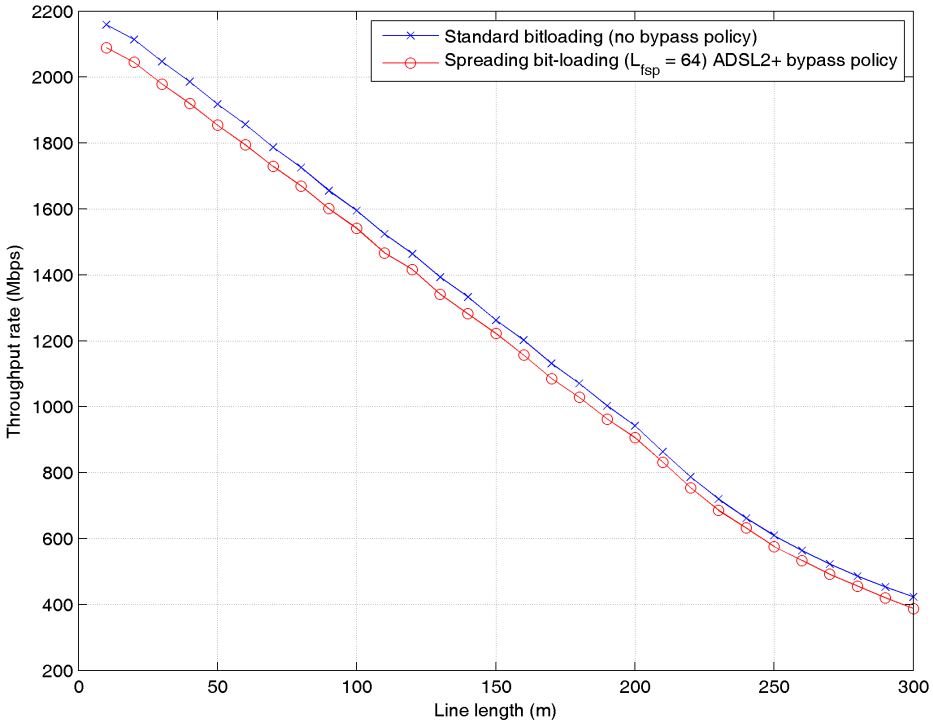

Figure 4.17. Throughput rate (Mbps) without spreading and bypass policy (blue crosses), compared to L_{fsp} = 64 spreading with ADSL2+ bypass policy (red circles) vs. line length.

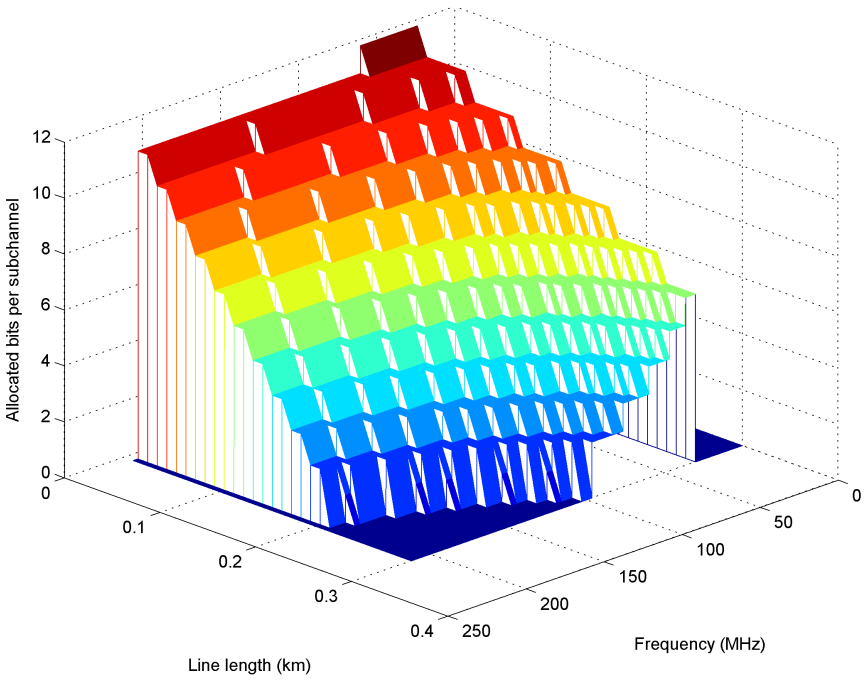

Figure 4.18. Bit allocation per subchannel with L_{fsp} = 64 spreading when VDSL2 Profile 30a bypass policy is applied vs. line length and frequency.

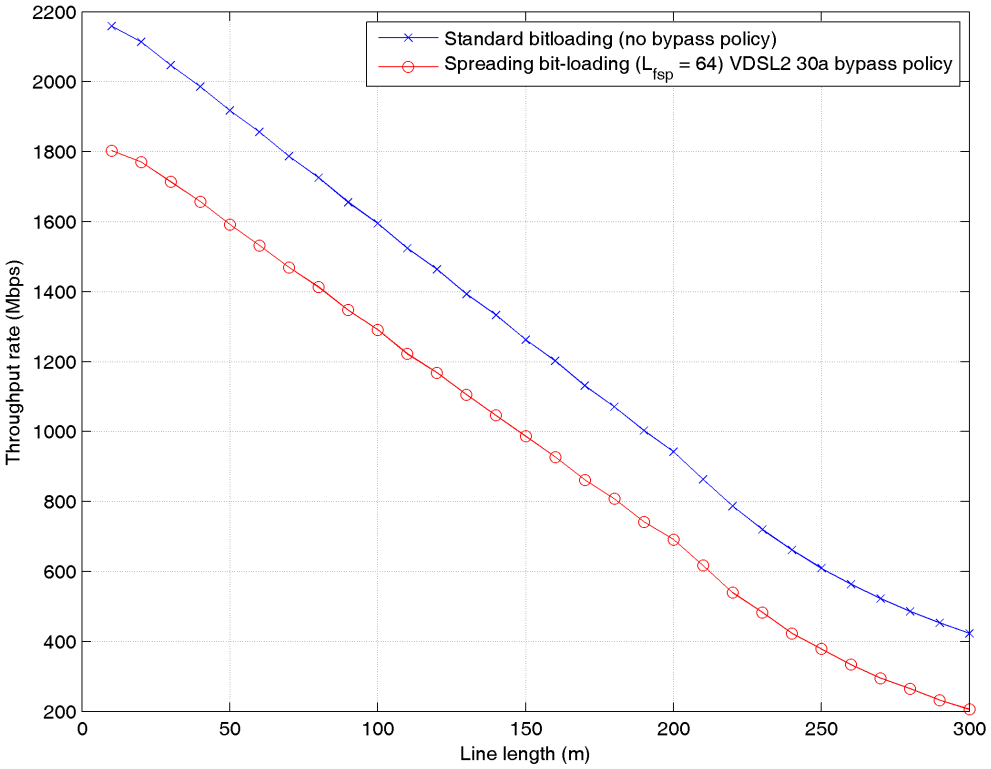

Figure 4.19. Throughput rate (Mbps) without spreading and bypass policy (blue crosses), compared to L_{fsp} = 64 spreading with VDSL2 Profile 30a bypass policy (red circles) vs. line length.

CHAPTER 5 SIMULATION MODEL AND RESULTS

5.1 INTRODUCTION

In this chapter the simulation model of the GDSL system is discussed in Section 5.2. A detailed encoding example is also provided to explain how the RS/LDPC encoding and modulation queues work. In Section 5.3.1 basic transmitter/receiver results of the GDSL modem are provided. In Section 5.3.2 the operation of the SOCC in the NEXT/FEXT environment is analysed and BER tests are performed, using a practical MIMO crosstalk environment.

5.2 SIMULATION MODEL

A SIMULINK-like simulation model is shown in Figure 5.1.

At the transmitter, bits to be transmitted need to be converted to bytes, since the RS encoder/decoder pair operate on byte-sized codewords ($GF(256)$). If the information is already in byte format (like files stored on your computer), it can be sent directly to the RS encoder. The encoding process for LDPC is shown in Figure 5.2, but is similar for RS. With a RS(255,239) encoder, 1912 (239*8) data bits converted to 239 data symbols will be input to the RS encoder, which will then produce 255 encoded symbols at its output. These 2040 encoded bits will be placed in a queue for the M-QAM modulator. This process is repeated as long as there are bits to be transmitted, else the Modulator queue is padded with zeros and a zero padding message, indicating the number of padding zeros, is sent to the receiver.

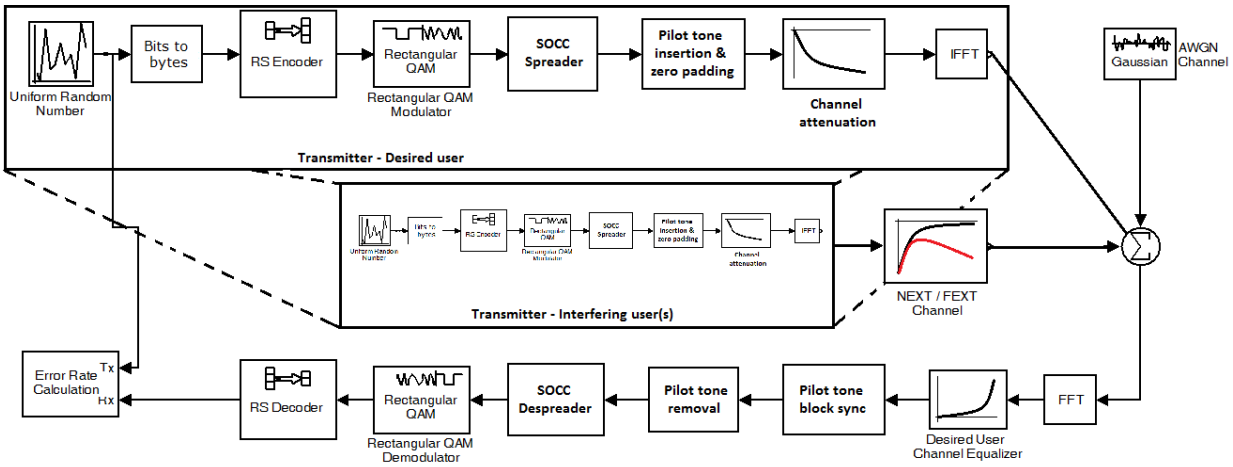

Figure 5.1. Simulation model of the GDSL system. The transmitter is shown top left (boxed) and the receiver bottom right. Interfering users have the same transmitter structure, as indicated by the hashed lines.

Based on the *BpRB* allocated per RB, bits will be taken from the Modulator queue and a corresponding M-QAM symbol will be created. This symbol is then sent to the SOCC Spreader, where it is spread with its unique allocated code within the current RB. The modulation / spreading process above is repeated within the current RB till all allocated spreading codes are used, and then also for all active RBs. The resultant will be a super-vector of spreaded symbols over the 4096 subchannels. The next step is to add the pilot symbols or messages, depending on which ones are used. Channel attenuation is performed in the frequency domain, rather than the time domain, since it is a multiplication process, rather than a slow convolution process. The IFFT process is then performed to create a time signal which spans $1/\Delta f = 1/51{,}750 = 19.323\ \mu s$.

In Figure 5.3 detailed encoding messages of a modem operating over a 200 m length 0.5 mm diameter copper wire, with RS(255,239) coding, square root raised cosine filtering and VDSL30a bypass active, are shown. The transmitter starts with 999.998 Mbits of data, as indicated in line [1]. A RS(255,239) encoder takes 1,912 bits (239 bytes) at a time and encodes it to 2,040 bits (255 symbols), which are placed in a modulator queue [3]. The encoding process continues till enough bits are available for the modulator (indicated by the long red bar, [1] to [24]). The total number of modulator bits for every FFT block of 19.323 μs is the sum over all active RBs, of the product of the bits per RB (*BpRB*) and the number of spreading codes allocated per RB (*CpRB*). Obtaining *BpRB*, as well as the code allocation algorithm is discussed in Chapter 6. For this encoding example, the modulator takes 15,936 bits

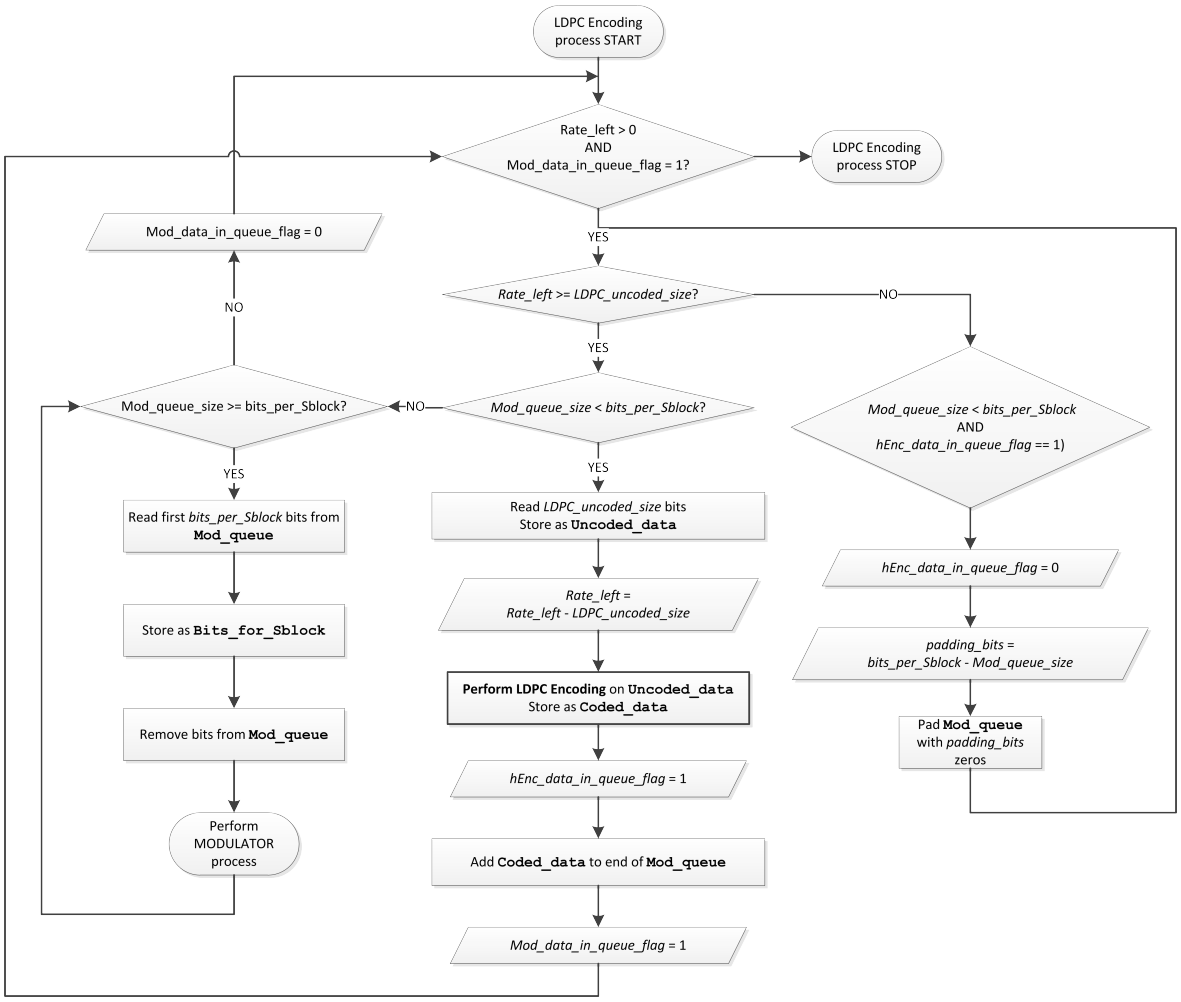

Figure 5.2. Flow diagram showing the forward error correction coding process for LDPC (similar for RS) and how coded bits are added to the Modulator queue.

(16,320-384) every 19.323 μs (indicated by the short green bar, 24 to 26), giving a total throughput of 824.688 Mbps, for a 200 m 0.5 mm twisted pair.

For all interfering users, the resultant signal after channel attenuation is sent through the NEXT/FEXT channel (once again a multiplication process in frequency), followed by the IFFT process. In Figure 5.1 this process is indicated as a convolution process in time (transmitter followed by the NEXT/FEXT channel).

For the receiver, the effect of AWGN as well as adding all interfering users (with associated crosstalk coupling) are performed by the summation function ($\sum$). Channel equalization is performed in the frequency domain, followed by block synchronization using the pilot tones. The pilot tones are then

```
TRANSMITTER
Rate left = 999.998 Mbits
....RS encode
Mod_queue size: 2040
Rate left = 999.996 Mbits
....RS encode
Mod_queue size: 4080
Rate left = 999.994 Mbits
....RS encode
Mod_queue size: 6120
Rate left = 999.992 Mbits
....RS encode
Mod_queue size: 8160
Rate left = 999.990 Mbits
....RS encode
Mod_queue size: 10200
Rate left = 999.989 Mbits
....RS encode
Mod_queue size: 12240
Rate left = 999.987 Mbits
....RS encode
Mod_queue size: 14280
Rate left = 999.985 Mbits
....RS encode
Mod_queue size: 16320
..Modulate
Mod_queue size: 384
Rate left = 999.983 Mbits
....RS encode
Mod_queue size: 2424
Rate left = 999.981 Mbits
....RS encode
Mod_queue size: 4464
Rate left = 999.979 Mbits
....RS encode
Mod_queue size: 6504
Rate left = 999.977 Mbits
....RS encode
Mod_queue size: 8544
```

Figure 5.3. Detailed messages of the RS FEC encoding and modulation process for a 200 m length 0.5 mm diameter copper wire.

removed, despreading and demodulation performed for each unique set of codes for each RB, over all active RBs. Bits are once again placed in a Decoder queue, which is then used by the RS decoder. The decoding process for LDPC is shown in Figure 5.4. With a RS(255,239) decoder, 2040 (255*8) bits are converted to 255 symbols, used as input to the RS decoder, which will then produce 1912 bits (239

symbols) at its output.

Figure 5.4. Flow diagram showing the forward error correction decoding process for LDPC (similar for RS) and how decoded bits are added to the Demodulated queue.

5.3 SIMULATION RESULTS

5.3.1 Basic Transceiver Results

The measured SNR is averaged over a number of IFFT/FFT blocks. With an FFT block (OFDM block) signal duration of 1/Δf = 1/51,750 = 19.323 μs, either 5, 52, 518, 5,175 or 51,750 FFT blocks are respectively needed for averaging over 100 μs, 1 ms, 10 ms, 100 ms or 1 s. A comparison was made for 0.5 mm diameter line lengths of 0 m (no attenuation), 100 m, 200 m, and 300 m respectively, implementing the VDSL2 Profile 30a bypass policy. The real and imaginary parts of the transmitted signal (blue) and the received signal (red), as a function of time, are shown in Figs. 5.5-5.8.

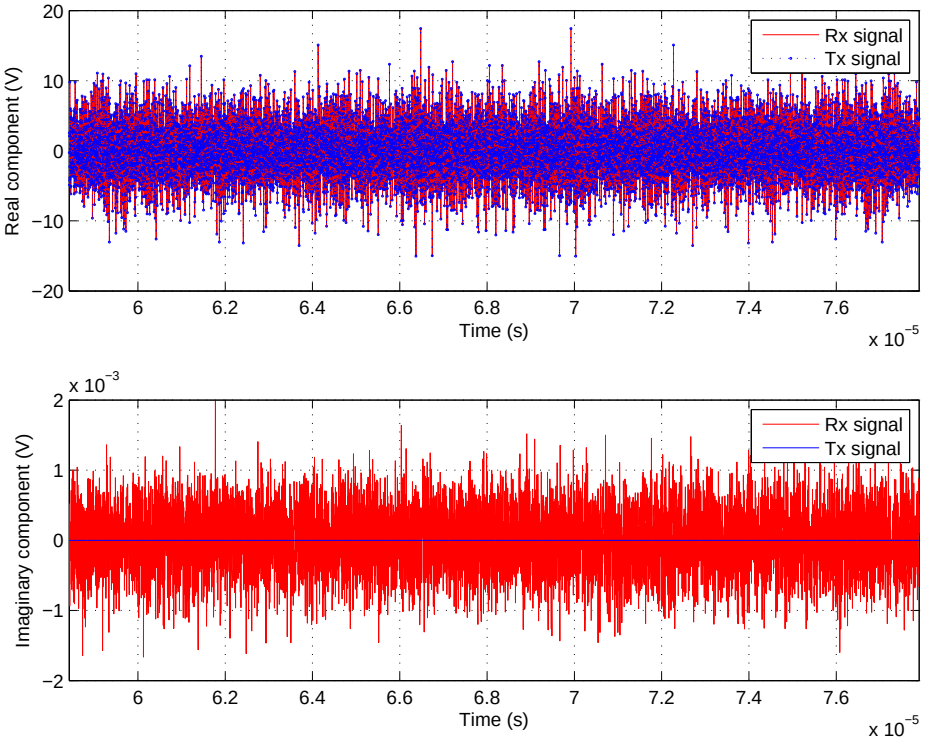

Figure 5.5. Real and imaginary representation of the transmitted signal (blue) and the received signal (red) for a 0 m long 0.5 mm diameter twisted copper pair.

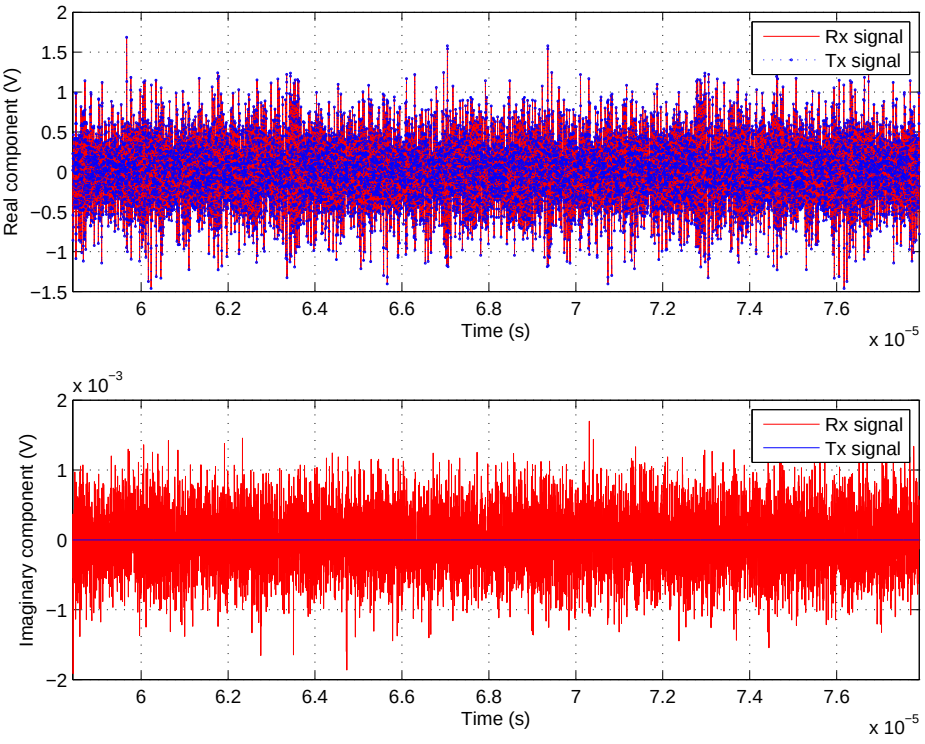

Figure 5.6. Real and imaginary representation of the transmitted signal (blue) and the received signal (red) for a 100 m long 0.5 mm diameter twisted copper pair.

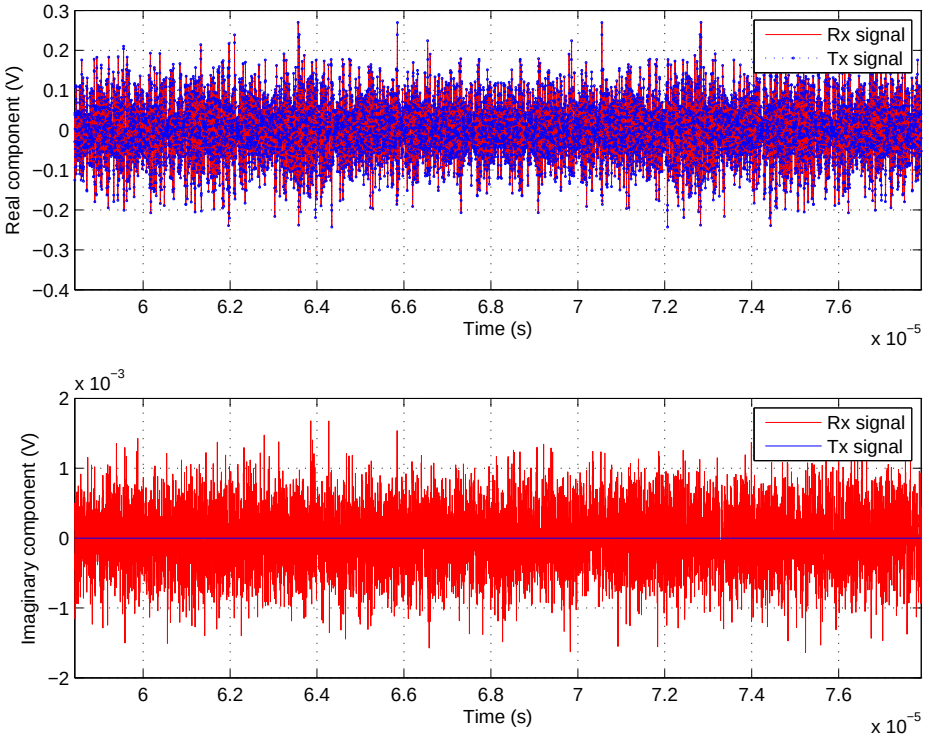

Figure 5.7. Real and imaginary representation of the transmitted signal (blue) and the received signal (red) for a 200 m long 0.5 mm diameter twisted copper pair.

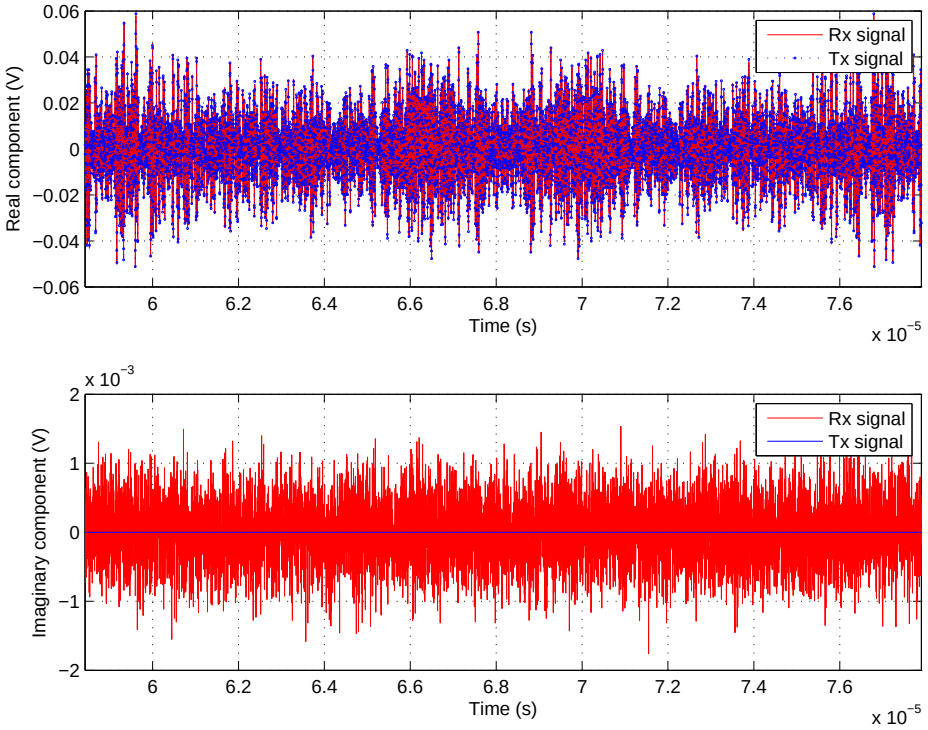

Figure 5.8. Real and imaginary representation of the transmitted signal (blue) and the received signal (red) for a 300 m long 0.5 mm diameter twisted copper pair.

Note that the imaginary component of the transmitted signal is zero, due to the Hermitian symmetry of the IFFT/FFT, as explained in Section 4.4.5 and shown in Figure 4.2 (p. 54). PSDs and SNRs for 100 ms averaging, for various line lengths, are shown in Figs. 5.9-5.12 and Figs. 5.13-5.16 respectively.

It should be observed that the averaging time is acceptable to provide a statistically smoothed profile where the effect of AWGN is smoothed out. The vertical lines that are visible in the PSDs and SNRs indicate the position of the pilot tones / RB signalling carriers.

An example of the pilot tones inserted (2x (6 dB) amplified) is shown in Figure 5.17. In Figure 5.18 the Amateur radio band mask (purple), FM radio mask (green) and DVB-T band mask (blue) is shown.

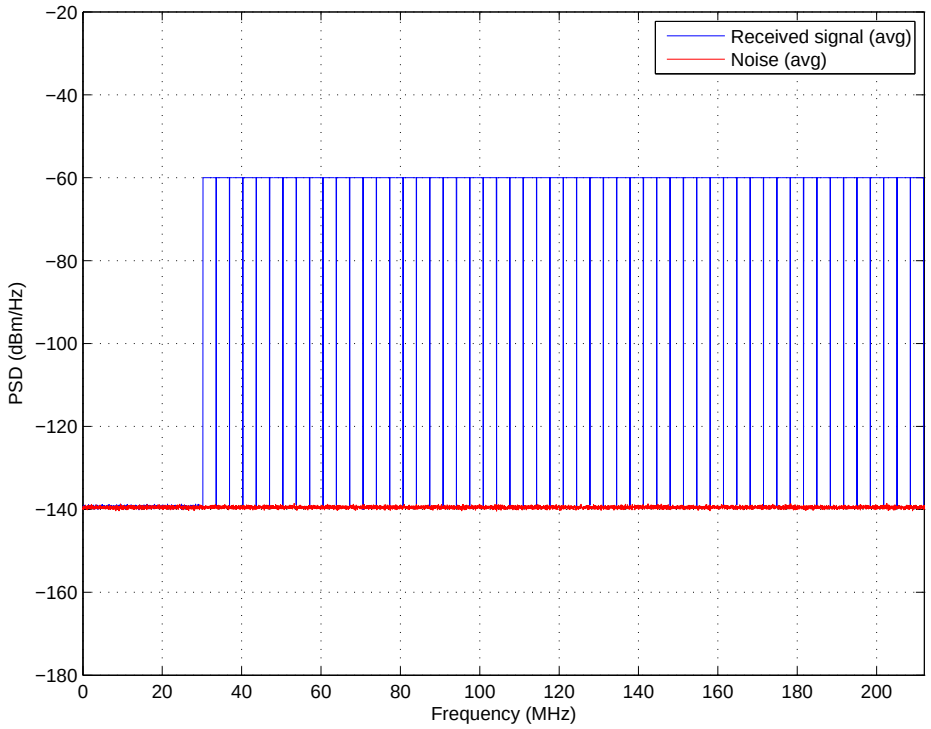

Figure 5.9. Power spectral density at the receiver for a 0 m long 0.5 mm diameter twisted copper pair.

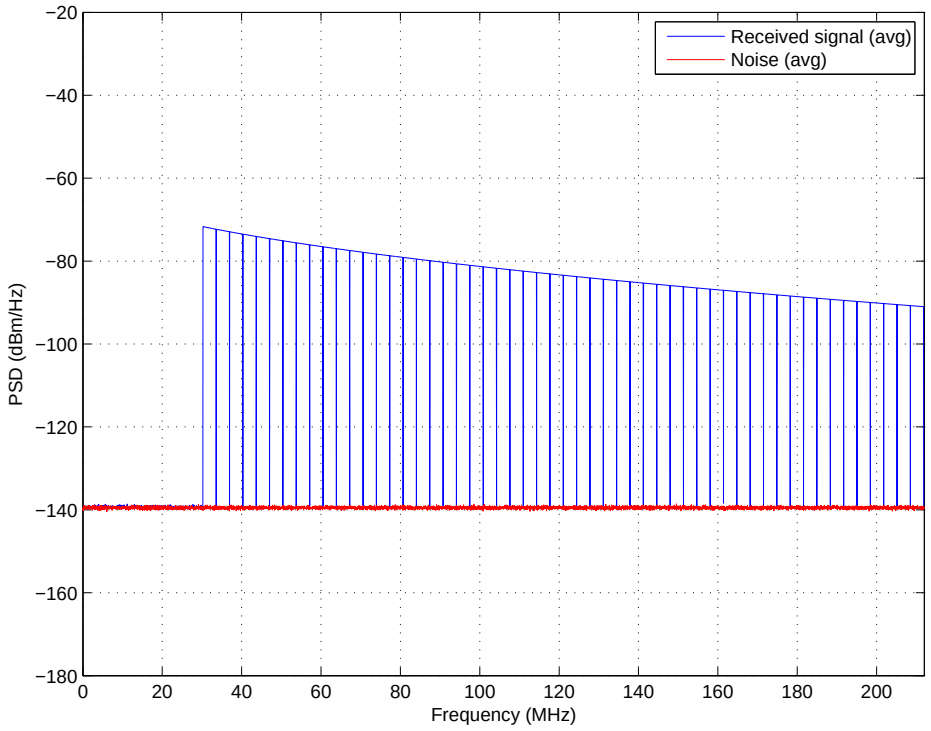

Figure 5.10. Power spectral density at the receiver for a 100 m long 0.5 mm diameter twisted copper pair.

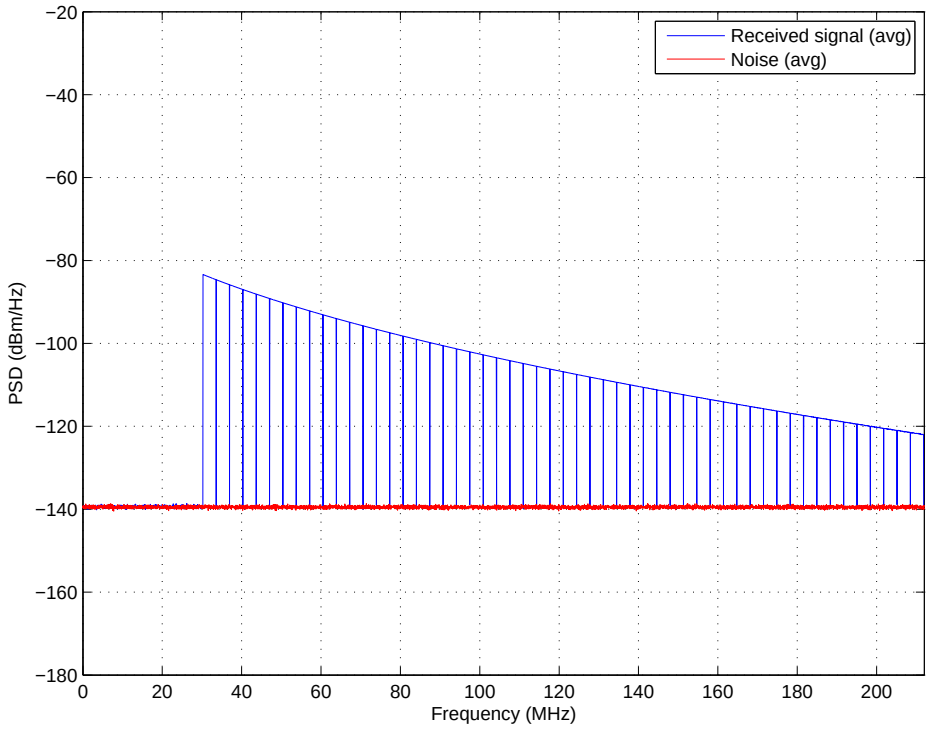

Figure 5.11. Power spectral density at the receiver for a 200 m long 0.5 mm diameter twisted copper pair.

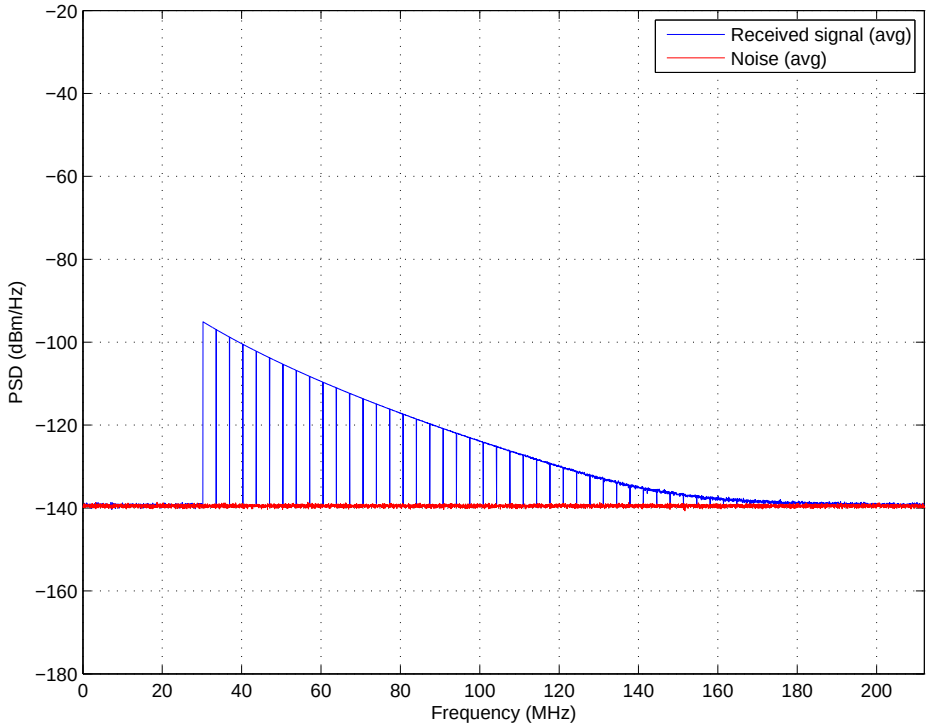

Figure 5.12. Power spectral density at the receiver for a 300 m long 0.5 mm diameter twisted copper pair.

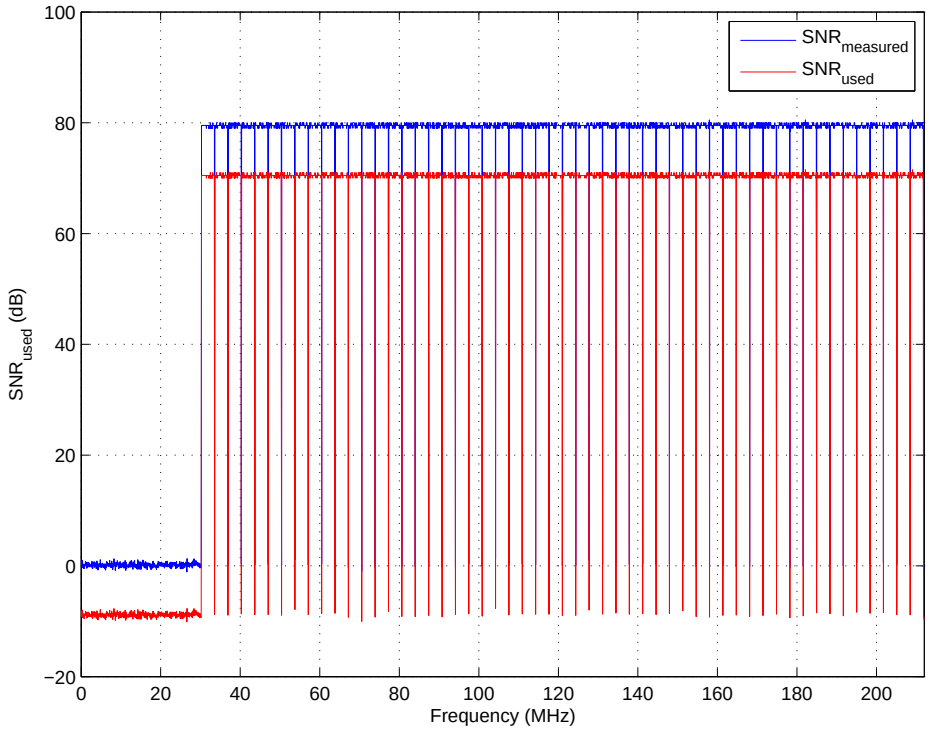

Figure 5.13. $SNR_{measured}$ and SNR_{used} for a 0 m long 0.5 mm diameter twisted copper pair.

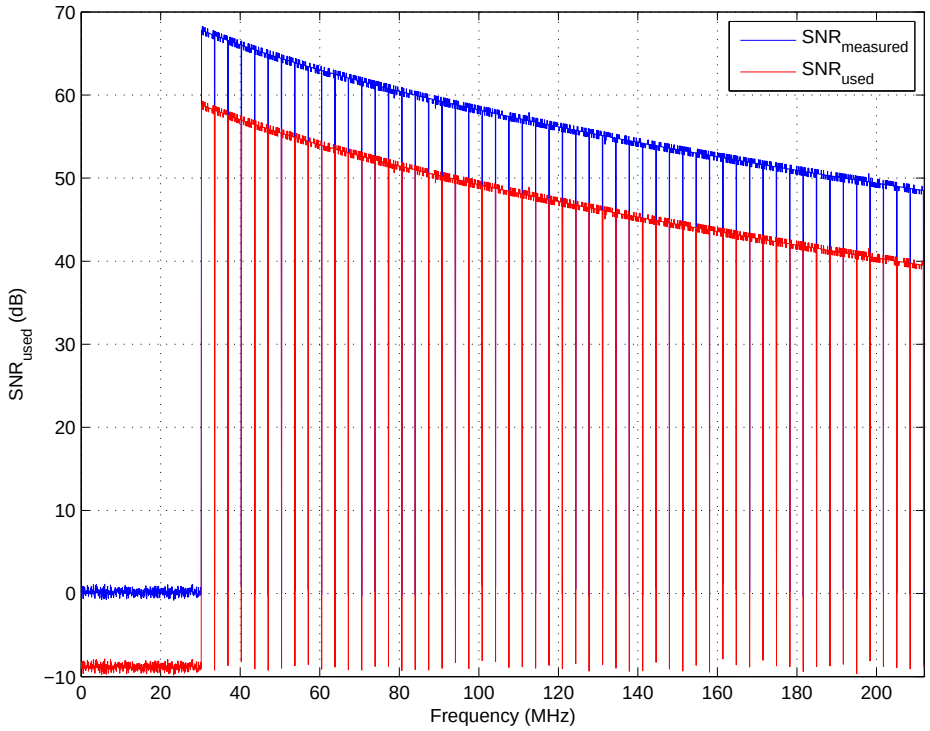

Figure 5.14. $SNR_{measured}$ and SNR_{used} for a 100 m long 0.5 mm diameter twisted copper pair.

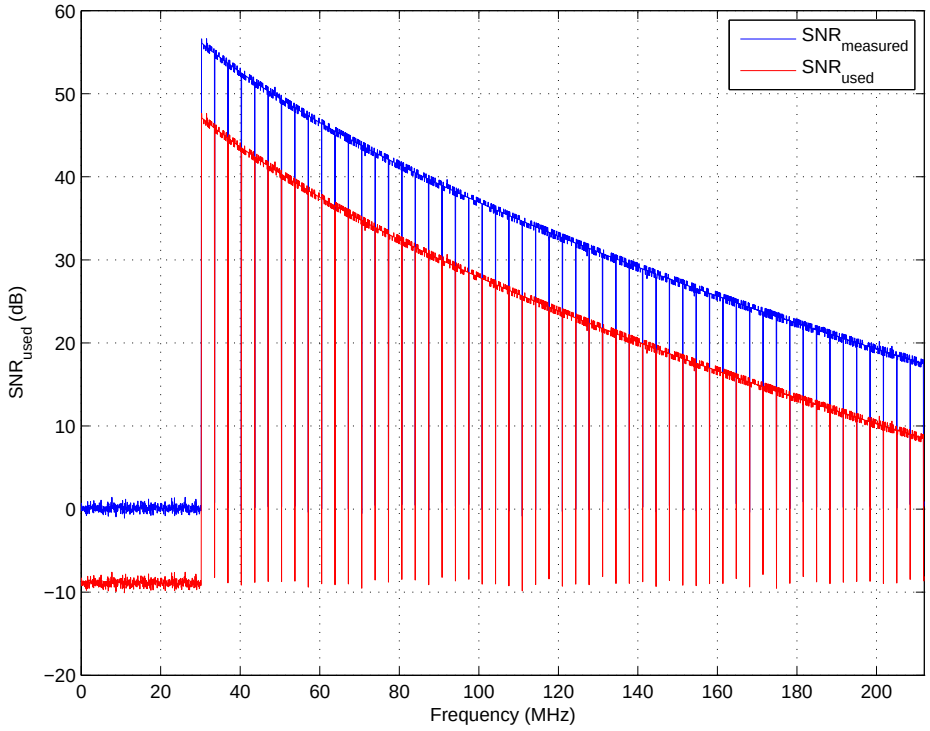

Figure 5.15. $SNR_{measured}$ and SNR_{used} for a 200 m long 0.5 mm diameter twisted copper pair.

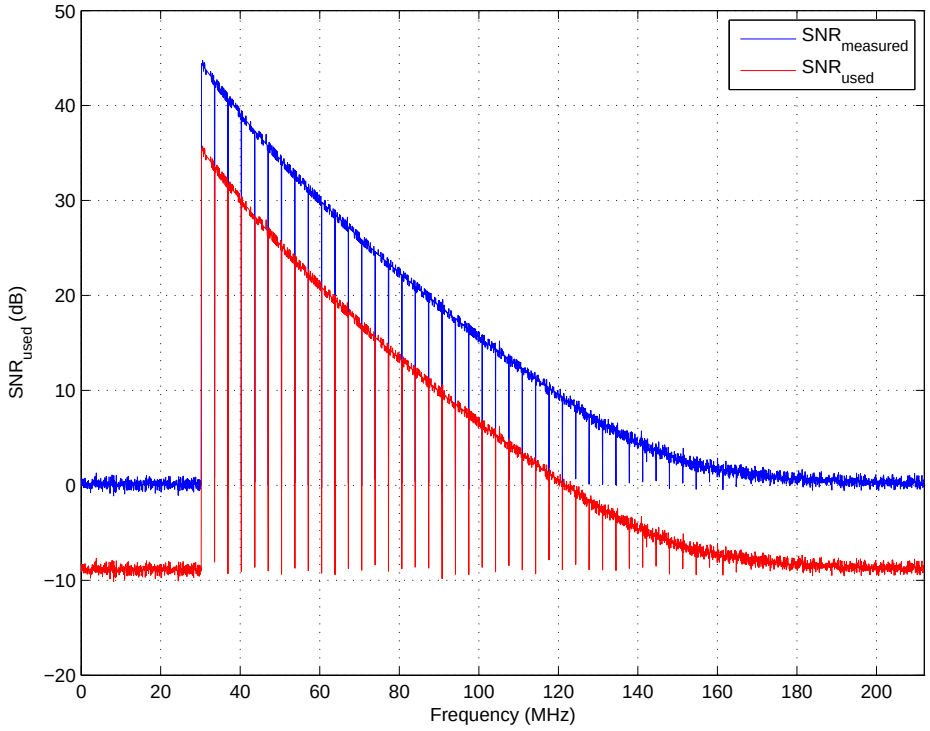

Figure 5.16. $SNR_{measured}$ and SNR_{used} for a 300 m long 0.5 mm diameter twisted copper pair.

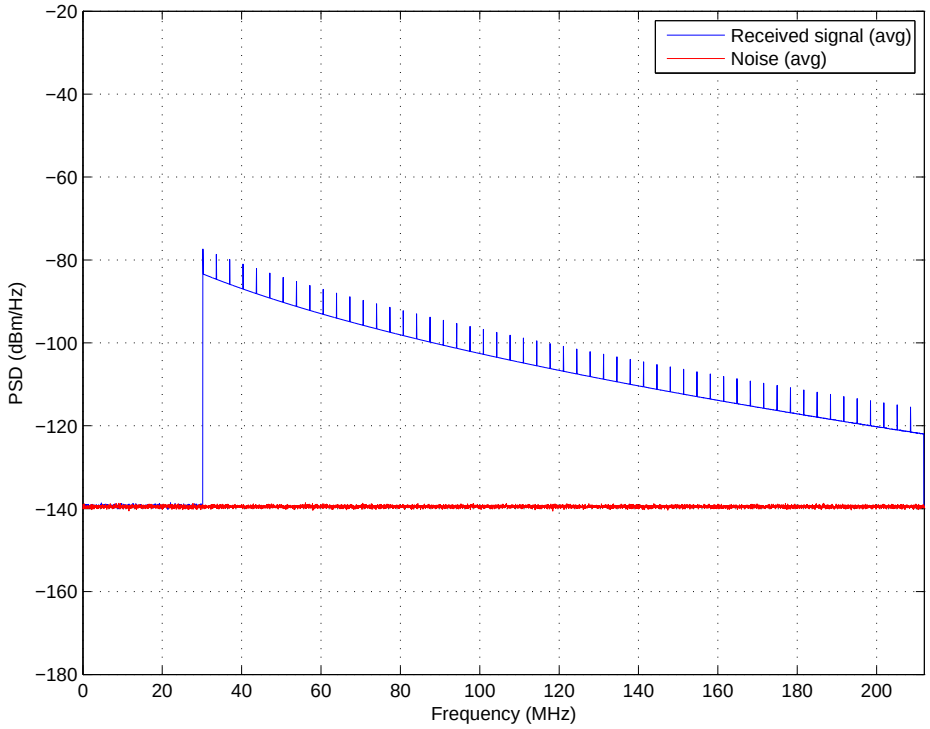

Figure 5.17. Power spectral density at the receiver with 6 dB amplified pilot tones inserted for a 200 m long 0.5 mm diameter twisted copper pair.

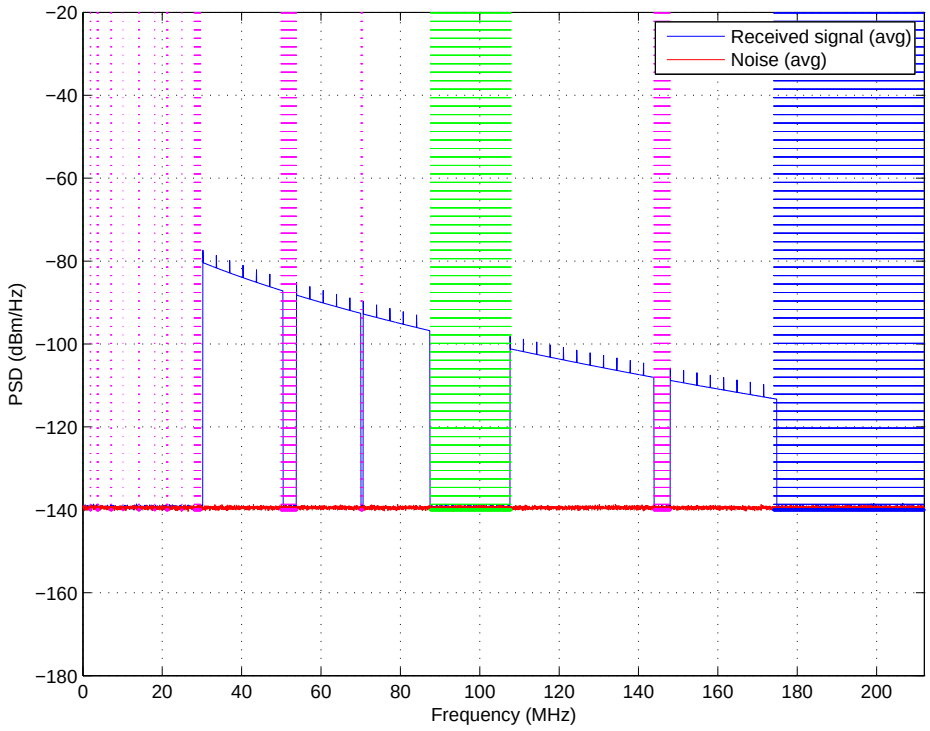

Figure 5.18. Power spectral density at the receiver with 6 dB amplified pilot tones and HAM, FM AND DVB-T masks applied for a 200 m long 0.5 mm diameter twisted copper pair.

If these profiles are activated, the bit mask profile (bit allocated per tone or RB) will be made zero - during code allocation and modulation, no information (bits) will be transmitted in these bands. All pilot tones are also zeroed. In Figure 5.19 the effect of square root raised cosine filtering on the high frequency tail from 200 MHz is shown.

5.3.2 SOCC correlation properties in a NEXT/FEXT environment

In order to determine how the SOCC spreading codes will perform under NEXT and FEXT conditions, the disturbing signal (including background noise, NEXT interferer and/or FEXT interferer) should be considered. It is equivalent to determining the Interference Noise. Referring to Figure 3.12, consider the case of sending information downstream for User i. If Tx_{DOWN} have a power spectrum of $S_{DOWN}(f)$, the transmitter's received version at the downstream receiver (Rx_{DOWN}) will be $S_{DOWN}(f).\mid H_{ins}(f)\mid^2$ (basically an attenuated version of the transmitter's spectrum). The interfering received signal from User(s) j will be a power sum of NEXT and FEXT terms [135], each respectively of the form $S_{UP}(f).NEXT(f)$ and $S_{DOWN}(f).FEXT(f)$. If N_o is the background noise, the Interference Noise

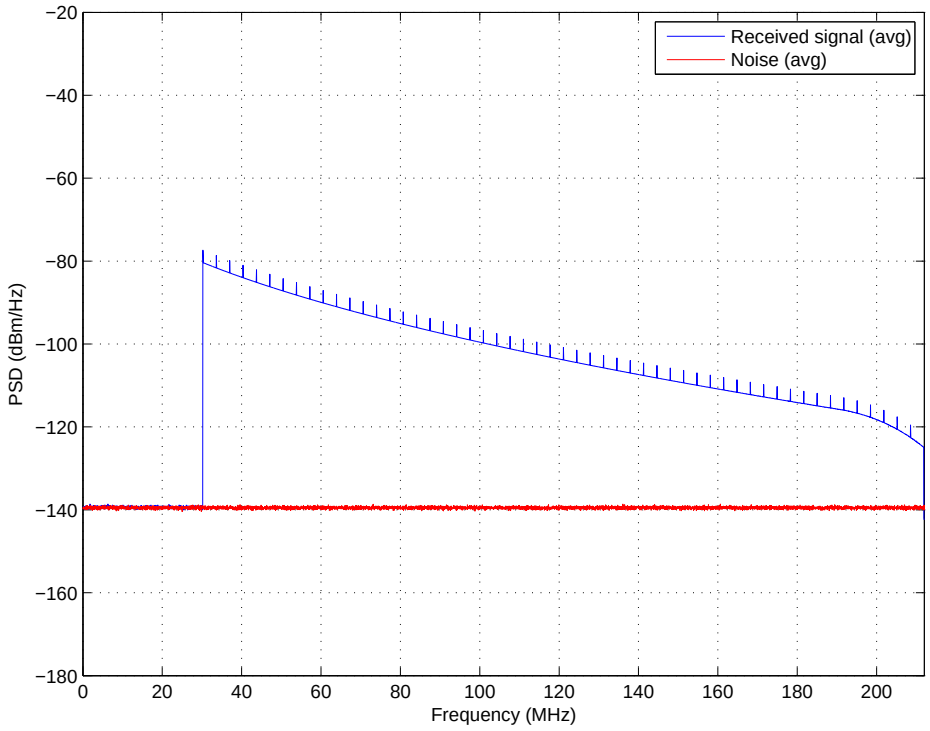

Figure 5.19. Effect of square root raised cosine filtering for a 200 m long 0.5 mm diameter twisted copper pair.

will be:

$$N_{\text{int}} = N_0 + \left(\frac{N_j}{N_{dis\_total}}\right)^{0.6} .S^j_{up}(f).NEXT(f) + \left(\frac{N_j}{N_{dis\_total}}\right)^{0.6} .S^j_{down}(f).FEXT(f) \qquad (5.1)$$

for all Users j.

During Modem Initialization the channel attenuation profile is determined and synchronized between the GTU-C and GTU-R. Since both receivers of User i have knowledge of the channel, the 1-tap decision feedback equalizer (DFE) can remove the effect of insertion loss. This is equivalent to dividing the received signal by $|\,H_{ins}(f)\,|^2$. The equalized Interference Noise then becomes:

$$N_{\text{int}} = \frac{N_0}{\left|H^i_{ins}(f)\right|^2} + \left(\frac{N_j}{N_{dis\_total}}\right)^{0.6} .\frac{S^j_{up}(f).NEXT(f)}{\left|H^i_{ins}(f)\right|^2} + \left(\frac{N_j}{N_{dis\_total}}\right)^{0.6} .\frac{S^j_{down}(f).FEXT(f)}{\left|H^i_{ins}(f)\right|^2} \qquad (5.2)$$

where N_j is the number of similar disturbers from Users j and N_{dis_total} is the total number of disturbers. Note that the equalization is performed using the channel profile of User i. Considering Figure 3.13, NEXT and FEXT (for short loops) provide the most detrimental effect for current xDSL systems. It

can be observed from this figure that the crosstalk coupling is relatively high (where a higher negative valued dB value means lower coupling and vice versa). NEXT is usually avoided by using a FDD approach (upstream and downstream bands in separate frequency bands) or a TDD approach (sending upstream packets and downstream packets after each other).

The GDSL system was tested for different users using only 99% worse case NEXT coupling, with operation in the lowest RB (RB1), as shown in Figure 5.20, and in the highest RB (RB63), as shown in Figure 5.21 ('4 Users' mean that there is the desired user and 3 other NEXT coupled users). It can be observed that the performance for up to 16 users are still acceptable, but for up to 64 users the performance deteriorates. In Figure 5.22 a 64 users QPSK system is used to compare NEXT and FEXT for different line lengths (l = 10 m, 100 m and 200 m respectively). The system performance is acceptable for line lengths of 100 m or more, provided that NEXT is not present.

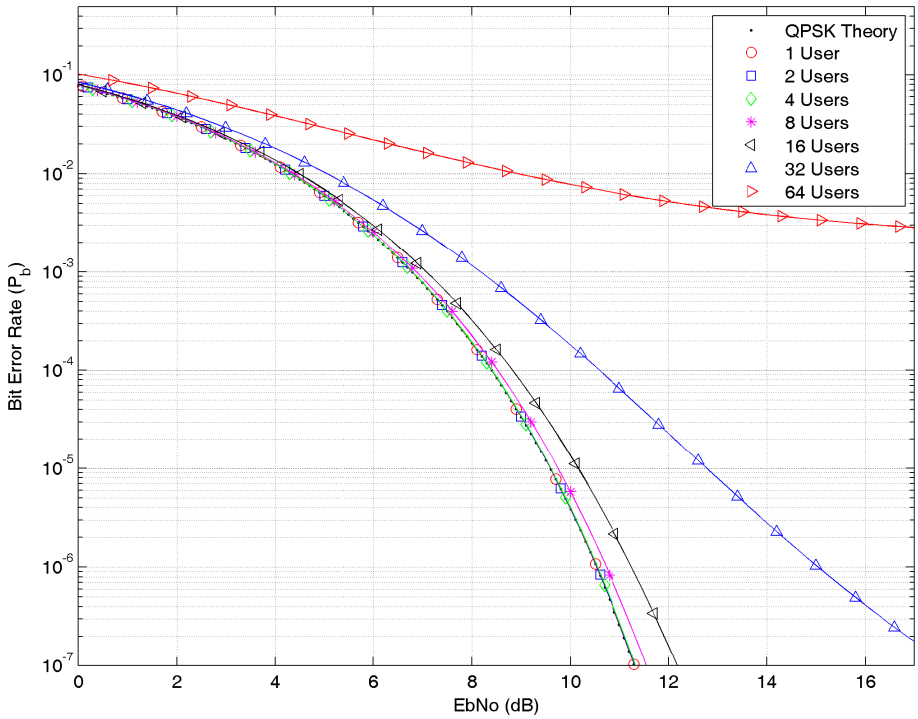

Figure 5.20. BER for a QPSK system for different NEXT coupled users, operating in the lowest frequency Resource Block (RB1).

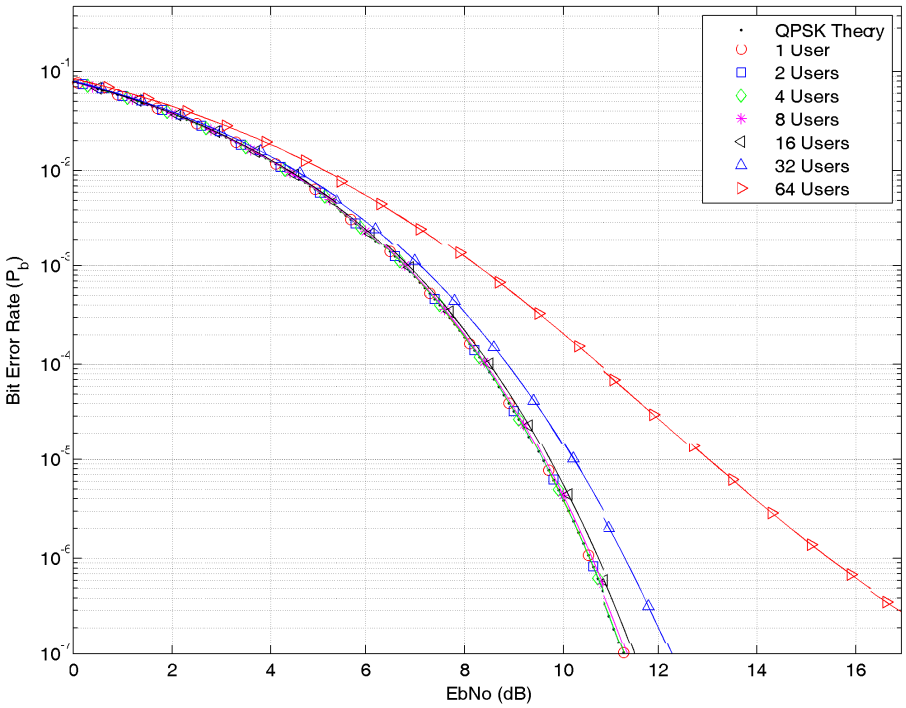

Figure 5.21. BER for a QPSK system for different NEXT coupled users, operating in the highest frequency Resource Block (RB63).

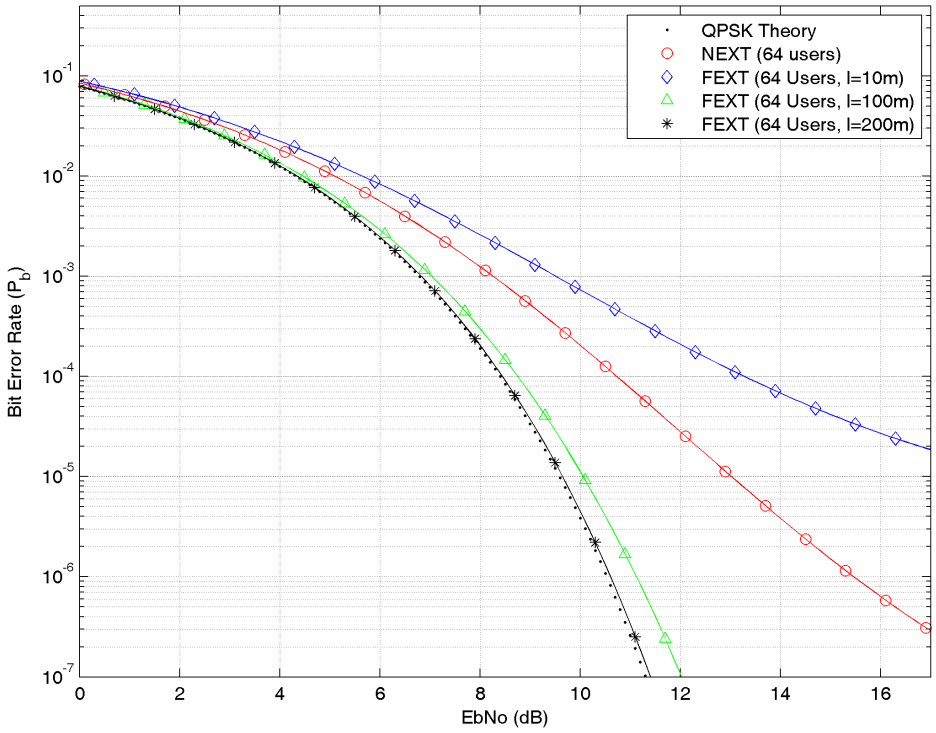

Figure 5.22. BER for a 64 users QPSK system, comparing NEXT and FEXT (l = 10 m, 100 m and 200 m respectively) for the high frequency Resource Block (RB63).

In Section 3.8.2 a more practical MIMO Crosstalk model is explained. If crosstalk coupling attenuation values X_{dB} of Table 3.2 are also taken into consideration, the performance for low and high RBs respectively, are shown in Figure 5.23 and Figure 5.24. It can be observed that the performance for up to 64 users are still acceptable. In Figure 5.25 a 64 users QPSK system is used to compare NEXT and FEXT (l = 10 m, 100 m and 200 m respectively) when practical crosstalk coupling attenuation (XdB) values are also taken into account. The system performance is acceptable, even with NEXT and FEXT at a very short line lengths of 10 m. The non-linear behaviour of NEXT and FEXT creates

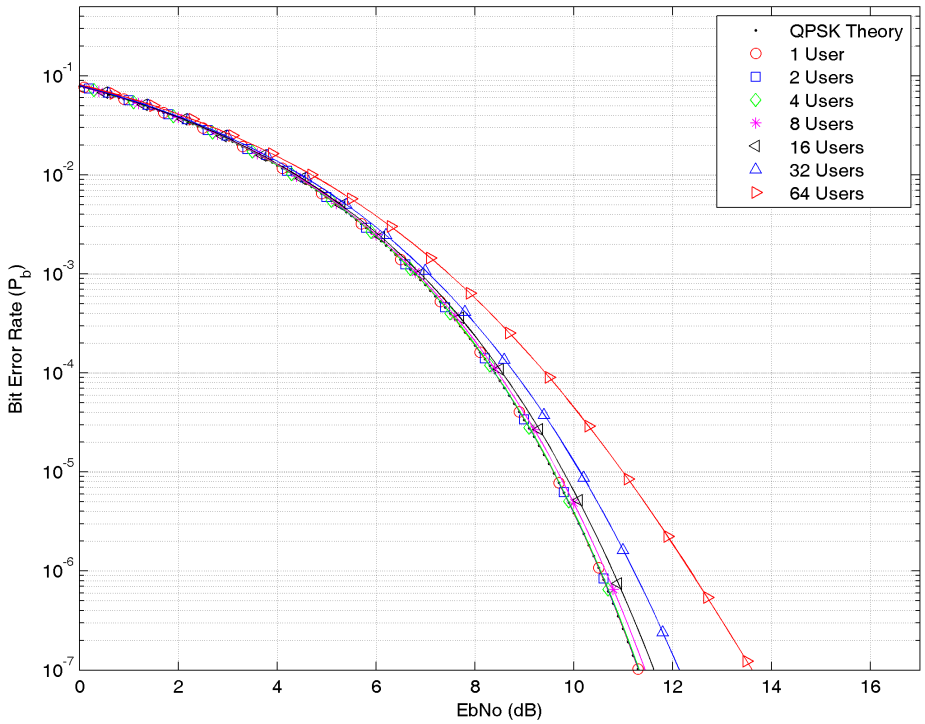

Figure 5.23. BER for a QPSK system for different NEXT coupled users, with practical MIMO model, operating in the lowest frequency Resource Block (RB1).

an orthogonality distortion effect on the correlation properties of the SOCC family. The attenuation level of the relevant NEXT / FEXT function also plays a role in further amplifying this effect. This is evident when comparing Figure 5.20 and Figure 5.21, with Figure 3.13 used to determine the degree of non-linearity (the gradient of the respective crosstalk functions at low and high frequencies).

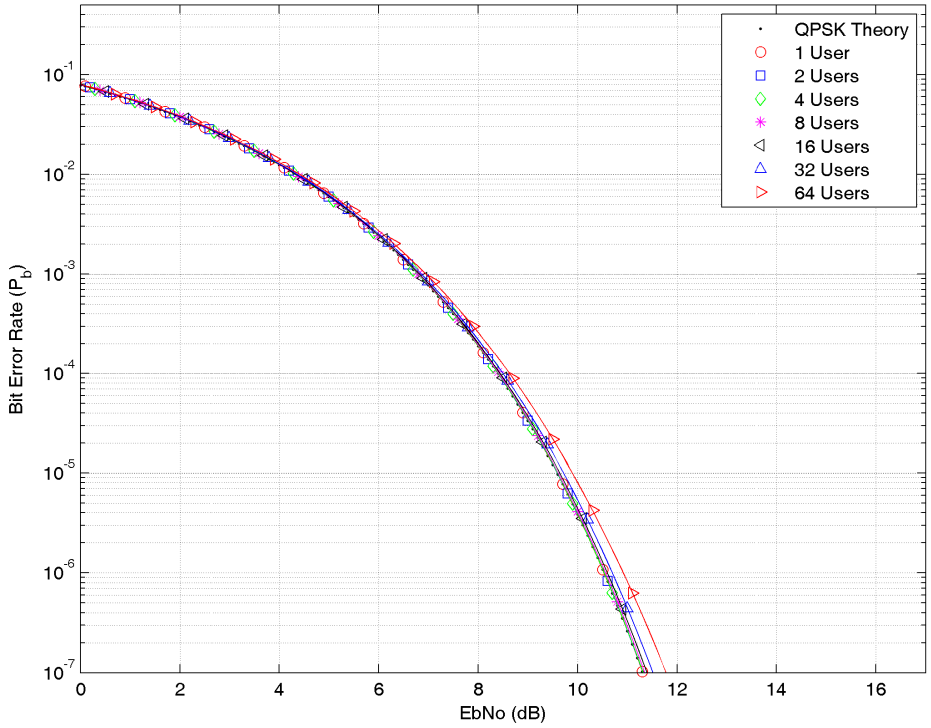

Figure 5.24. BER for a QPSK system for different NEXT coupled users, with practical MIMO model, operating in the highest frequency Resource Block (RB63).

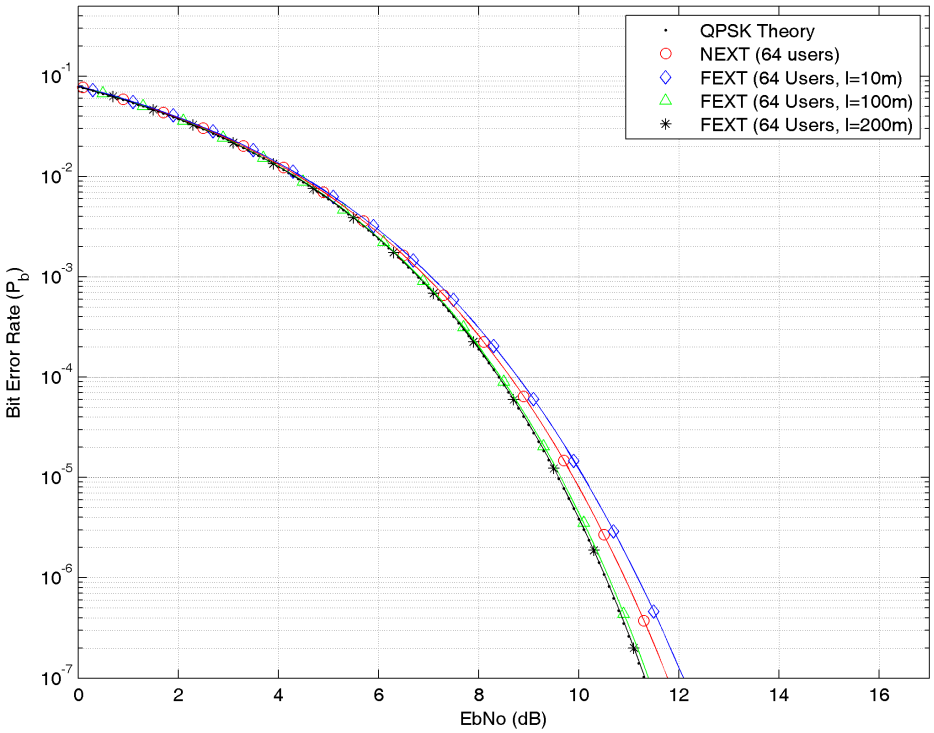

Figure 5.25. BER for a 64 users QPSK system, with practical MIMO model, comparing NEXT and FEXT (l = 10 m, 100 m and 200 m respectively) for the high frequency Resource Block (RB63).

5.4 CHAPTER SUMMARY

In this chapter the simulation model of the GDSL system was described and simulation results presented. The BER analysis performed proved that the GDSL system, using SOCC frequency spreading, is capable of operating in a heavily NEXT/FEXT dominated environment under full-load conditions (64 users), even for very short line lengths (extreme FEXT conditions), to provide MUI-free communication.

CHAPTER 6 RESOURCE BLOCK CODE ALLOCATION ALGORITHM

6.1 INTRODUCTION

This chapter describes the novel code allocation algorithm (CAA) that was designed to ensure that unique codes are allocated to all active users for each of the active or used RBs. RBs were described in Section 4.5. General operation of the CAA is described in Section 6.2. In Section 6.3 the determination of the Bit allocation per RB ($BpRB$) profile is discussed, followed by a detailed description of the CAA in Section 6.4. A detailed example is provided in Section 6.5. In Section 6.6 the operation of the GDSL modem under random data arrival is discussed, followed by a complexity analysis of the CAA in Section 6.7.

6.2 GENERAL OPERATION

The algorithm uses the offered number of bits of each user and the Bit allocation per RB ($BpRB$) profile to allocate spreading codes uniquely to each user, such that MUI-free operation is obtained and each user obtain the same ratio of transferred bits to offered bits. In extreme cases, users with bad or long line profiles (having a bit allocation profile that quickly becomes zero for higher frequencies) can also have a comparable good transfer ratio performance, since more codes are allocated to them in lower frequency RBs. Users with better line profiles are then allocated more codes in their higher frequency RBs. Users will also only use RBs (or equivalently higher spectrum) where codes have been allocated.

6.3 DETERMINATION OF BIT ALLOCATION PER RESOURCE BLOCK

During modem initialization, the BpT profile for the current user is obtained. Within the `Code_alloc_GDSL` process the BpT profile is converted to a *BpRB* profile for each user using Algorithm 1. This is to ensure that the bits per tone profile within a RB is uniform (the same) across all subchannels allocated to the RB.

Algorithm 1 Calculation of *BpRB* for RBs

```
1 for n = 1 step L_fsp to N,
2    temp = max([BpT(n), BpT(n+1), BpT(n+2), ..., BpT(n+L-1)]);
3    if temp > 15,
4      temp = 15;
5    end
6    if temp < 2,
7      temp = 0;
9    end
10   [BpRB(n), BpRB(n+1), BpRB(n+2), ..., BpRB(n+L-1)] = temp;
11   while ∑_{j=n}^{n+L-1} BpRB(j)-0.5 > ∑_{j=n}^{n+L-1} b(j),
12     BpRB(n:n+L-1) = BpRB(n:n+L-1) - 1;
13   end
14 end
```

To illustrate this principle, consider the bit allocation for a 200 m line, using $L_{fsp} = 64$ spreading, as shown in Figure 6.1. The standard bit allocation (*BpT*) is shown as red circles. The adapted spreading bit allocation (*BpRB*) is shown as blue crosses. It should be observed that there is little difference between the two bit allocations. The difference becomes more pronounced for $L_{fsp} = 256$. Figures 6.2 and 6.3 show a 3D plot of the spreading bit allocation per subchannel for $L_{fsp} = 64$ and $L_{fsp} = 256$ respectively, as a function of line length and frequency.

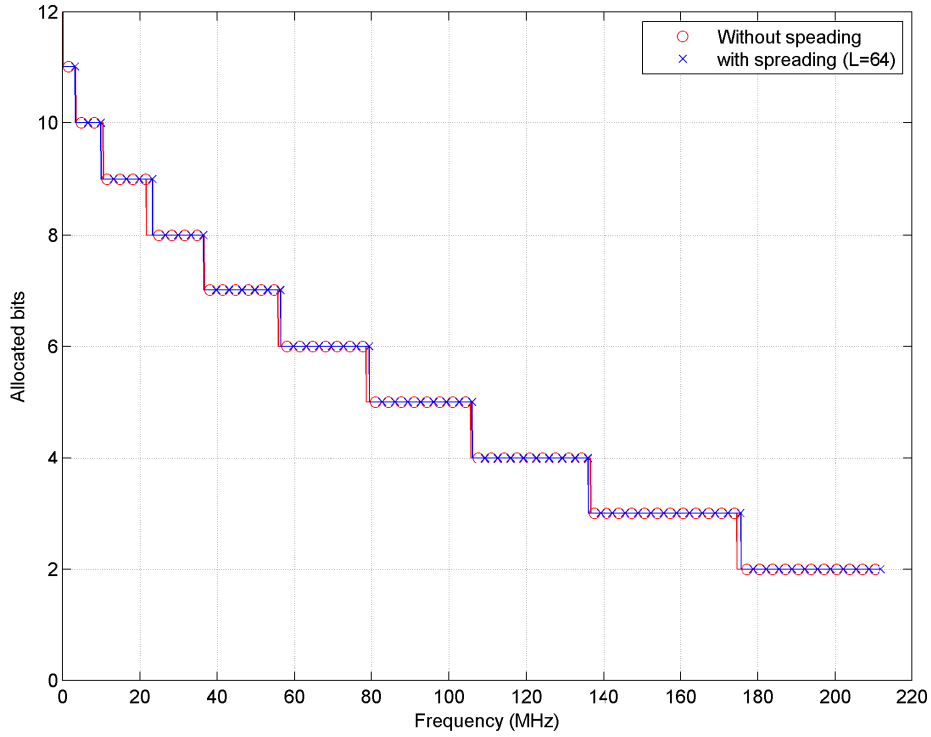

Figure 6.1. Bit allocation per subchannel without spreading (red circles) and with spreading (blue crosses) vs. frequency.

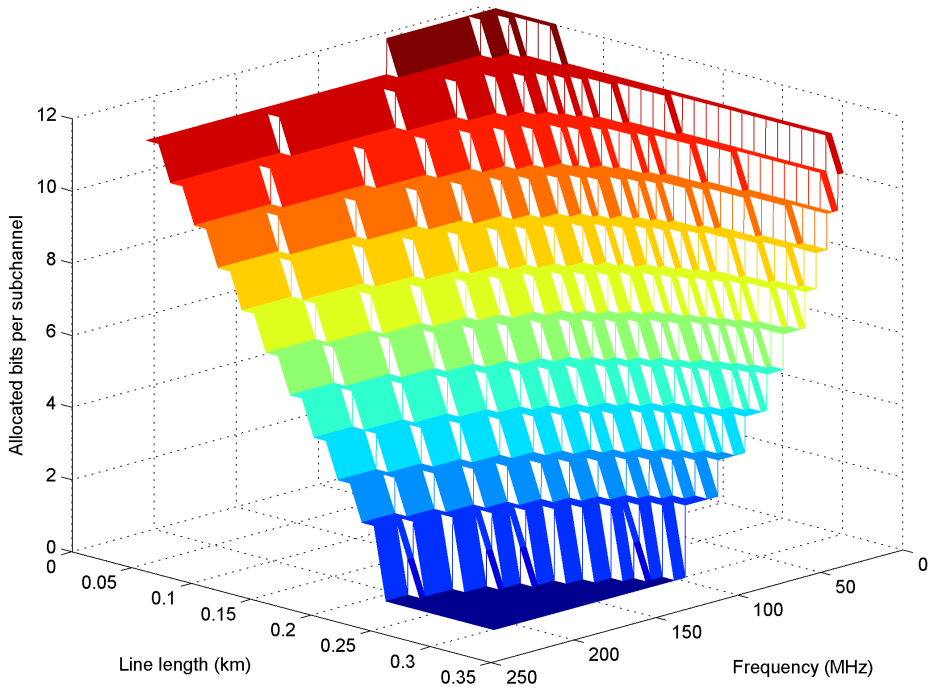

Figure 6.2. Bit allocation per subchannel with L_{fsp} = 64 vs. line length and frequency.

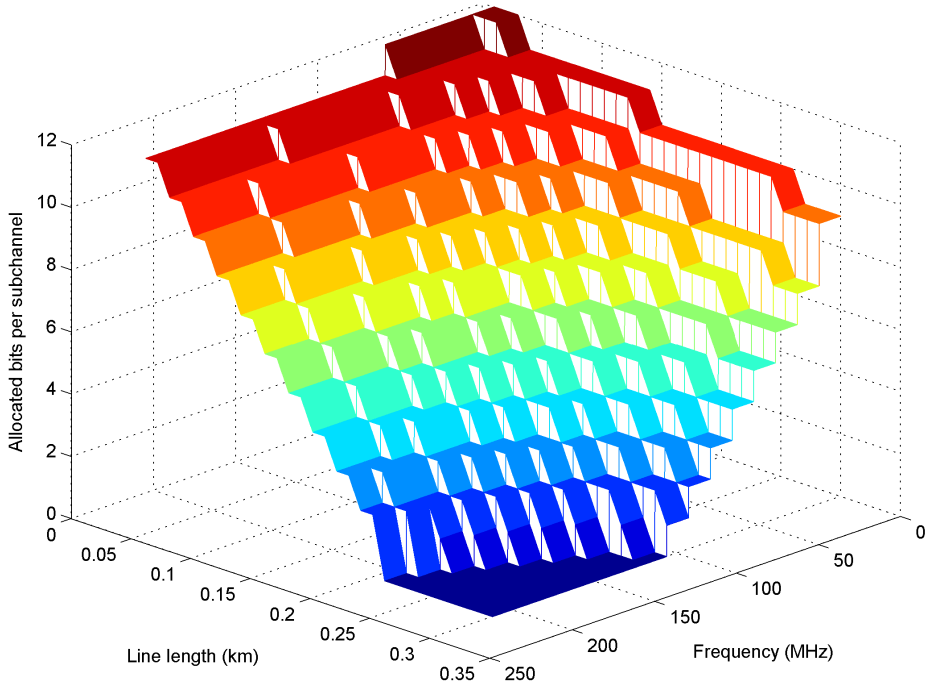

Figure 6.3. Bit allocation per subchannel with $L_{fsp} = 256$ vs. frequency.

6.4 CODE ALLOCATION ALGORITHM

The allocation of spreading codes is explained in Algorithm 2, where $Bits\_left$ is the offered bits that are left after processing the calculated bits to be sent for the current RB ($Bits\_used$), K is the number of active users in the system (up to L_{fsp}), M is the total number of RBs that are considered (based on the active bypass profile), $BpRB$ is the Bit allocation per RB based on the bit allocation profile of each user, $Codes\_RB$ is the number of allocated codes for the current RB, $\|\cdot\|$ is the nearest integer function and $\lfloor\cdot\rfloor$ is the floor function.

The CAA will also work based on the amount of data (MB) that needs to be transferred, or the required transfer rate (Mbps). To illustrate the operation of the algorithm, consider the detailed example in Section 6.5.

The CAA will typically be updated every 1.004831 ms (52 FFT blocks), 10.009662 ms (518 FFT blocks) or 100 ms (5175 FFT blocks). This has been incorporated using a Code Change Rate (CCR) parameter that should be provided to the `Code_alloc_GDSL` process. The allocated codes per RB should also be communicated to each user when changed. The code allocation process is also

Algorithm 2 Code allocation algorithm

Step 1: Specify the offered bits (Mb) of each user in the system as $Bits\_left$(k), for k = 1 to K (K the number of users)

Step 2: Obtain the bit allocation profiles based on RBs for each user as $BpRB$(k,m), for k = 1 to K and for m = 1 to M (M the total number of RBs)

Step 3: Iteratively calculate the codes allocated for each RB:

```
for m = 1 to M
  for k = 1 to K
    if BpRB(k,m) ≠ 0
      Bits_used(k,m) = Bits_left(k,m) - RB_bits(k,m-1)
      Determine ∑_{l=m+1}^{M} BpRB(k,l)
      Determine BpRB(k,m)_ratio from 5
      Codes_RB(k,m) = ‖BpRB(k,m)_ratio.L_fsp‖
      Determine RB_bits(k,m)
      if RB_bits(k,m) > Bits_left(k,m)
        Codes_RB(k,m) = ⌊RB_bits(k,m)/Bits_left(k,m)+1⌋
        Determine RB_bits_adj(k,m)
      end
  end
end
```

independently performed for upstream and downstream. For N = 4096 and $L_{fsp} = 64$ there are 63 RBs (refer to Section 4.5). For each user in each RB, the start index $CpRB_{start}$ and end index $CpRB_{end}$ of spreading codes to be used, should be communicated. As an example, if User 1 was allocated 9 codes ($Codes\_RB(1,m)$), it will use spreading codes 1 to 9; if User 2 was allocated 10 codes ($Codes\_RB(2,m)$), it will use spreading codes 10 to 19; and so on, up to say User 5, using spreading codes 36 to 64.

6.5 DETAILED EXAMPLE

Consider 5 users, each with 3 RBs and offered bits (here in kbits to keep the example small) as indicated in Table 6.1. User 1 has an average line profile $BpRB$ = [8, 6, 2] in the first 3 RBs. Users 2 and 3 have

Table 6.1. 5 Users' Bits per RB profiles ($BpRB$) and offered bits (kbits).

User	RB 1	RB 2	RB 3	Offered bits (kbits)
1	8	6	2	4
2	12	12	11	10
3	12	12	11	5
4	6	5	3	4
5	3	2	0	4

good profiles, but different offered bits. Users 4 and 5 have the same offered bits as User 1, but with worse line profiles. User 5's line profile is especially bad and for existing DSL systems not using the CAA, it will not nearly obtain its required transfer rate. It will be shown that the proposed algorithm adapts code allocation per RB to ensure that actual transfer ratios for all users lead to approximately the same transfer ratio.

For this example the CCR is 5 FFT blocks. User 2 only joins the CAA process during the 3rd FFT block of CCR Cycle 1. This will illustrate that User 2 will not take part in data transmission during CCR Cycle 1 and also how the CAA adapts over following CCA cycles to ensure the same transfer ratio for all users.

6.5.1 CCR Cycle 1

The CAA is executed. The CAA starts by setting $Bits\_left$ equal to the number of offered bits for each user. Since User 2 has not joined yet, its value is zero.

$$Bits\_left = \begin{bmatrix} 4000 \\ 0 \\ 5000 \\ 4000 \\ 4000 \end{bmatrix}$$

The status of $Codes\_RB$, as well as the number of bits transmitted per RB, for CCR Cycle 1 over 5 FFT blocks, as a function of time t (in μs), user and RB, is shown in Table 6.2 and Table 6.3 respectively. A summary of $Bits\_left$ after each FFT block, the total bits sent for CCR Cycle 1 and the transfer ratio are shown in Table 6.4.

Table 6.2. Status of *Codes_RB* for CCR Cycle 1.

t (μs) $\Rightarrow$	0			19.323			38.647			57.971			77.295		
FFT Block	1			2			3			4			5		
User	RB1	RB2	RB3	RB1	RB2	RB3	RB1	RB2	RB3	RB1	RB2	RB3	RB1	RB2	RB3
1	11	10	34	11	10	34	11	10	34	11	10	34	11	10	34
2	0	0	0	0	0	0	0	0	0	0	0	0	0	0	0
3	6	4	7	6	4	7	6	4	7	6	4	7	6	4	7
4	12	10	23	12	10	23	12	10	23	12	10	23	12	10	23
5	35	40	0	35	40	0	35	40	0	35	40	0	35	40	0

Table 6.3. Bits transmitted per RB for CCR Cycle 1.

t (μs) $\Rightarrow$	0			19.323			38.647			57.971			77.295		
FFT Block	1			2			3			4			5		
User	RB1	RB2	RB3	RB1	RB2	RB3	RB1	RB2	RB3	RB1	RB2	RB3	RB1	RB2	RB3
1	88	60	68	88	60	68	88	60	68	88	60	68	88	60	68
2	0	0	0	0	0	0	0	0	0	0	0	0	0	0	0
3	72	48	77	72	48	77	72	48	77	72	48	77	72	48	77
4	72	50	69	72	50	69	72	50	69	72	50	69	72	50	69
5	105	80	0	105	80	0	105	80	0	105	80	0	105	80	0

Table 6.4. *Bits_left* after each FFT Block, total bits sent at the end of CCR Cycle 1 and the transfer ratio.

t (μs) $\Rightarrow$	0	19.323	38.647	57.971	77.295		
FFT Block	1	2	3	4	5		
User	*Bits_left* (bits)					Total bits sent	Transfer ratio
1	3784	3568	3352	3136	2920	1080	27.00%
2	0	0	0	0	0	0	0
3	4803	4606	4409	4212	4015	985	19.70%
4	3809	3618	3427	3236	3045	955	23.875%
5	3815	3630	3445	3260	3075	925	23.125%

It should be observed for CCR Cycle 1 that:

- No codes are allocated to User 2, since it has not joined when the CAA was executed, and also not when it joined at FFT block 3. No data is also transmitted;

- The codes allocated does not change for the duration of the CCR cycle;
- The sum of all codes allocated per RB is not more than 64;
- User 5 is allocated more spreading codes to be able to transfer more bits relative to the other users in order to compensate for its bad profile;
- The bits transmitted per RB is equal to the product of the codes allocated to that RB (*Codes_RB*) and the Bit allocation profile for that RB (*BpRB*) for each user respectively.
  Example: For User 1, RB1 has 11 codes allocated to it (from Table 6.2). The *BpRB* in RB1 is 8 (from Table 6.1). The number of bits sent in RB1 is 88 (from Table 6.3)

6.5.2 CCR Cycle 2

The CAA is executed again. This time the starting $Bits\_left$ is equal to the last $Bits\_left$ of CCR Cycle 1 (FFT Block 5), except for User 2, where the value of $Bits\_left$ is now equal to the offered bits. Thus,

$$Bits\_left = \begin{bmatrix} 2920 \\ 10000 \\ 4015 \\ 3045 \\ 3075 \end{bmatrix}$$

The status of *Codes_RB*, as well as the number of bits transmitted per RB, for CCR Cycle 2 over 5 FFT blocks, as a function of time t (in μs), user and RB, is shown in Table 6.5 and Table 6.6 respectively. A summary of $Bits\_left$ after each FFT block, the total bits sent for CCR Cycle 2 and the transfer ratio are shown in Table 6.7.

Table 6.5. Status of *Codes_RB* for CCR Cycle 2.

t (μs) $\Rightarrow$	96.618			115.942			135.266			154.589			173.913		
FFT Block	6			7			8			9			10		
User	RB1	RB2	RB3	RB1	RB2	RB3	RB1	RB2	RB3	RB1	RB2	RB3	RB1	RB2	RB3
1	25	2	9	25	2	9	25	2	9	25	2	9	25	2	9
2	15	39	29	15	39	29	15	39	29	15	39	29	15	39	29
3	7	15	11	7	15	11	7	15	11	7	15	11	7	15	11
4	17	4	15	17	4	15	17	4	15	17	4	15	17	4	15
5	0	4	0	0	4	0	0	4	0	0	4	0	0	4	0

Table 6.6. Bits transmitted per RB for CCR Cycle 2.

t (μs) $\Rightarrow$	96.618			115.942			135.266			154.589			173.913		
FFT Block	6			7			8			9			10		
User	RB1	RB2	RB3	RB1	RB2	RB3	RB1	RB2	RB3	RB1	RB2	RB3	RB1	RB2	RB3
1	200	12	18	200	12	18	200	12	18	200	12	18	200	12	18
2	180	468	319	180	468	319	180	468	319	180	468	319	180	468	319
3	84	180	121	84	180	121	84	180	121	84	180	121	84	180	121
4	102	20	45	102	20	45	102	20	45	102	20	45	102	20	45
5	0	8	0	0	8	0	0	8	0	0	8	0	0	8	0

Table 6.7. *Bits_left* after each FFT Block, total bits sent at the end of CCR Cycle 2 and the transfer ratio.

t (μs) $\Rightarrow$	96.618	115.942	135.266	154.589	173.913		
FFT Block	6	7	8	9	10		
User	*Bits_left* (bits)					Total bits sent	Transfer ratio
1	2690	2460	2230	2000	1770	2230	55.75%
2	9033	8066	7099	6132	5165	4835	48.35%
3	3630	3245	2860	2475	2090	2910	58.2%
4	2878	2711	2544	2377	2210	1790	44.75%
5	3067	3059	3051	3043	3035	965	24.125%

It should be observed for CCR Cycle 2 that:

- User 2 is allocated a lot more spreading codes to compensate for its relatively larger *Bits_left* since becoming an active user;
- The spreading codes allocated does not change for the duration of the CCR cycle;
- User 5 now has a lower spreading code allocation due to User 2;
- The transfer ratio of all users are approximately equal, except for User 5.

6.5.3 CCR Cycle 3

The status of *Codes_RB*, as well as the number of bits transmitted per RB, for CCR Cycle 3 over 5 FFT blocks, as a function of time t (in μs), user and RB, are shown in Table 6.8 and Table 6.9 respectively.

A summary of *Bits_left* after each FFT block, the total bits sent for CCR Cycle 3 and the transfer ratio are shown in Table 6.10.

Table 6.8. Status of *Codes_RB* for CCR Cycle 3.

t (μs) $\Rightarrow$	193.237			212.560			231.884			251.208			270.531		
FFT Block	11			12			13			14			15		
User	RB1	RB2	RB3	RB1	RB2	RB3	RB1	RB2	RB3	RB1	RB2	RB3	RB1	RB2	RB3
1	6	6	12	6	6	12	6	6	12	6	6	12	6	6	12
2	16	15	23	16	15	23	16	15	23	16	15	23	16	15	23
3	6	5	9	6	5	9	6	5	9	6	5	9	6	5	9
4	12	11	20	12	11	20	12	11	20	12	11	20	12	11	20
5	24	27	0	24	27	0	24	27	0	24	27	0	24	27	0

Table 6.9. Bits transmitted per RB for CCR Cycle 3.

t (μs) $\Rightarrow$	193.237			212.560			231.884			251.208			270.531		
FFT Block	11			12			13			14			15		
User	RB1	RB2	RB3	RB1	RB2	RB3	RB1	RB2	RB3	RB1	RB2	RB3	RB1	RB2	RB3
1	48	36	24	48	36	24	48	36	24	48	36	24	48	36	24
2	192	180	253	192	180	253	192	180	253	192	180	253	192	180	253
3	72	60	99	72	60	99	72	60	99	72	60	99	72	60	99
4	72	55	60	72	55	60	72	55	60	72	55	60	72	55	60
5	72	54	0	72	54	0	72	54	0	72	54	0	72	54	0

Table 6.10. *Bits_left* after each FFT Block, total bits sent at the end of CCR Cycle 3 and the transfer ratio.

t (μs) $\Rightarrow$	193.237	212.560	231.884	251.208	270.531		
FFT Block	11	12	13	14	15		
User	*Bits_left* (bits)					Total bits sent	Transfer ratio
1	1662	1554	1446	1338	1230	2770	69.25%
2	4540	3915	3290	2665	2040	7960	79.60%
3	1859	1628	1397	1166	935	4065	81.30%
4	2023	1836	1649	1462	1275	2725	68.125%
5	2909	2783	2657	2531	2405	1595	39.87%

It should be observed for CCR Cycle 3 that:

- User 2 is still allocated a lot of spreading codes;

- User 5 has been allocated a lot more spreading codes in RB1 and RB2 to compensate for its bad profile;
- The transfer ratio of all users are approximately equal, with User 5 steadily improving.

6.5.4 CCR Cycle 4

The status of *Codes_RB*, as well as the number of bits transmitted per RB, for CCR Cycle 4 over 5 FFT blocks, as a function of time t (in μs), user and RB, are shown in Table 6.11 and Table 6.12 respectively. A summary of $Bits\_left$ after each FFT block, the total bits sent for CCR Cycle 4 and the transfer ratio are shown in Table 6.13.

Table 6.11. Status of *Codes_RB* for CCR Cycle 4.

t (μs) $\Rightarrow$	289.855			309.179			328.502			347.826			367.150		
FFT Block	16			17			18			19			20		
User	RB1	RB2	RB3	RB1	RB2	RB3	RB1	RB2	RB3	RB1	RB2	RB3	RB1	RB2	RB3
1	7	7	16	7	7	16	7	7	16	7	7	16	7	7	16
2	8	8	18	8	8	18	8	8	18	8	8	18	8	8	18
3	4	4	8	4	4	8	4	4	8	4	4	8	4	4	8
4	10	9	22	10	9	22	10	9	22	10	9	22	10	9	22
5	35	36	0	35	36	0	35	36	0	35	36	0	35	36	0

Table 6.12. Bits transmitted per RB for CCR Cycle 4.

t (μs) $\Rightarrow$	289.855			309.179			328.502			347.826			367.150		
FFT Block	16			17			18			19			20		
User	RB1	RB2	RB3	RB1	RB2	RB3	RB1	RB2	RB3	RB1	RB2	RB3	RB1	RB2	RB3
1	56	42	32	56	42	32	56	42	32	56	42	32	56	42	32
2	96	96	198	96	96	198	96	96	198	96	96	198	96	96	198
3	48	48	88	48	48	88	48	48	88	48	48	88	48	48	88
4	60	45	66	60	45	66	60	45	66	60	45	66	60	45	66
5	105	72	0	105	72	0	105	72	0	105	72	0	105	72	0

It should be observed for CCR Cycle 4 that:

- User 4 and especially User 5 are allocated most of the spreading codes in each RB;
- User 5 has been allocated a lot more spreading codes in RB1 and RB2 to compensate for its bad profile;

Table 6.13. *Bits_left* after each FFT Block, total bits sent at the end of CCR Cycle 4 and the transfer ratio.

t (μs) $\Rightarrow$	289.855	309.179	328.502	347.826	367.150		
FFT Block	16	17	18	19	20		
User	*Bits_left* (bits)					Total bits sent	Transfer ratio
1	1100	970	840	710	580	3420	85.50%
2	1650	1260	870	480	90	9910	99.10%
3	751	567	383	199	15	4985	99.70%
4	1104	933	762	591	420	3580	89.50%
5	2228	2051	1874	1697	1520	2480	62.00%

- Users 2 and 3 have almost transferred all their offered bits, based on the transfer ratio. User 5's transfer ratio is still improving based on more allocated spreading codes.

6.5.5 CCR Cycle 5

The status of *Codes_RB*, as well as the number of bits transmitted per RB, for CCR Cycle 5 over 5 FFT blocks, as a function of time t (in μs), user and RB, are shown in Table 6.14 and Table 6.15, respectively. A summary of *Bits_left* after each FFT block, the total bits sent for CCR Cycle 5 and the transfer ratio are shown in Table 6.16.

Table 6.14. Status of *Codes_RB* for CCR Cycle 5.

t (μs) $\Rightarrow$	386.473			405.797			425.121			444.444			463.768		
FFT Block	21			22			23			24			25		
User	RB1	RB2	RB3	RB1	RB2	RB3	RB1	RB2	RB3	RB1	RB2	RB3	RB1	RB2	RB3
1	7	7	31	7	7	31	7	7	31	7	7	31	7	7	31
2	1	1	3	1	1	3	1	1	3	1	1	3	1	1	3
3	0	0	1	0	0	1	0	0	1	0	0	1	0	0	1
4	7	7	29	7	7	29	7	7	29	7	7	29	7	7	29
5	49	49	0	49	49	0	49	49	0	49	49	0	49	49	0

It should be observed for CCR Cycle 5 that:

- User 2 and 3 have been allocated a few spreading codes, since their transfer ratio is almost 100%;

Table 6.15. Bits transmitted per RB for CCR Cycle 5.

t (μs) ⇒	386.473			405.797			425.121			444.444			463.768		
FFT Block	21			22			23			24			25		
User	RB1	RB2	RB3	RB1	RB2	RB3	RB1	RB2	RB3	RB1	RB2	RB3	RB1	RB2	RB3
1	56	42	62	56	42	62	56	42	62	56	42	**2**	0	0	0
2	12	12	33	12	12	**11**	0	0	0	0	0	0	0	0	0
3	0	0	11	0	0	**11**	0	0	0	0	0	0	0	0	0
4	42	35	87	42	35	87	42	35	**15**	0	0	0	0	0	0
5	147	98	0	147	98	0	147	98	0	147	98	0	147	98	0

Table 6.16. *Bits_left* after each FFT Block, total bits sent at the end of CCR Cycle 5 and the transfer ratio.

t (μs) ⇒	386.473	405.797	425.121	444.444	463.768		
FFT Block	21	22	23	24	25		
User	*Bits_left* (bits)					Total bits sent	Transfer ratio
1	420	260	100	0	0	4000	100%
2	33	0	0	0	0	10002	100%
3	4	0	0	0	0	5007	100.001%
4	256	92	0	0	0	4000	100%
5	1275	1030	785	540	295	3705	92.625%

- User 5 has been allocated the most spreading codes in RB1 and RB2 to compensate for its bad profile;
- All users, except for User 5, complete their transfers of the offered bits. This occurs in Table 6.15 at the positions where the numbers are bold (termination points);
- At these terminations points, not all the spreading codes are used. User 1, for example, only transmit 2 bits at the termination point at FFT Block 24 RB3. User 1 has a bit allocation of 2 bits for RB3 (from Table 6.1), thus it will only use 1 code of the 31 allocated. Similarly User 2 uses 1 of its 3 codes, User 3 uses its assigned code and User 4 uses 5 of its 29 allocated codes.

6.5.6 CCR Cycle 6

The status of *Codes_RB*, as well as the number of bits transmitted per RB, for CCR Cycle 6 over 5 FFT blocks, as a function of time t (in μs), user and RB, *only for User 5*, are shown in Table 6.17 and Table 6.18 respectively. A summary of $Bits\_left$ after each FFT block, the total bits sent for CCR Cycle 6 and the transfer ratio, only for User 5, are shown in Table 6.19.

Table 6.17. Status of *Codes_RB* for CCR Cycle 6.

t (μs) ⇒	483.092			502.415			521.739			541.063			560.386		
FFT Block	26			27			28			29			30		
User	RB1	RB2	RB3	RB1	RB2	RB3	RB1	RB2	RB3	RB1	RB2	RB3	RB1	RB2	RB3
5	64	52	0	0	0	0	0	0	0	0	0	0	0	0	0

Table 6.18. Bits transmitted per RB for CCR Cycle 6.

t (μs) ⇒	483.092			502.415			521.739			541.063			560.386		
FFT Block	26			27			28			29			30		
5	192	**104**	0	0	0	0	0	0	0	0	0	0	0	0	0

Table 6.19. $Bits\_left$ after each FFT Block, total bits sent at the end of CCR Cycle 6 and the transfer ratio.

t (μs) ⇒	483.092	502.415	521.739	541.063	560.386		
FFT Block	26	27	28	29	30		
User	$Bits\_left$ (bits)					Total bits sent	Transfer ratio
5	0	0	0	0	0	4001	100%

It should be observed for CCR Cycle 6 that User 5 completes transferring all its offered bits and uses all allocated codes.

This example illustrates that the CAA allocates spreading codes uniquely and ensures that all users get the same ratio of transferred bits to offered bits (not always at a specific point in time, but over an acceptable period of time).

6.5.7 Spreading code-RB allocation diagram

Figure 6.4 shows the allocation of spreading codes as a function of FFT Blocks and RBs for the different users.

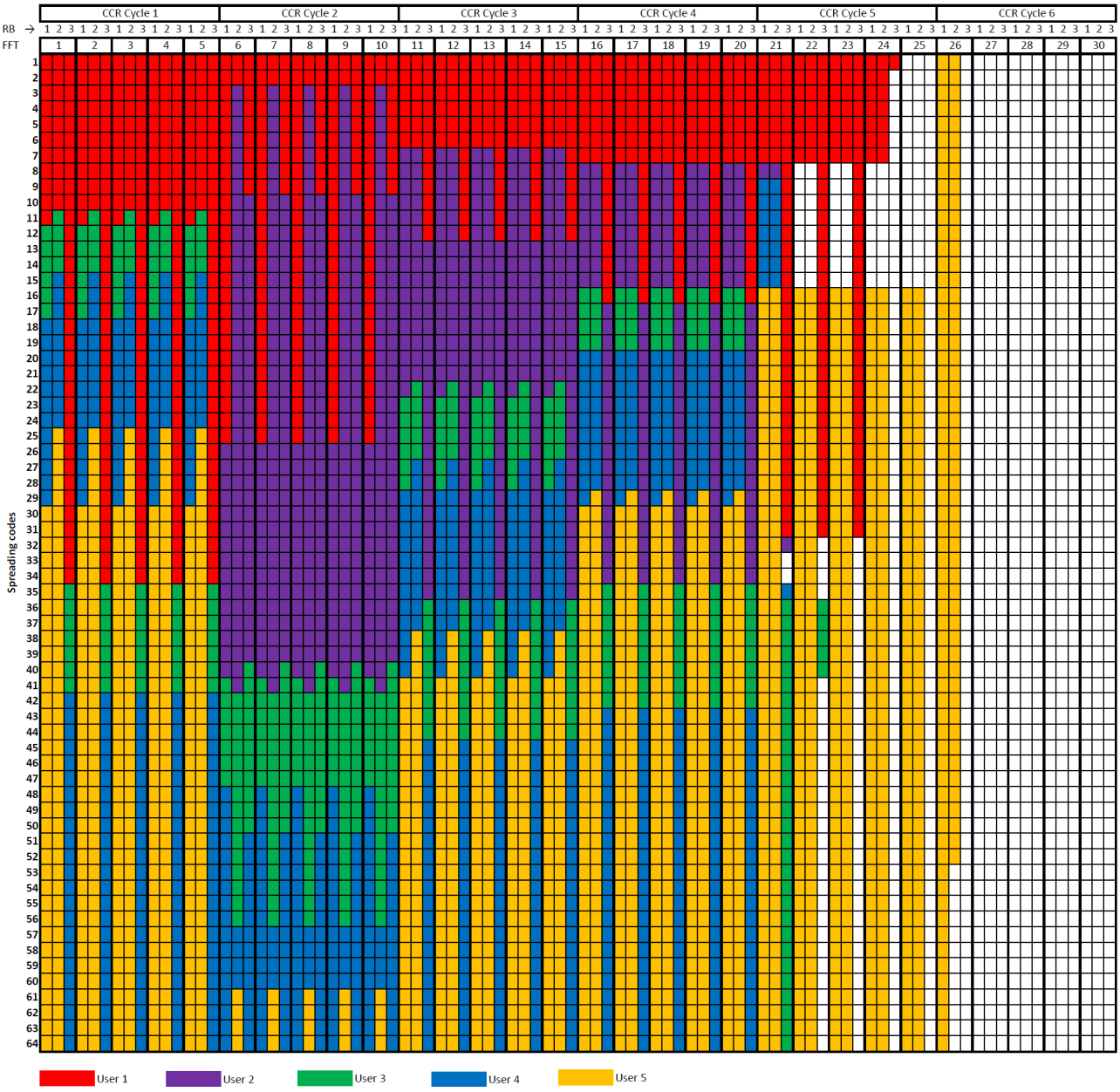

Figure 6.4. Spreading code-RB code allocation diagram.

6.6 OPERATION OF THE CODE ALLOCATION ALGORITHM UNDER RANDOM DATA ARRIVAL

To illustrate the behavior of the code allocation algorithm under random data arrival conditions, two situations were considered:

- 4 lines with similar attenuation profiles
- 4 lines with different attenuation profiles

Data of random sizes between 1 and 100 Mb, distributed over random time of arrival (in this case the FFT blocks), randomly distributed over the 4 users, were used. For 4 similar length lines (attenuation profiles), the result is shown in Figure 6.5. It can be observed that the algorithm ensures that all users' obtain the same ratio of actual data (rate) to required data (rate), ending at the same point in time. For 4 different line lengths, the result is shown in Figure 6.6. Here it is observed that lines 1 and 2, which is within the 200 m range, end at the same point in time (5.384 s), while lines 3 and 4, end at the same point in time (6.296 s). After 5.384 s, all available codes are allocated only between users 3 and 4, as users 1 and 2 have no further data to send.

6.7 COMPLEXITY OF THE PROPOSED CODE ALLOCATION ALGORITHM

In theoretical analysis of algorithms, it is common to estimate their complexity in the asymptotic sense, using for instance the Big-O notation. The complexity can also be based on a time analysis, but this will be dependent on the speed of the processor being used. Big-O is not dependent on processing speed. From Algorithm 2, Step 3 there are 2 for-loops, one for the number of active RBs (M) and one for the number of active users (K). The complexity of the system is thus $O(MK)$, $0 \leq K \leq 64$, $0 < M \leq 63$. Looking more from an Engineering perspective, the number of multiply-accumulate (MAC) operations can be used. From a more detailed analysis, the algorithm uses $15MK$ multiplications, $3MK + 4M(K\text{-}1)$ additions, $2MK$ nearest integer (rounding) operations and $9MK$ decision (if) operations.

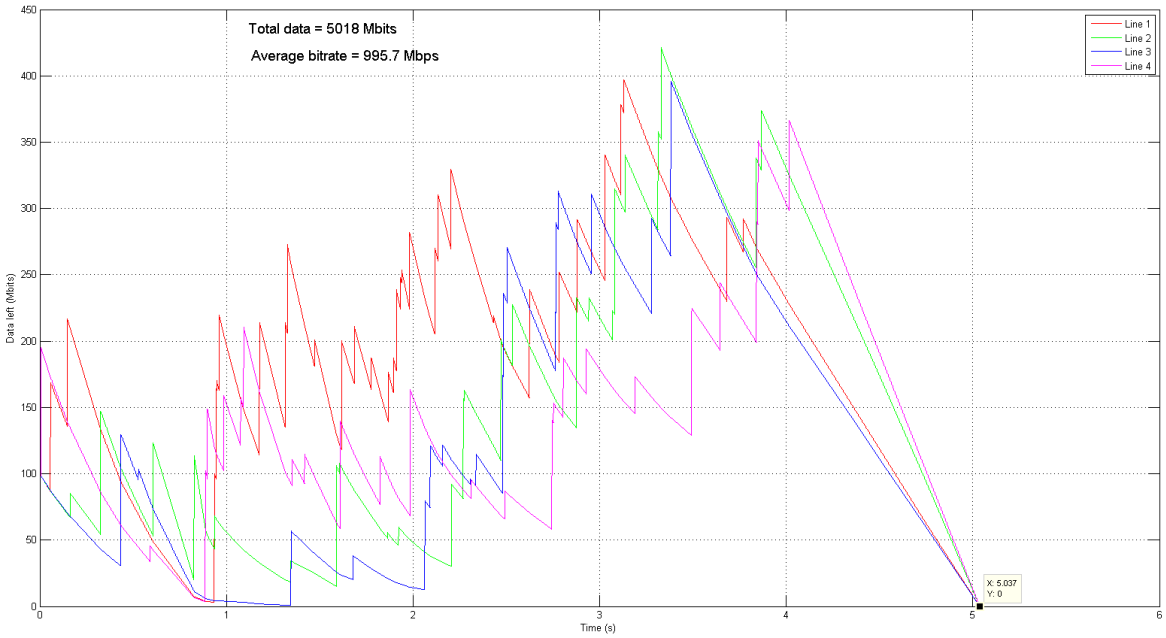

Figure 6.5. RB code allocation algorithm behaviour under random data arrival condition for similar line lengths.

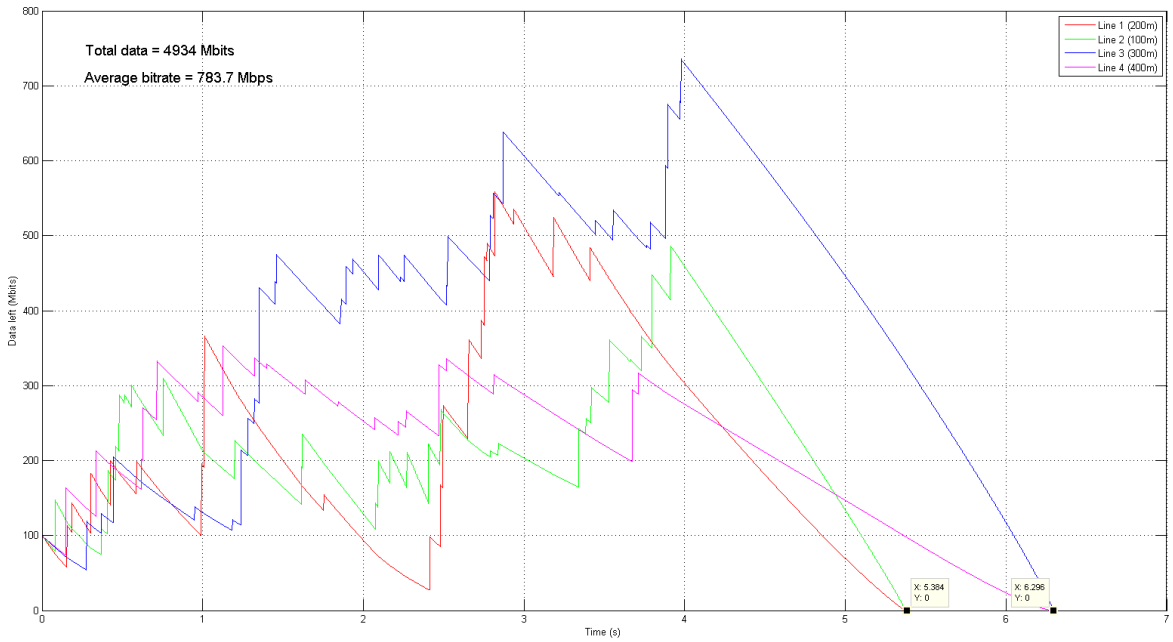

Figure 6.6. RB code allocation algorithm behaviour under random data arrival condition for different line lengths.

6.8 CHAPTER SUMMARY

This chapter described the novel code allocation algorithm (CAA) that was designed to ensure that unique codes are allocated to all active users for each of the active or used RBs. The general operation of the CAA was described and a detailed example was provided to illustrate the operation and status of the CAA. The example illustrated how the CAA adapts to changing conditions (users joining (or leaving) the pool), as well as ensuring that all users obtain the same transfer ratio (transmitted bits to offered bits). Operation of the GDSL modem under random data arrival as well as a complexity analysis of the CAA was also provided.

CHAPTER 7 CONCLUSION

7.1 THESIS SUMMARY

This thesis addressed the design of a GDSL modem capable of delivering 1 Gbps aggregated throughput over a single 200 m length of 0.5 mm diameter twisted copper pair, and ensuring MUI-free communication in a severe NEXT/FEXT dominated environment. Related background material was provided in Chapter 2. Channel modelling was addressed in Chapter 3, including channel and system capacity, channel impulse response, SNR margin, cable parameters, two-port networks and models, background noise, NEXT and FEXT crosstalk models and the practical MIMO crosstalk model. In Chapter 4 the GDSL system architecture was described, mainly covering the transmitter and receiver structure, Resource Blocks were explained, SOCC spreading properties were investigated, modem operation was described and xDSL bypass policies were provided. In Chapter 5 the simulation environment and results were provided. Basic transceiver results, as well as BER analysis of the GDSL system in a MIMO practical crosstalk environment was performed. This provided the main proof of MUI-free communication. In Chapter 6 the novel Code Allocation Algorithm (CAA) was presented and a detailed example was provided.

7.2 UNIQUE CONTRIBUTIONS

In this thesis the following contributions were made:

- A new Multi-carrier Code Division Multiple Access (MC-CDMA) modem, for use within the xDSL domain, capable of delivering 1 Gbps aggregated throughput was developed;
- 1 Gbps aggregate throughput was achieved with only GDSL modems present over a 190 m length **single** twisted-pair of 0.5 mm diameter copper wire, in contrast to either 1 Gbps over 4

pairs of 200 m long 0.5 mm diameter wire, or 1 Gbps over a single pair of 100 m long 0.5 mm diameter wire. Distances of between 185 m to 148 m are obtained for ADSL2+ and VDSL2 Profile 30a bypass profiles respectively;

- A SOCC frequency spreading block was developed to provide MUI-free communication, even in the presence of severe FEXT (short loops) or even NEXT. This was illustrated in Figure 5.25. This SOCC spreading block can be modularly added to existing DSL systems to provide MUI-free communication;
- A novel code allocation scheme was developed and implemented, as described in Chapter 6. The algorithm uses the offered bits of each user and the bits per RB profile to allocate spreading codes uniquely to each user (which ensures MUI-free operation), while ensuring that each user obtain the same transfer ratio. A detailed example was also provided. An accredited ISI publication was accepted on this topic.
- The use of spreading codes and the novel CAA ensure that system resources are more optimally used. Spreading codes are allocated where and when they are needed, rather than being permanently allocated to a specific user.
- Orthogonal code division (using spreading) vs. existing pre-coding was implemented to mitigate MUI, even in severe crosstalk conditions. Vectored DSL makes use of pre-coding in downstream transmission and makes use of MUD-IC in upstream transmission [4]. Overall these techniques (pre-coding and MUD-IC) have a high computational overhead. Using SOCC spreading codes the effect of crosstalk is mitigated, since the SOCC spreading/despreading process inherently provide IC and does not require overhead for pre-coding and MUD-IC.

7.3 FUTURE RESEARCH WORK

The developed GDSL modem is a novel improvement over existing G.fast implementations. For future research:

- the current design can be extended towards XG-Fast. Due to much shorter line lengths, attenuation will also be much less, providing the opportunity for the use of longer spreading sequences, $L_{fsp} = 256$ or higher;
- the existing unshielded twisted pair (UTP) wire can be replaced with foiled twisted pair (FTP) or shielded twisted pair (STP), providing better crosstalk coupling attenuation. This creates

a possibility to operate complete GDSL systems over a single FTP, in contrast to the existing GDSL system (several users) operating over several UTPs;

- SOCC spreading and CAA can be investigated for use in powerline communication systems as well as wireless communication.

REFERENCES

[1] M. K. Rudberg and M. Hjelm, "Method and device for reducing crosstalk interference," *US Patent US6647067 B1*, November 2003, (http://www.google.ca/patents/US6647067).

[2] J. A. C. Bingham, *ADSL, VDSL and Multicarrier Modulation*, ser. Wiley Series in Telecommunication and Signal Processing. John Wiley & Sons, Inc., 2000, ISBN 0-471-29099-8.

[3] L. Hu, S. Nooshabadi, and T. Mladenov, "Forward error correction with Raptor GF(2) and GF(256) codes on GPU," *IEEE Trans. Cons. Electr.*, vol. 59, no. 1, pp. 273–280, February 2013.

[4] C. Leung, S. Huberman, K. Ho-Van, and T. Le-Ngoc, "Vectored DSL: Potential, Implementation Issues and Challenges," *IEEE Commun. Surveys Tuts.*, vol. 15, no. 4, pp. 1907 – 1923, Q4 2013.

[5] G.992.1, *Asymmetric Digital Subscriber Line (ADSL) Transceivers*, ITU, Jul 1999, Available: https://www.itu.int/rec/T-REC-G.992.1/en (Last accessed: 29 August 2016).

[6] G.993.1, *Very-high-speed Digital Subscriber Lines (VDSL)*, ITU, Jun 2004, Available: https://www.itu.int/rec/T-REC-G.993.1/en (Last accessed: 29 August 2016).

[7] G.9700, *Fast access to subscriber terminals (G.fast) - Power spectral density specification*, ITU, Apr 2014, Available: https://www.itu.int/rec/T-REC-G.9700/en (Last accessed: 29 August 2016).

[8] J. M. Cioffi, "Friendly DSLs," obtained from the author, Stanford University.

[9] J. M. Cioffi and Ölçer, "Guest Editorial: Very High-Speed Digital Subscriber Line," *IEEE Commun. Mag.*, vol. 38, no. 5, pp. 62,64, May 2000.

[10] P. Chetty, "Telkom's Superfast Broadband rollout speeds ahead," Website media release, 14 June 2013, Available: http://www.telkom.co.za/about_us/mediacentre/press_release/articles/2013/article_1171.html (Last accessed: 29 August 2016).

[11] G.993.2, *Very high speed digital subscriber line transceivers 2 (VDSL2)*, ITU, Jan 2015, Available: https://www.itu.int/rec/T-REC-G.993.2/en (Last accessed: 29 August 2016).

[12] F. Sjöberg, "High Speed Communication on Twisted-pair Wires and Low Complexity Multiuser Detectors," Ph.D. dissertation, Luleå University of Technology, Division of Signal Processing, April 1998.

[13] G.9701, *Fast access to subscriber terminals (G.fast) - Physical layer specification*, ITU, Dec 2014, Available: https://www.itu.int/rec/T-REC-G.9701/en (Last accessed: 29 August 2016).

[14] J. Cioffi, B. Lee, M. Mohseni, A. Leshem, and L. Youming, "GDSL (Gigabit DSL)," ITU Working group T1E1.4 (DSL Access), Washington DC, Contribution T1E1.4/2003-487R1, 9 August 2003.

[15] B. Lee, J. Cioffi, S. Jagannathan, and M. Mohseni, "Gigabit DSL," *IEEE Trans. Commun.*, vol. 55, no. 9, pp. 1689–1692, September 2007.

[16] H. Lei, "Giga DSL: Gigabit access over copper," *Huawei COMMUNICATE*, no. 68, pp. 22–23, January 2013, Available: http://www.huawei.com/en/static/HW-201354.pdf (Last accessed: 29 August 2016).

[17] J. M. Cioffi, K. Cheong, A. Salvekar, and J. Lauer, "Mitigation of DSL Crosstalk via Multiuser Detection and Code-Division Multiple Access," *ANSI Contribution T1E1.4/98-253*, Austin, TX, USA, September 1998.

[18] M. L. Honig, P. Crespo, and K. Steiglitz, "Suppression of Near- and Far-End Crosstalk by Linear Pre- and Post-Filtering," *IEEE JSAC*, vol. 10, no. 3, pp. 614–629, April 1992.

[19] G. Ginis and J. M. Cioffi, "A Multi-user Precoding Scheme achieving Crosstalk Cancellation with Application to DSL Systems," in *Proc. 34th Asilomar Conference*, ser. Pacific Grove, CA, October 2000, pp. 1627–1631.

[20] A. B. Sesay and M. R. Gibbard, "Asymmetric signal processing for indoor wireless LANs," in *IEEE PIMRC '95*, ser. Toronto, Canada, September 1995, pp. 6–10.

[21] J. W. Cook, R. H. Kirkby, M. G. Booth, K. T. Foster, D. E. A. Clarke, and G. Young, "The noise and crosstalk environment for ADSL and VDSL systems," *IEEE Commun. Mag.*, vol. 37, no. 5, pp. 73–78, May 1999.

[22] J. H. van Wyk, "ADSL Capacity in a Generic Exchange Environment," Master's thesis, Department of Electrical, Electronic & Computer Engineering, University of Pretoria, Lynnwood Road, Pretoria, South Africa, January 1999, Available: http://repository.up.ac.za/handle/2263/30451 (Last accessed: 29 August 2016).

[23] ANSI.T1.413, *Network and Customer Installation Interface – Asymmetric Digital Subscriber Line (ADSL) Metallic Interface*, ANSI, 4 December 1998, T1.413-1998 standard, Issue 2, Rev. 5, *ANSI T1E1.4 Workgroup*.

[24] T. Starr, J. M. Cioffi, and P. J. Silverman, *Understanding Digital Subscriber Line Technology*. Prentice Hall Communications Engineering and Emerging Technologies Series,Prentice Hall, New York, 1999, ISBN 0-13-780545-4.

[25] H. Visagie, "Digital subscriber line basics," *Electron*, pp. 51–54, October 1998.

[26] G.992.2, *Splitterless Asymmetric Digital Subscriber Line (ADSL) Transceivers*, ITU, Jul 1999, Available: https://www.itu.int/rec/T-REC-G.992.2/en (Last accessed: 29 August 2016).

[27] G.992.3, *Asymmetric digital subscriber line transceivers 2 (ADSL2)*, ITU, Apr 2009, Available: https://www.itu.int/rec/T-REC-G.992.3/en (Last accessed: 29 August 2016).

[28] G.992.5, *Asymmetric digital subscriber line 2 transceivers (ADSL2)- Extended bandwidth ADSL2 (ADSL2plus)*, ITU, Jan 2009, Available: https://www.itu.int/rec/T-REC-G.992.5/en (Last accessed: 29 August 2016).

[29] J. H. van Wyk and L. P. Linde, "Current Research on VDSL Technology," in *Proc. SATCAM '00*, 10-12 September 2000.

[30] P. Vetter, D. Goderis, L. Verpooten, and A. Granger, "Systems aspects of APON/VDSL deployment," *IEEE Commun. Mag.*, vol. 38, no.5, pp. 66–72, May 2000.

[31] P. Warrier and B. Kumar, *xDSL Architecture*. McGraw-Hill, 2000, ISBN 0-07-135006-3.

[32] W. Coomans, R. B. Moraes, K. Hooghe, A. Duque, J. Galaro, and M. Timmers, "XG-FAST: The 5th Generation Broadband," *IEEE Commun. Mag.*, vol. 53, no. 12, pp. 83 – 88, December

2015.

[33] H. Lui, *Signal Processing Applications in CDMA Communications*. Artech House Publishers, Boston, London, 2000. ISBN 1-58053-042-7.

[34] L. Vandendorpe, "Multitone spread spectrum multiple access communications system in a multipath Rician fading channel," in *Proc. ICC '94*, New Orleans, LA, USA, 1-5 May 1994, pp. 1638–1642.

[35] V. M. DaSilva and E. S. Sousa, "Performance of orthogonal CDMA codes for quasi-synchronous communication systems," in *Proc. IEEE ICUPC '93*. Ottowa, Canada, October 1993, pp. 995–999.

[36] A. Chouly, A. Brajal, and S. Jourdan, "Orthogonal multicarrier techniques applied to direct sequence spread spectrum CDMA systems," in *Proc. GLOBECOM '93*, Houston, TX, USA, 29 November - 2 December 1993, pp. 1723–1728.

[37] S. Kondo and L. B. Milstein, "Performance of multicarrier DS-CDMA systems," *IEEE Trans. Commun.*, vol. 44, no. 2, pp. 238–246, February 1996.

[38] N. Yee and J. P. Linnartz, "BER of multicarrier CDMA in an indoor Rician fading channel," in *Proc. ACSSC '93*. Volume 1: Pacific Grove, CA, USA, November 1993, pp. 426–430.

[39] K. Fazel and L. Papke, "On the Performance of Convolutionally-coded CDMA/OFDM for Mobile Communication Systems," in *Proc. IEEE PIMRC '93*, Yokohama, Japan, September 1993, pp. 468–472.

[40] S. Hara and R. Prasad, "Overview of multicarrier CDMA," *IEEE Commun. Mag.*, vol. 35, no. 2, pp. 126–133, December 1997.

[41] ——, "Design and performance of multicarrier CDMA system in frequency-selective Rayleigh fading channels," *IEEE Trans. Vech. Tech.*, vol. 48, no. 5, pp. 1584–1595, September 1999.

[42] P. Švač, "Variable Two-Shift Complete Complementary Code," in *Proc. EUROCON 2005*, 21-24 November 2005, pp. 482–485.

[43] C. W. You and D. S. Hong, "Multicarrier CDMA systems using time-domain and frequency-domain spreading codes," *IEEE Trans. Commun.*, vol. 51, no. 1, pp. 17–21, January 2003.

[44] M. B. Pursley, "Performance evaluation of phase coded spread-spectrum multiple access communication - Part 1: System analysis," *IEEE Trans. Commun.*, vol. COM-25, no. 8, pp. 795–799, August 1977.

[45] S. Stańczak and H. Boche, "Aperiodic properties of generalized binary Rudin-Shapiro sequences and some recent results on sequences with a quadratic phase function," in *Proc. IZSBC 2000*, Zurich, 15-17 February 2000, pp. 279–286.

[46] D. Sarwate and M. Pursley, "Crosscorrelation Properties of Pseudorandom and Related Sequences," *Proc. IEEE*, vol. 68, no. 5, pp. 593–619, May 1980.

[47] S. Stańczak, B. J. Boche, and M. Haardt, "Are LAS-codes a miracle?" in *Proc. GLOBECOM '01*, San Antonio, Texas, 25-29 November 2001, pp. 589–593.

[48] X. Zhou and W. Lu, "Performance analysis of LA codes in LAS-CDMA," *Proc. ICSP '02*, pp. 1307–1311, 26-30 August 2002.

[49] S. Ni, H. Wei, J. S. Blogh, and L. Hanzo, "Network performance of asynchronous UTRA-like FDD/CDMA systems using loosely synchronised spreading codes," in *Proc. VTC '03*, Orlando, Florida, USA, 6-9 October 2003, pp. 1359–1363.

[50] S. Ni, H. Wei, and L. Hanzo, "Loosely synchronised spreading code aided network performance of quasi-synchronous UTRA-like TDD and FDD CDMA systems," *IEEE Elect. Let.*, vol. 41, no. 15, pp. 861–863, 21 July 2005.

[51] C. Y. Lai, H. C. Chu, S. S. Liao, and C. M. Huang, "On LA code performance analysis for LAS-CDMA communications," in *Proc. CASSET '04*, Shanghai, China, 31 May - 2 June 2004, pp. 341–344.

[52] ——, "LA code construction and performance analysis for LAS-2000," in *Proc. APCCAS '04*, Tainan, Taiwan, 6-9 December 2004, pp. 793–796.

[53] H. Xu and S. Yang, "LAS-OFDMA for Power Line Carrier Communications in Home Networks," in *Proc. ICCE '05*, Las Vegas, Nevada, USA, 8-12 January 2005, pp. 387–388.

[54] Z. Wang, Y. Zhao, and Y. Zhang, "A novel LS-code access method in MC-CDMA system to overcome frequency offset," in *Proc. CCECE '05*, Saskatoon, Saskatchewan Canada, 1-4 May 2005, pp. 1145–1148.

[55] X. Tang and W. H. Mow, "Design of Spreading Codes for Quasi-Synchronous CDMA With Intercell Interference," *IEEE JSAC*, vol. 24, no. 1, pp. 84–93, January 2006.

[56] C. R. Nassar, B. Natarajan, and S. Shattil, "Introduction of Carrier Interference to Spread Spectrum Multiple Access," in *Proc. IEEE Emerging Technologies Symp.*, April 1999, pp. 11–15.

[57] Y. Wu, BFarhang-Boroujeny, and S. Attallah, "Clipping noise mitigation methods in DMT-based ADSL systems," in *Proc. ICC '01*, vol. 6. Helsinki, Finland, 11-14 June 2001, pp. 1670–1673.

[58] B. Natarajan, Z. Wu, C. R. Nassar, and S. Shattil, "Large set of CI spreading codes for high-capacity MC-CDMA," *IEEE Trans. Commun.*, vol. 52, no. 11, pp. 1862–1866, November 2004.

[59] B. M. Popovic, N. Suehiro, and P. Z. Fan, "Orthogonal sets of quadriphase sequences with good correlation properties," *IEEE Trans. Inf. Theory*, vol. 48, no. 4, pp. 956–959, April 2002.

[60] B. M. Popovic, "Spreading sequences for multicarrier CDMA systems," *IEEE Trans. Commun.*, vol. 47, no. 6, pp. 918–926, June 1999.

[61] B. Natarajan, C. R. Nassar, S. Shattil, M. Michelini, and Z. Wu, "High-performance MC-CDMA via carrier interferometry codes," *IEEE Trans. Vech. Tech.*, vol. 50, no. 6, pp. 1344–1353, November 2001.

[62] B. Natarajan and C. R. Nassar, "Crest Factor Considerations in MC-CDMA with Carrier Interferometry Codes," in *Proc. PACRIM 2001*, 26-28 August 2001, pp. 445–448.

[63] M. R. Schroeder, "Synthesis of low-peak-factor signals and binary sequences with low autocorrelation," *IEEE Trans. Inf. Theory*, vol. IT-16, pp. 85–89, January 1970.

[64] Z. Wu and C. R. Nassar, "Novel orthogonal codes for MC-CDMA with low crosscorrelation in frequency selective fading channels," in *Proc. ACSSC 2002*, 3-6 November 2002, pp. 1444–1447.

[65] D. A. Wiegandt, Z. Wu, and C. R. Nassar, "High-throughput, high-performance OFDM via pseudo-orthogonal carrier interferometry spreading codes," *IEEE Trans. Commun.*, vol. 51, no. 7, pp. 1123–1134, July 2003.

[66] Y. Chung, "Performance evaluation of adaptive OFDM with carrier interferometry codes in frequency selective fading channels," in *Proc. ICC '04*, 20-24 June 2004, pp. 3276–3279.

[67] N. Taylor, M. A. Cooper, S. M. D. Armour, and J. P. McGeehan, "Performance evaluation of carrier interferometry implementations of MC-CDMA over a wideband channel suffering phase noise," in *Proc. VTC 2005-Spring*, 30 May-1 June 2005, pp. 3043–3047.

[68] Z. Wu and C. R. Nassar, "Narrowband Interference Rejection in OFDM via Carrier Interferometry Spreading Codes," *IEEE Trans. Wireless Commun.*, vol. 4, nr. 4, pp. 1491–1505, July 2005.

[69] S. I. Park, I. Song, K. S. Kim, N. Suehiro, and J. Lee, "An Analysis of a Modulated Orthogonal Sequence," in *Proc. ICASSP '98*, 12-15 May 1998, pp. 3197–3200.

[70] N. Suehiro and M. Hatori, "Modulatable Orthogonal Sequences and their Application to SSMA Systems," *IEEE Trans. Inf. Theory*, vol. 34, no. 1, pp. 93–100, January 1988.

[71] R. Frank, "Polyphase Codes with Good Nonperiodic Correlation Properties," *IRE Trans. Inf. Theory*, vol. 9, no. 1, pp. 43–45, January 1963.

[72] R. Heimiller, "Phase shift codes with good periodic correlation properties," *IRE Trans. Inf. Theory*, vol. IT-7, pp. 254–257, October 1961.

[73] S. Golomb and R. Scholtz, "Generalized Barker sequences," *IEEE Trans. Inf. Theory*, vol. IT-11, pp. 533–537, October 1965.

[74] N. Chang and S. Golomb, "On n-Phase Barker Sequences," *IEEE Trans. Inf. Theory*, vol. 40, no. 4, pp. 1251–1253, July 1994.

[75] D. C. Chu, "Polyphase codes with good periodic correlation properties," *IEEE Trans. Inf. Theory*, vol. IT-18, pp. 531–533, July 1972.

[76] R. L. Frank, "Polyphase complementary codes," *IEEE Trans. Inf. Theory*, vol. IT-26, pp. 641–647, November 1980.

[77] M. J. E. Golay, "Complementary Series," *IEEE Trans. Inf. Theory*, vol. 7, no. 2, pp. 82–87, April 1961.

[78] R. Sivaswamy, "Multiphase complementary codes," *IEEE Trans. Inf. Theory*, vol. 24, no. 5, pp. 546–552, September 1978.

[79] B. M. Popovic, "Generalized Chirp-Like Polyphase Sequences with Optimum Correlation Properties," *IEEE Trans. Inf. Theory*, vol. 38, no. 4, pp. 1406–1409, July 1992.

[80] ——, "GCL polyphase sequences with minimum alphabets," *IEE Elect. Let.*, vol. 30, no. 2, pp. 106–107, January 1994.

[81] N. Suehiro and M. Hatori, "N-Shift Cross-Orthogonal Sequences," *IEEE Trans. Inf. Theory*, vol. 34, no.1, pp. 143–146, January 1988.

[82] A. Milewski, "Periodic Sequences with Optimal Properties for Channel Estimation and Fast Start-Up Equalization," *IBM J. Res. Develop.*, vol. 27, no. 5, pp. 426–431, September 1983.

[83] B. Popovic, "Complementary sets of chirp-like polyphase sequences," *IEEE Electr. Let.*, vol. 27, no.3, pp. 254–255, January 1991.

[84] S. Park, S. Park, I. Song, and N. Suehiro, "Multiple-access Interference Reduction for QS-CDMA Systerms with a Novel Class of Polyphase Sequences," *IEEE Trans. Inf. Theory*, vol. 46, no. 4, pp. 1448–1458, July 2000.

[85] L. Lu and V. K. Dubey, "Extended orthogonal polyphase codes for multicarrier CDMA system," *IEEE Commun. Let.*, vol. 8, no 12, pp. 700–702, December 2004.

[86] Y. Tsai, G. Zhang, and X. Wang, "Polyphase Codes for Uplink OFDM-CDMA Systems," *IEEE Trans. Commun.*, vol. 56, no. 3, pp. 435–444, March 2008.

[87] H. Hu and B. Lui, "Genetic Algorithm for Designing Polyphase Orthogonal Code," in *Proc. WiCOM '08*, Dalian, 12-14 October 2008, pp. 1–4.

[88] J. Pereira and H. da Silva, "Generalized Chu Polyphase Sequences," in *Proc. ICT '09*, Marrakech, 25-27 May 2009, pp. 47–52.

[89] G. Welti, "Quaternary Codes for Pulsed Radar," *IRE Trans. Inf. Theory*, vol. 6, no. 3, pp. 400–408, June 1960.

[90] H. Lüke, "Sets of One and Higher Dimensional Welti Codes and Complementary Codes," *IEEE Trans. AES*, vol. AES-21, no. 2, pp. 170–179, March 1985.

[91] R. Turyn, "Ambiquity Function of Complementary Sequences," *IEEE Trans. Inf. Theory*, vol. 9, no.1, pp. 46–47, January 1963.

[92] H. H. Chen, J. F. Yeh, and N. Suehiro, "A multicarrier CDMA architecture based on orthogonal complementary codes for new generations of wideband wireless communications," *IEEE Commun. Mag.*, vol. 39, no. 10, pp. 126–135, October 2001.

[93] J. Zhou and D. Li, "Notes on the balance property of Golay complementary pairs," in *Proc. WAC '12*, Puerto Vallarta, Mexico, 24-28 June 2012, pp. 1–4.

[94] C. C. Tseng and C. L. Liu, "Complementary sets of sequences," *IEEE Trans. Inf. Theory*, vol. IT-18, pp. 644–652, September 1972.

[95] L. Bömer and M. Antweiler, "Periodic Complementary Binary Sequences," *IEEE Trans. Inf. Theory*, vol. 36, no. 6, pp. 1487–1494, November 1990.

[96] S. Golomb and H. Taylor, "Two-dimensional synchronization patterns for minimum ambiquity," *IEEE Trans. Inf. Theory*, vol. 28, no. 4, pp. 600–604, July 1982.

[97] X. Huang and Y. Li, "Scalable complete complementary sets of sequences," in *Proc. GLOBECOM 2002*, vol. 2, 17-21 November 2002, pp. 1056–1060.

[98] ——, "Polyphase scalable complete complementary sets of sequences," in *Proc. ICCS 2002*, vol. 2, 25-28 November 2002, pp. 810–814.

[99] H. H. Chen, "A new CDMA architecture based on complementary codes enabling isotropic MAI-free operation," in *Proc. ISCC '03*, Kemer - Antalya, Turkey, 30 June - 3 July 2003, pp. 936–941.

[100] S. Matsufuji, R. Shigemitsu, Y. Tanada, and N. Kuroyanagi, "Construction of Complementary Arrays," in *Proc. SympoTIC '04*, Bratislava, Slovakia, 24-26 October 2004, pp. 78–81.

[101] Y. Tu, P. Fan, S. Matsufuji, and X. Li, "Construction of Complementary Sequence Sets Based on Generating Function," in *Proc. WiCOM '09*, Beijing, 24-26 September 2009, pp. 1–4.

[102] X. Long, F. Zeng, W. Zhang, C. Sun, and L. Guo, "Complementary sequences and its anti-interference performance in multi-carrier CDMA system," in *Proc. WOCC 2010*, Shanghai, 14-15 May 2010, pp. 1–4.

[103] F. Zeng and Z. Zhang, "Two Dimensional Periodic Complementary Array Sets," in *Proc. WiCOM 2010*, Chengdu, 23-25 September 2010, pp. 1–4.

[104] H. Chen, *The Next Generation CDMA Technologies*. John Wiley & Sons, 2007, ISBN: 978-0-470-02294-8.

[105] H. Torii, N. Suehiro, and M. Nakamura, "A new class of Zero-Correlation-Zone sequences," *IEEE Trans. Inf. Theory*, vol. 50, no. 3, pp. 559–565, March 2004.

[106] P. Farkaš and M. Turcsańy, "Two-dimensional orthogonal complete complementary codes," in *Proc. SympoTIC '03*, 26-28 October 2003, pp. 21–24.

[107] ——, "Three-dimensional Orthogonal Complete Complementary Codes," in *Proc. SympoTIC '04*, 24-26 October 2004, pp. 98–101.

[108] D. Gerakoulis and S. Ghassemzadeh, "Extended orthogonal code designs with applications in CDMA," in *Proc. ISSTA 2000*, Portland, Oregon, 6-8 September 2000, pp. 657–661.

[109] A. M. Tulino, L. Li, and S. Verdu, "Spectral Efficiency of Multicarrier CDMA," *IEEE Trans. Inf. Theory*, vol. 51, no. 2, pp. 479–505, February 2005.

[110] L. L. Yang and L. Hanzo, "Multicarrier DS-CDMA: A Multiple Access Scheme for Ubiquitous Broadband Wireless Communications," *IEEE Commun. Mag.*, vol. 41, no. 10, pp. 116–124, October 2003.

[111] X. K. Zhao and X. D. Zhang, "Peak-to-average power ratio analysis in multicarrier DS-CDMA," *IEEE Trans. Vech. Tech.*, vol. 52, no. 3, pp. 561–568, May 2003.

[112] H. H. Chen, S. W. Chu, and M. Guizani, "On Next Generation CDMA Technologies: The REAL Approach for Perfect Orthogonal Code Generation," *IEEE Trans. Vech. Tech.*, vol. 57, no. 5, pp. 2822 – 2833, September 2008.

[113] C. R. Paul, *Analysis of Multiconductor Transmission Lines*, 2nd ed. John Wiley and Sons, 2008.

[114] J. S. Chow, J. C. Tu, and J. M. Cioffi, "A Discrete Multitone Transceiver System for HDSL Applications," *IEEE JSAC*, vol. 9, no. 6, pp. 895–908, August 1991.

[115] J. M. Cioffi, *Lecture Notes for Advanced Digital Communications*. Stanford University, Fall 1997.

[116] R. van den Brink, "G.fast: Wideband modeling of twisted pair cables as two-ports," ITU Study Group 15, Tech. Rep., 3-10 November 2011, Available:

http://www.joepeesoft.com/Public/DSL_Corner/Docs/Publications_ITU_T/PUB_2011_09_ITU_T_SG15_11GS3-028_RefModel_Theory.pdf (Last accessed: 29 August 2016).

[117] J. J. Werner, "The HDSL Environment," *IEEE JSAC*, vol. 9, no. 6, pp. 785–800, August 1991.

[118] A. Dutta-Roy, "A Second Wind for Wiring," *IEEE Spectrum*, vol. 36, no. 9, pp. 52–60, September 1999.

[119] W. Y. Chen, *DSL: Simulation Techniques and Standards Development for Digital Subscriber Line Systems*. MacMillan Technology Series 1998, Indianapolis, 1998, ISBN 0-57-870017-5.

[120] G.994.1, *Handshake procedures for digital subscriber line transceivers*, ITU, Jun 2012, Available: https://www.itu.int/rec/T-REC-G.994.1/en (Last accessed: 29 August 2016).

[121] ATIS, "Multiple-input Multiple-output Crosstalk Channel Model," NIPP-NAI-2009-014R3, Tech. Rep., 2009.

[122] J. Campello, "Optimal Discrete Bit Loading for Multicarrier Modulation Systems," *Obtained from the author*, 1999.

[123] L. Hanzo, M. Munster, B. J. Choi, and T. Keller, *OFDM and MC-CDMA for Broadband Multi-user Communications, WLANs and Broadcasting*. Wiley, 2003.

[124] R. Gallager, "Low-Density Parity-Check Codes," Ph.D. dissertation, Cambridge, MA, MIT Press, 1963.

[125] ETSI, *Digital Video Broadcasting (DVB): Second generation framing structure, channel coding and modulation systems for Broadcasting, Interactive Services, News Gathering and other broadband satellite applications: Part 1: DVB-S2*, ETSI EN 302 307-1 V1.4.1 (2014-11), Available: http://www.etsi.org/deliver/etsi_en/302300_302399/30230701/01.04.01_60/en_30230701v010401p.pdf (Last accessed: 29 August 2016).

[126] IEEE, *802.11n-2009 - IEEE Standard for Information technology– Local and metropolitan area networks– Specific requirements– Part 11: Wireless LAN Medium Access Control (MAC)and Physical Layer (PHY) Specifications Amendment 5: Enhancements for Higher Throughput*, IEEE 802.11n-2009, Available: https://standards.ieee.org/findstds/standard/802.11n-2009.html (Last accessed: 29 August 2016).

[127] ——, *802.3an-2006 - Standard for Information Technology - Telecommunications and Information Exchange Between Systems Ű LAN/MAN - Specific Requirements Part 3: CSMA/CD Access Method and Physical Layer Specifications - Amendment: Physical Layer and Management Parameters for 10 Gb/s Operation, Type 10GBASE-T*, IEEE 802.3an-2006, Available: https://standards.ieee.org/findstds/standard/802.3an-2006.html (Last accessed: 29 August 2016).

[128] G.9960, *G.9960 : Unified high-speed wireline-based home networking transceivers - System architecture and physical layer specification*, ITU, Jul 2015, Available: https://www.itu.int/rec/T-REC-G.9960/en (Last accessed: 29 August 2016).

[129] R. Neal, *Software for Low Density Parity Check Codes*, Available: http://www.cs.utoronto.ca/∼radford/ftp/LDPC-2012-02-11/index.html (Last accessed: 29 August 2016).

[130] D. MacKay, *Converting alist to binary*, Available: http://www.inference.phy.cam.ac.uk/mackay/perl/A2H.p (Last accessed: 29 August 2016).

[131] IEC, "Information technology equipment - radio disturbance characteristics limits and methods of measurement," IEC, Tech. Rep. EN55022:1998 (CISPR 22:1997), 1998.

[132] A. Y. Wu and T. S. Chan, "Computationally efficient fast algorithm and architecture for the IFFT/FFT in DMT/OFDM systems," in *Proc. SIPS '98*. Cambridge, MA, USA, 8-10 October 1998, pp. 356–365.

[133] ——, "Cost-efficient parallel lattice VLSI architecture for the IFFT/FFT in DMT transceiver technology," in *Proc. ICASSP '98*, vol. 6. Seattle, WA, USA, 12-15 May 1998, pp. 3517–3520.

[134] G.994.1, *Additional codepoints for the support of ITU-T G.9701*, ITU, Dec 2014, Available: https://www.itu.int/rec/T-REC-G.994.1-201412-I!Amd4/en (Last accessed: 29 August 2016).

[135] S. Galli and K. Kerpez, "Methods of summing crosstalk from mized sources - Part I: Theoretical Analysis," in *IEEE Trans. Commun.*, vol. 50, no. 3, Mar. 2002, pp. 453 – 461.